THE SYNTHESIS, OPTICAL PROPERTIES AND BIOLOGICAL APPLICATIONS OF Mn^{2+},Cu^{2+} AND Ag^{+} DOPED ZnS NANOPARTICLES

by

LUN MA

Presented to the Faculty of the Graduate School of

The University of Texas at Arlington in Partial Fulfillment

of the Requirements

for the Degree of

DOCTOR OF PHILOSOPHY

THE UNIVERSITY OF TEXAS AT ARLINGTON

August 2011

To my Mother

ACKNOWLEDGEMENTS

To begin with, I would like to thank my advisor, Dr. Wei Chen for his support, understanding and patience during the past four years over my work. He is a great teacher and researcher and always approachable. He has been a source of advice when I need any. I greatly appreciate the opportunity to work with and learn from him. Without his guidance and helpful suggestions, this work would not have been possible.

I am grateful to my other committee members, who take their time and serve in my committee, and put forth the effort to read and comment on this dissertation. I also would like to give my gratitude to Dr. Qiming Zhang, my graduate supervisor, who provides lots of suggestions on my academics.

The postdoctoral scholars Marius Hossu, Xiaoju Zou, Ke Jiang and visiting professor ZhongXin Liu, also give great help and ideas from various perspectives. They have explained and discussed many issues and problems I have met. I also want to thank all the other members in my group. I really enjoy the time working with them.

Finally, I would like to give my deepest thanks to my wife and family, for their love and support all the time.

July 29, 2011

ABSTRACT

THE SYNTHESIS, OPTICAL PROPERTIES AND BIOLOGICAL APPLICATIONS OF Mn^{2+},Cu^{2+} AND Ag^{+} DOPED ZnS NANOPARTICLES

LUN MA, PhD

The University of Texas at Arlington, 2011

Supervising Professor: Wei Chen

As a typical wide-band gap IIB-VI semiconductor, ZnS and ZnS based materials have been extensively studied and used in a variety of applications such as electroluminescence and cathodoluminescence displays, solar cells, and other optoelectronic devices. The most attractive feature of ZnS is its ability to be doped with most transition and/or rare earth metal ions, which allows a wide range of tunable electronic and optical properties. The nano-sized ZnS based particles perform unique physical and chemical properties that dramatically differ from their bulk materials due to quantum size confinement. In this dissertation, Mn^{2+}, Cu^{2+} and Ag^{+} doped ZnS water soluble nanoparticles were synthesized for biological applications.

Luminescent nanoparticles have gained immense attention as versatile fluorescent agents for bio-medical imaging because of their unique luminescence and photophysical properties. ZnS:Mn is a representative member in ZnS based material family. The red emission from Mn^{2+} ions is very intensive and can be excited by various energy sources, including X-ray. In this work, the synthesized water soluble ZnS:Mn nanoparticles are first applied to cell imaging and fingerprint detection. Satisfactory results have been obtained due to intensive

luminescence of ZnS:Mn nanoparticles and their relative long lifetime. Subsequently, hydrophobic ZnS:Mn nanoparticles were prepared and encapsulated together with photosensitizer into polylactic-co-glycolic acid (PLGA) spheres for photodynamic therapy (PDT) applications. Results show that more cells were killed by using PLGA encapsulated ZnS:Mn-photosensitizer composites after X-ray treatment.

Water soluble afterglow nanoparticles are the key factor for the new strategy of “Nanoparticle Self-Lighting Photodynamic Therapy for Cancer Treatment”, in which the light activating photosensitizers is generated by afterglow nanoparticles. Therefore, water soluble ZnS:Cu,Co green afterglow nanoparticles were synthesized and their optical properties including afterglow properties were discussed. The result from the preliminary application of ZnS:Cu,Co afterglow nanoparticles and photosensitizer conjugation on human prostate cancer cells shows that the energy transfer occurs and the composite materials killed more cells comparing to either photosensitizers or nanoparticles after UV light treatment.

High fluorescence or afterglow intensity is required for an efficient light source in PDT. The afterglow enhancement is observed by sample aging. Further measurement and analysis revealed that the oxidation process occurring on particle surface could produce more defects which act as electron traps and result in the enhancement on both afterglow intensity and longevity. Moreover, blue afterglow was obtained from ZnS:Ag,Co water soluble nanoparticles by using the same strategy, which may further contribute to the development of new afterglow materials from ZnS-based nanoparticles.

TABLE OF CONTENTS

LIST OF ILLUSTRATIONS

Figure Page

LIST OF TABLES

CHAPTER 1

INTRODUCTION

Chapter 1 introduces the fundamental phenomenon and concepts in luminescence. Basic mechanisms of fluorescence, phosphorescence and afterglow are discussed. ZnS based luminescent nanoparticles are briefly described, particularly on manganese doped ZnS nanoparticles, while Chapter 2 mainly focuses on their experimental synthesis and biological applications. On the other hand, water soluble ZnS:Cu,Co and ZnS:Ag,Co afterglow nanoparticles are also important part in this dissertation. Due to their relatively lower popularity, afterglow materials will be extensively introduced in this chapter and the synthesis, properties and applications of afterglow nanoparticles will be explicated in Chapter 3. Chapter 4 opens and discusses the enhancement of ZnS:Cu,Co afterglow nanoparticles. Aging is found as an efficient method to enhance ZnS based water soluble afterglow nanoparticles. As a consequence, blue afterglow has been obtained from ZnS:Ag,Co nanoparticles by using the same preparation strategy and is described in chapter 5.

1.1 Luminescence

1.1.1 The Phenomenon of Luminescence – A "Cold" Light

The term "lumen" is originally from Latin which means light. In general, luminescence refers to a phenomenon in which materials emit light after they absorb some kind of energy. The light here usually stays in a visible wavelength range (380 nm ~ 750 nm) or an extended range from near-ultraviolet to near-infrared sometimes. In another common phenomenon existing in nature, substances at a certain temperature release thermal radiation to their environment. Those light emitted from hot surfaces (usually above 900 K) during the thermal radiation process could also be seen by human eyes and this emission is actually called incandescence, which does not need to absorb extra energy for emitting light. On the contrary, luminescence

means a non-thermally produced or a “cold” light. It is a light emitting process related to electron transitions from their higher energy states to lower energy states.

1.1.2 A Brief History of Luminescence

The observation of luminescence could be dated back to ancient time. However, the first well documented luminescence phenomenon was considered from a Spanish physician and botanist N. Monardes who obtained some liquid infusion from the wood of a small Mexican tree in 1565. In 17th century, a famous scientist Robert Boyle (known as “the father of chemistry”) made much detailed description about luminescence and even firstly tried to use this phenomenon as a PH indicator. The concept of luminescence did not get more clear in the next century until professor George Gabriel Stokes published his paper – “On the Change of Refrangibility of Light” in 1852. Stokes studied the light emitted from quinine sulphate and realized that the substance actually re-emits light at longer wavelength than the light wavelength absorbed. The wavelength shifting between emission and excitation wavelengths was later named as “Stokes Shift”. Stokes also firstly promoted the term “fluorescence” and it is now widely used in the field of luminescence. Starting from the early 20th century, the explanation of luminescence phenomenon got improved much because of Alexander Jablonski’s work. The electron transitions between excited and ground energy states in light absorption and emission were clearly illustrated in an energy band diagram. The diagram was named after him as Jablonski Diagram and is now widely accepted as fundamental tools to analyze the mechanism of luminescence.

1.1.3 The Different Types of Luminescence

The knowledge of luminescence and its applications were developed quickly after the World War II, much more luminescent materials appeared and have been applied to many fields. People had noticed that luminescence can be induced by various of energy forms. Based on different excitation energy sources, luminescence is now categorized into many types, such as cathodoluminescence, chemiluminescence, radioluminescence, photoluminescence,

thermoluminescenc and triboluminescence. In this dissertation, my work is focused on the photoluminescence in which the luminescence is excited by photons or electromagnetic radiations.

Despite of different excitation sources, once the material is excited and emits luminescence, it lasts for a certain time which could be very short in nanoseconds or long in hours. Depending on how long the emission light can last after the excitation is turned off, luminescence has been divided into fluorescence, phosphorescence and afterglow.

1.2 The Fundamental Mechanism of Fluorescence, Phosphorescence and Afterglow

1.2.1 Fluorescence

The lifetime of a luminescent material means the time cost when the luminescence intensity drops to its 1/e intensity after the excitation is ceased. Fluorescence typically has a lifetime around 10^{-8} s, although this value can also reach a time scale of milliseconds in some cases (e.g. ZnS:Mn, 1.8 ms). Illustrated by the energy band diagram in Figure 1.1, when a phosphor (materials that can emit luminescence) absorbs energy and is excited, the electrons in valence band can jump up to higher energy states – excited states S_1 or S_2. This process is very quick and usually costs about 10^{-15} s. The excited electrons have very short life time (10^{-11} ~ 10^{-13} s) and then quickly release their energy by vibrations or internal conversions to the lowest energy level of the first excited state S_1. The transitions from the lowest excited state to ground states can release energy in either radiative or nonradiative process. The radiative process produces photons in fluorescence and nonradiative process releases energy by vibrations and generates heat. As electron transitions from higher excited states to the lowest energy level of the first excited state S_1 are several orders faster and usually nonradiative, the wavelength of fluorescence emitted finally is not affected by the excitation energy significantly.

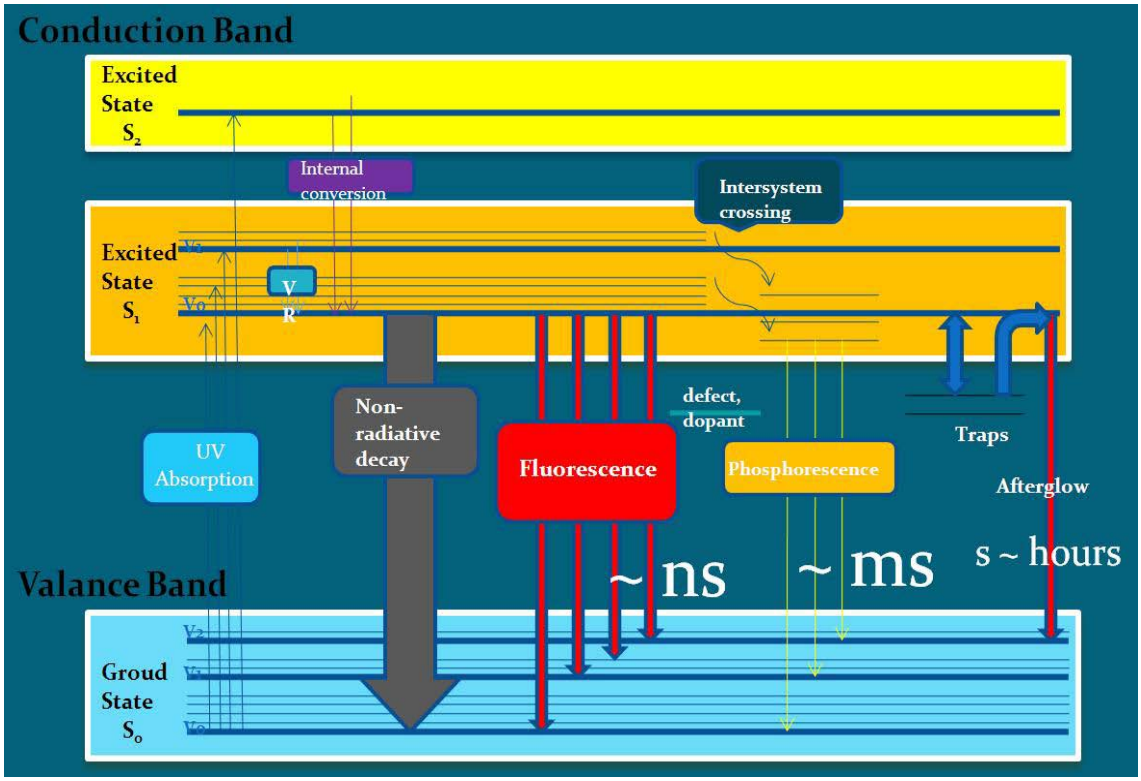

Figure 1.1 The energy band gap diagram for the illustration of typical fluorescence, phosphorescence and afterglow.

1.2.2 Phosphorescence and Afterglow

It is necessary to introduce the concept of singlet and triplet state before further discussions on phosphorescence and afterglow. An excited state may have multiple energy status that is indexed by 2S+1, where S is the total spin quantum number of a molecule. From knowledge of quantum mechanics, the spin of an electron can only be “up” (+1/2) or “down” (-1/2). In general, the electrons in ground states of most material molecules are paired and the total spin quantum number S is 0 as the two electrons in one orbit must stay in opposite spins. Therefore the ground state is usually a singlet state (2S+1 = 1). Most electron transitions do not change spin orientation, thus those excited states remain in singlet states. However, there are cases in which the electron spin is changed after the transition process and result in two unpaired electrons with S = 1. The excited state now is in “triplet” as 2S+1 =3 and it contains

three energy statues in an applied magnetic field. The diagram illustration of the singlet and triplet state is shown in Figure 1.2.

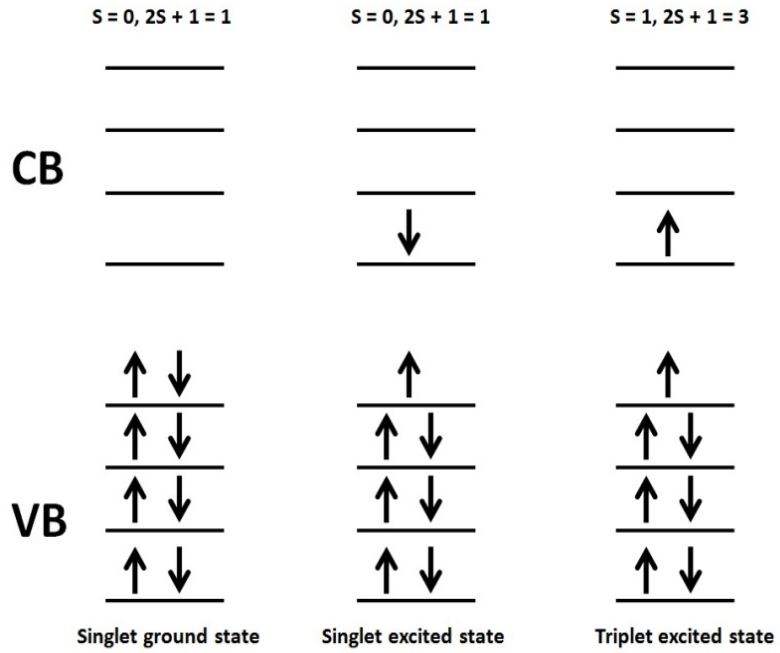

Figure 1.2 The diagram illustration of singlet ground state, singlet excited state and triplet excited state.

Afterglow (persistent luminescence) means the phosphors can emit luminescence for a long time after the excitation source has been turned off. The afterglow luminescence remains from several seconds to hours or even days. The phenomenon of afterglow is frequently found to be mixed with another term “phosphorescence” and some researchers have tried to distinguish them from each other because phosphorescence has been explained by electron transitions from an energy triplet state to singlet state, while the afterglow is generally proposed with a different mechanism related to electron traps.[1-3] As shown in Figure 1.1, phosphorescence takes longer time in the radiative decay process than fluorescence and typically lasts from milliseconds to seconds because the transition from triplet state to singlet state is spin forbidden. In further comparison, afterglow has much longer life time from minutes to hours. Thermal energy is generally required to release those electrons that are trapped.

Certainly, electrons could be re-trapped and released later and this process could be repeated for many times. In general, afterglow is temperature related. The entrapped electrons may obtain enough thermal energy and escape very quickly if the ambient temperature is too high. On the other hand, they cannot be released if the temperature is too low. A proper energy trap depth has been suggested as 0.65 eV for the room temperature in the afterglow study of Eu^{2+} and Dy^{3+} doped strontium aluminates.[4,5] However, it should be noticed that the actual detailed afterglow mechanism is much complicated and still unclear. The type of electron traps varies from material to material and how the traps are formed as well as their quantities and locations are still in debate. Meanwhile, new afterglow materials keep developing but mostly are suggested with their own particular explanation.[6-9] In some areas, the terms of afterglow and phosphorescence or long lasting luminescence are not distinguished strictly and used as substitutions with each other. In this work, the phrase afterglow is generally used as the experiment products continuously emitting light for minutes (much longer than usual phosphorescence) after the excitation source has been removed. The model of electron traps is consequently applied for the long lasting luminescence from our nanoparticles.

1.3 ZnS Based Luminescent Nanoparticles

1.3.1 Bulk and Nano-sized ZnS Based Materials

ZnS is a typical wide-band gap IIB-VI semiconductor and has been extensively studied and used in commercial fields for many years. ZnS based luminescent materials emit different colors and can be excited by a variety of sources to display photoluminescence, cathodoluminescence and electroluminescence. It is such an important inorganic material which can be found in many applications including photoconductors, solar cells, field effect transistors, optical sensors, and light emitting displays. Zinc blende and wurtzite are two crystal structures usually seen in ZnS based materials. The energy band gap in bulk ZnS is 3.6 eV and 3.8 eV for zinc blende and wurtzite structures, respectively.[10-12] Both of them are located in ultraviolet (UV) range and not visible. Nano-sized ZnS materials may have higher band gap energy due to

quantum confinement effect from their small sizes. In fact, a violet/blue emission peaking from 420 nm to 470 nm due to crystal defects is very common in ZnS materials.[11,13-20] This defect emission could be very intensive from ZnS nanoparticles as the surface area becomes a dominant role in nano-sized materials. The band-band emission from ZnS nanoparticles has also been observed with defect emission together.[12,20,21] However, the key reason for the wide applications of ZnS is its ability to be doped with most transition and/or rare earth metal ions. The dopants can alter the electronic and optical properties of the doped system significantly.[16,18,22,23] By the large amount of dopant candidates, ZnS based luminescent materials are able to cover the luminescence from blue to red.[24-26]

Nanomaterials have attracted much attention in recent decades because of their unusual physical and chemical properties in comparison with their bulk materials. Here, the changes of optical properties are focused. As the particle size decreases to Bohr radius of exciton, quantum confinement causes an increased band gap. This makes the wavelength of luminescence from nanomaterials tunable. As a typical example, CdTe nanoparitcles display a red shift of absorption and emit light from green to red when their size increase from 3.1 nm to 3.8 nm.[27] In ZnS based materials, a remarkable optical property change due to the ZnS band gap increasing can be seen from ZnS:Eu^{2+}.[28,29] The bulk ZnS:Eu^{2+} barely shows emission at room temperature because the lowest excited state of Eu^{2+} still merges inside of bulk ZnS (host) conduction band. In ZnS:Eu^{2+} nanoparticles, the band gap is enlarged and the conduction band is higher than Eu^{2+} excited states, hence the f-f transition of Eu^{2+} occurs and emits light.[29] The quantum confinement also increases the overlap of electrons and holes, which induces higher electron-hole recombination rate and absorption strength of the material.[30] Thus, it is expected that nanomaterials may have much efficient luminescence than their bulk materials.

The small particles have very high surface/volume ratio and this ratio increases dramatically when the size of the particles shrinks to nanometers. A 10 nm particle usually contains tens of thousands atoms and the surface atoms count about 20%, while a 2 nm

particle has several hundred atoms and 80% of them are on the surface. As the surface area becomes dominant for small nanoparticles, defects located in the particle surface also play an important role in nanoparticle properties. The defect emission can be very noticeable in ZnS luminescent nanoparticles and thus reduce the luminescence from other luminescent centers. Surface passivations are good methods reducing surface defects and obtain high quantum efficiency through adding surfactants or coating with a shell of another material.

Water solubility is a general requirement for biological applications. Comparing with bulk materials, it is much easier for nanoparticles to be water soluble as they are light and small. However, nanoparticles have high surface energy and strong tendency to aggregate. One of the efficient methods obtaining water soluble nanoparticles is to apply surface stabilizers (surfactants) on particle surface. The stabilizers generally own functional groups on their one end which have affinity to attach on particle surface and other groups on the other end which are hydrophilic. With the modification by stabilizers, the surface energy is reduced and the hydrophilic chemical groups help the nanoparticle dispersion in water. As for ZnS based nanoparticles, because of the strong affinity to Zn^{2+} ions, stabilizers having thio groups (-SH) are mostly used, such as thioglycolic acid (TGA), 3-mercaptopropionic acid (MPA), L-cysteine, and 2-Mercaptoethylamine hydrochloride (CA). The other way of dispersing nanoparticles in water is by using electrolyte. Because of the high surface/volume ratio of nanoparicles, dangling bonds are commonly found on nanoparticle surfaces and this makes the particle lose its electric neutrality and capable to adsorb oppositely charged ions onto its surface area. The charged nanoparticles repel each other by Coulomb force and thus can disperse in water.

Moreover, nanoparticles have advantages to enter cells in biological systems as they are small enough. ZnS based luminescent nanoparticles are cyto-friendly materials and have started to be used as labeling agent for biological imaging instead of organic dyes.[24] The light emitted from nanoparticles further allow them to be used for medical treatment.[31] ZnS based afterglow water soluble nanoparticles may also find new applications in biological imaging and

photodynamic therapy for deep cancer treatment. This dissertation involves some work in such interesting fields and they will be discussed in the following content.

1.3.2 Preparation of ZnS Based Nanoparticles

Nanoparticles can be prepared from gaseous, liquid and solid environments. Depending on whether chemical reactions are involved, the synthesis processes are categorized into physical method and chemical method. A typical physical method to synthesize nanoparticles is to grind bulk materials mechanically into small sizes. For ZnS based materials, chemical methods have been mostly applied, including the methods of co-precipitation, hydrothermal, sol-gel and solid state reaction. In this dissertation, manganese, copper or silver doped ZnS nanoparticles are synthesized by precipitation method in water or organic solvents. Hydrophilic and hydrophobic ZnS based nanoparticles have been prepared by simply choosing proper stabilizers and reaction solvents.

In order to obtain water soluble nanoparticles, a straight forward method is to synthesize them directly in water. However, proper stabilizers must be applied. Firstly, it must have functional groups which can chemically bond with the particle surface. In general, nanoparticles adsorb other molecules or particles due to their high surface energy and aggregate to large clusters. Therefore, a strong chemical bond between nanoparticle and stabilizer is necessary to prevent particle-particle attachment. Secondly, the stabilizer should have hydrophilic groups which make the nanoparticle “water-like”. Thirdly, suitable environment needs to be considered because stabilizers work under appropriate conditions, such as PH value, temperature and solvent.

Hydrothermal method is also a very common way to prepare ZnS based nanoparticles in water. It reaches higher reaction temperature as the reaction container is tightly sealed. With high reaction temperature, particle nuclei form fast and it reduces the broadness of particle size distribution. Moreover, the doping could become more efficient as the dopant ions are earning more energy to diffuse in the host material. However, hydrothermal method presents less

safeness due to its high reaction pressure and it basically does not allows additional operations (e.g. adding other reactants) during the particle synthesis.

Synthesizing nanoparticles in oil phase is able to reach high reaction temperatures by using organic solvents with high boiling temperatures. Besides the advantages of higher doping efficiency and narrower particle size distribution, the reaction generally produces hydrophobic nanoparticles. As particle synthesis in oil phase usually needs lots of post-synthesis treatment and many high boiling temperature organic solvents are not environment-friendly, this type of synthesis is not treated as a “green” chemistry.

It should be noticed that hydrophobic nanoparticles can be converted to hydrophilic by phase transfer method.[32] For ZnS based hydrophobic nanoparticles, a phase exchange ligand with thio group is generally preferred as the strong affinity between thio group and Zn^{2+} ions. In addition, hydrophobic nanoparticles can be encapsulated into some polymer spheres (e.g. PLGA) or coated by a silica shell This strategy also makes the hydrophobic nanoparticles dispersed in water without changing much of their optical properties.

1.4 Afterglow Materials

1.4.1 The Afterglow Materials in Ancient Time

People noticed the phenomenon of afterglow from more than 2000 years ago. In ancient China, stones with persistent luminescence have appeared in recorded stories and been treated as rare treasures because they are able to glow at night by themselves. Those stones were basically raw materials form nature, some might contain radioactive elements which emit nuclear radiation energy as the excitation source. As most of those old stories are not able to provide more details about afterglow, it is hard to know what type of materials they really belong to. The earliest well-documented persistent luminescence material was discovered by an Italian shoemaker Vencen cino Casciavolus in 1602. He tried to collect gold by heating different types of mineral ores but obtained some stones emitting red cold light at night. The stones were known later as Bolognian stone which contains mainly Ba_2SO_4 and some Bismuth and

Manganese. The ores turned to sulfide compound after calcination and actually impurities contained in the ores contributed to the afterglow.

1.4.2 ZnS Based Afterglow Materials

The afterglow materials were remaining their mystery until the first man-made persistent phosphors ZnS:Cu appeared in the late 19th century. However the real modern scientific study and industrialization on afterglow materials started from 1970s. As the typical first generation persistent phosphor products, ZnCdS:Cu, ZnS:Cu, CaS:Bi and CaSrS:Bi have found their applications in commercial market and military fields. Among those materials, ZnS:Cu (usually co-doped with cobalt) is very representative and extensively studied. The green afterglow emitted from it is visible to the human eye in darkness and is explained by the model of electron traps.[1,2] Co-doped cobalt makes this afterglow brighter and longer as co-doping can increase the depth of the electron traps.[1] Like ZnS based fluorescent nanoparticles, ZnS based afterglow materials may also have various afterglow wavelengths through different dopings (mostly transition and alkaline metal ions).[2,22,33] In addition, the doping with rare earth ions makes large improvement on afterglow properties of sulfide based materials, such as ZnS:Eu, CaBaS:Eu:Cu, CaSrS:Eu:Dy and etc. The Eu^{2+} ions are mainly used as activators and Dy^{3+} ions act as sensitizers or auxiliary activators. However, the intensity of persistent luminescence from these materials was still not very bright comparing to the general fluorescence with a stimulation source. In addition, their maximum persistent time can last for a few hours only. One of the solutions to prolong the duration of persistence is by adding radioactive elements as external excitation sources. The artificially added nuclear radiation sources continuously release energy to keep the material glowing even for years. However, from a strict view, it is not a real afterglow and should be called radioactive luminescence. Furthermore, the addition of radioactive elements brings a fatal disadvantage to the material development because they are harmful to environment and human health. What is more, the solid ZnS based phosphors are also not chemically stable under UV radiation or in a humid environment. The limitations greatly affect

more practical applications of ZnS based afterglow materials.

1.4.3 Aluminate and Silicate Afterglow Materials

The new development of afterglow materials were initiated with the study of strontium aluminate phosphor in 1946.[34] After that, Victor Abbruscato reported a long persistent luminescence from Eu^{2+} doped alkaline earth aluminates -- $SrAl_2O_4:Eu^{2+}$ in 1971 and suggested that Sr_{2+} vacancies could be the traps.[35] The research and development of new afterglow materials took place much faster after the mid of 1990s. In 1996, by introducing the rare earth element Dy^{3+} as co-dopant, Matsuzawa et al. synthesized $SrAl_2O_4:Eu^{2+},Dy^{3+}$ long afterglow phosphor which had large improvement in both afterglow brightness and longevity comparing with $SrAl_2O_4:Eu^{2+}$ materials.[7] Like Eu^{2+} and Dy^{3+} co-doped sulfide based afterglow materials, Dy^{3+} was still supposed to play the same role as auxiliary activators. Different preparation methods were then developed and similar aluminate afterglow phosphors such as $CaAl_2O_4:Eu^{2+}$ appeared soon after.[36-39] However, the properties of aluminate afterglow materials decreased much when they are under a water environment, thus largely limiting their applications in pigments, paints and other fields. Rare earth metal ions doped silicates (e.g. $Sr_2MgSi_2O_7:Eu^{2+},Dy^{3+}$) was introduced to improve the performance of afterglow materials in water.[40] Due to a better brightness and longer persistent time, aluminate based and silicate based afterglow materials are studied intensively in recent years.

1.5 Biological Applications of ZnS Based Fluorescent and Afterglow Nanoparticles

1.5.1 Applications in Fluorescence Imaging

Fluorescence imaging is a sensitive and quantitative imaging technique that is widely applied in molecular biology and biochemistry. Comparing with other bio-imaging methods (X-ray, CT and PET), fluorescence imaging uses visible or near infrared excitation which is non-ionizing and less hazardous. As labeling agents, organic dyes have been successfully used in fluorescence imaging for many years. However, shortages form the organic dyes, such as poor photo stability, narrow excitation spectra and short decay lifetime, limit their further steps in the

development of this imaging technique. In the recent two decades, luminescent nanoparticles started finding many exciting applications in the field of bio-imaging and medical treatment. These small fluorophores have attracted much attention due to their unique and remarkable optical properties. Compared to conventional organic dyes and fluorescent proteins, luminescent nanoparticles have numerous advantages, such as minimal photobleaching, higher quantum yields, broad excitation with narrower emission spectra and longer luminescence life time, which make them ideal to obtain high contrast bio-medical images. In addition, luminescent nanoparticles are able to be functionalized by proper surface groups for coupling with bio-molecules, so the particles can be effectively delivered to specific targeting locations of interest.

High luminescence intensity is one of the most important requirements of biological imaging. The core-shell CdSe/ZnS nanoparticle has firstly found its applications in cell imaging.[41-43] The shell of higher band-gap semiconductors can increase the luminescence quantum efficiency and physical/chemical stability of core particles. As cadmium is generally a toxic element, non-cadmium core-shell InP/ZnS nanoparticle was developed as a new non-toxic optical probe for imaging cancer cells.[44] However, the preparation of those core/shell nanostructures is generally complicated and hard to control. Recently, ZnS based luminescent nanoparticles have been reported as a non-cytotoxic cell image labeling agent by conjugating with folic acid.[24] As a long lifetime fluorescent material, ZnS:Mn nanoparticles have gained some attention, while further applications should be studied.

1.5.2 Applications in Photodynamic Therapy for Cancer Treatment

Photodynamic therapy (PDT) is a form of medical treatment in which disease cells or tissues are destroyed by applying a photosensitizer (photosensitizing drug) followed by light exposure. In addition, the presence of adequate molecular oxygen in the tissue is also required. The principle of PDT is that the photosensitizer absorbs the light energy and becomes activated, then the energy is transferred to oxygen molecules and generates singlet oxygen.

The singlet oxygen is highly reactive and it is able to immediately react with and damage vital cells and finally result in cell death.

While conventional chemotherapy usually affects the whole immune system, radiation therapy usually causes damages also to plenty of normal cells. In comparison, PDT is a site-specific treatment by targeting photosensitizers. The harmless visible light used in PDT leaves the immune system and normal cells intact. PDT has been applied in cancer treatment, precancerous lesions (actinic keratosis) and age-related macular degeneration. However, deep cancer treatment is a challenging problem existing in clinical PDT. To have an efficient energy transfer, the wavelengths of light source have to largely overlap with the maximum absorption of the photosensitizer applied. As the absorptions of most photosensitizers are located in UV range, PDT is limited on superficial area treatment because UV light cannot penetrate to deep tissues.

In order to resolve the problem, a new strategy “Nanoparticle self-lighting photodynamic therapy (NSLPDT)” was proposed[45] based on afterglow nanoparticle-photosensitizer conjugation. As afterglow material stores and then releases light energy in a long time, when it is conjugated with photosensitizer and targeted to tumors cells, afterglow is expected to be the light source activating photosensitizer. The afterglow particles can be excited ex vivo or in deep tissue by X-ray. Once the excitation is done, X-ray will be removed and this can largely reduce the harmful X-ray dosage.

The method opens a new promising field for afterglow materials. However, the current afterglow materials can be barely applied in biological systems as they are mostly not water soluble and in large sizes. Therefore, it is necessary to develop nano-sized and water soluble afterglow materials for biological applications. In this dissertation, ZnS:Cu,Co and ZnS:Ag,Co water soluble afterglow nanoparticles have been prepared by a simple wet chemistry method. Some preliminary results of ZnS:Cu,Co-photosensitizer conjugation are also discussed (Chapter 4). As the high afterglow intensity and longevity are required for efficient NSLPDT,

Chapter 4 shows ZnS:Cu,Co nanoparticle afterglow enhancement and possible mechanism of the enhancement is proposed.

Using scintillation nanoparticles as light source in PDT is another new method for deep cancer treatment.[45] X-ray is used to excite nanoparticles as it can penetrate body tissues. Some work by using LaF_3:Tb^{3+} and CdSe/ZnS nanoparticles has been reported.[46,47] ZnS:Mn is also a good luminescent material excited by X-ray . Due to a relative non-cytotoxic and environment friendly nature of its compounds, ZnS:Mn could be a very promising light source for PDT in deep cancer treatment. The application of ZnS:Mn-photosensitizer on cancer cell treatment is performed in the next chapter through encapsulating them inside polymer spheres.

CHAPTER 2

THE OPTICAL PROPERTIES OF ZnS:Mn NANOPARTICLES AND THEIR APPLICATIONS IN BIOLOGICAL IMAGING AND PHOTODYNAMIC THERAPY

2.1 Introduction

Among doped ZnS materials, ZnS:Mn is very representative and perhaps the most studied and applied member. The red emission form Mn^{2+} ions makes it largely used in flat panel displays and cathode ray tubes. ZnS:Mn is also an excellent candidate for magnetic and spintronic applications as Mn^{2+} has 5 unpaired 3d electrons. In biological imaging, core/shell luminescent nanoparticles have been mostly applied as they generally have high luminescence intensities.[43,44,48] However, the synthesis of those core/shell nanostructures is complicated and they are basically hydrophobic. More coatings and modifications have to be applied further to make them hydrophilic for biological environment. Sometimes very toxic element is seen in those nanostructures. ZnS:Mn material is non-toxic and easy-made in water by simple wet chemistry. It is also able to be excited by various sources, including UV light and X-ray, which further allows its application in both fluorescence imaging and light source in photodynamic therapy for deep cancer treatment. In this chapter, we first prepare ZnS:Mn luminescent nanoparticles and discuss the obtained nanoparticle structure and optical properties, then perform some applications in biological imaging and PDT.

2.2 Synthesis and Characterization

2.2.1 Preparation Method

$Zn(CH_3COO)_2$, $Mn(C_5H_8O_2)_2$, and thioglycolic acid (TGA,98%) were purchased from Sigma-Aldrich Inc., USA. Na_2S is also a product of Sigma but from Canada. All the chemicals were of analytical grade or of the highest purity available and used as received. De-ionized (DI) water was used as a solvent. A simple wet chemical method was applied to obtain water

soluble ZnS:Mn nanoparticles. Briefly, 183 mg $Zn(CH_3COO)_2$, 25 mg $Mn(C_5H_8O_2)_2$, and 72 mg Na_2S were added into 50 ml DI water following by adding 1.5 ml of 0.2 M TGA. The water solution was heated to boiling temperature and remained for 5 hours. Finally, the solution was allowed to be cooled in air to room temperature.

2.2.2 Characterization

The identity, crystalline structure, size and shape of the nanoparticles were observed by X-ray diffraction (XRD) and high-resolution transmission electron microscopy (HRTEM). The XRD pattern was recorded by using a Siemens Kristalloflex 810 D-500 x-ray diffractometer with a radiation beam λ = 1.5406 Å. The nanoparticles in solution were placed onto holey carbon-covered copper grids for HRTEM observations. The HRTEM images of the particles were obtained with a JEOL JEM-2100 electron microscope with accelerating voltage of 200 kV. The emission spectra were carried out with a Shimadzu RF-5301PC fluorescence spectrophotometer.

2.3 Structural and optical properties

2.3.1 XRD and TEM

The XRD pattern of ZnS:Mn nanoparticles is displayed in Figure 2.1. It can be identified as the cubic zinc blende structure with a comparison to the standard card (JCPDS, no. 05-0566). The three main peaks can be indexed with (111), (220) and (311) planes. The broadened peaks indicate the small particle sizes of the sample. From this pattern, the mean particle size is estimated to be 4 nm through the Scherrer equation $D=0.9\lambda/(\beta\cos\theta)$, where λ is the X-ray wavelength (here λ = 1.54060 Å), β is the full width at half maximum (FWHM) and θ is the diffraction angle.

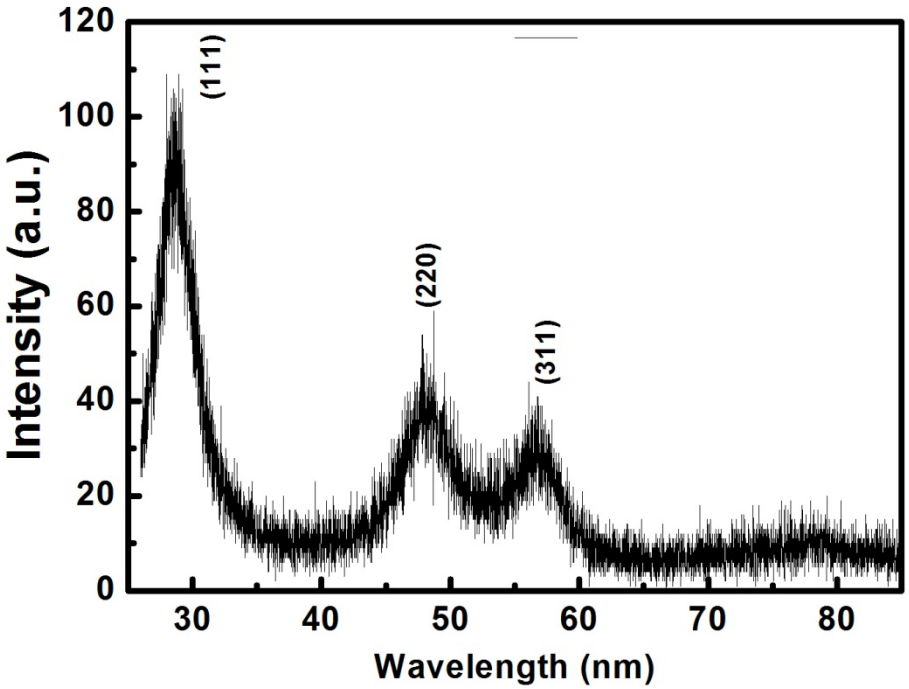

Figure 2.1 The XRD pattern of ZnS:Mn nanoparticles.

Figure 2.2 displays a typical high resolution transmission electron microscopy (HRTEM) image of ZnS:Mn nanoparticles. The particle aggregation is generally seen because of the drying process in TEM sample preparation. The average size of individual nanoparticles is found to be 4~5 nm, which matches well with the value estimated from the XRD measurement. The (111) lattice planes of some particles can be mainly observed and this lattice spacing is estimated to be about 0.31 nm from the HRTEM image, which is consistent with the (111) spacing of bulk ZnS (JCPDS 05-0566, 0.312 nm).

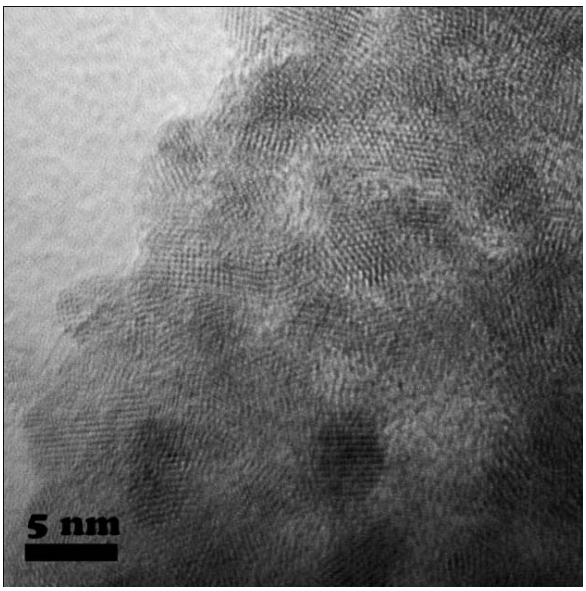

Figure 2.2 HRTEM image of ZnS:Mn nanoparticles dispersed in water.

2.3.2 Photoluminescence

Figure 2.3 The photo pictures of ZnS:Mn nanoparticles dispersed in water under normal light (left) and UV light (right).

The chemically synthesized ZnS:Mn nanoparticles are able to be well dispersed in water, which makes them easier to be applied in biological systems. Figure 2.3 shows the photo pictures of ZnS:Mn nanoparticles dispersed in water. The aqueous ZnS:Mn sample is transparent (left image) and emits strong red fluorescence under UV light (right image). Their photoluminescence spectra are shown in Figure 2.4. The ZnS exciton emission has been

obseved peaking at 373 nm by excitation of 240 nm. To obtain the maxium intensive red emission from Mn^{2+} due to $^4T_1 - {}^6A_1$ transition,[16,18,49,50] the excitation wavelength was changed to 340 nm. The defect emission centered at 441 nm is obseved but it is weak and broad.

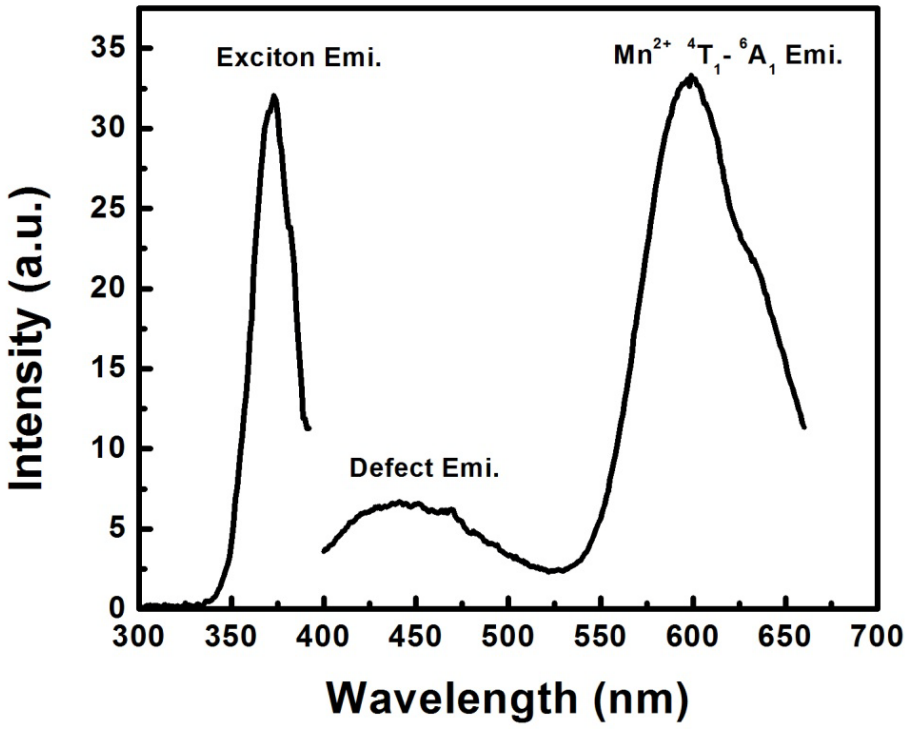

Figure 2.4 The luminescence spectra of water soluble ZnS:Mn nanoparticles. The exciton emission at 373 nm was excited by 240 nm. The emissions from defects and Mn^{2+} were excited by 340 nm.

2.4 Applications in Cell Imaging and Fingerprint Detection

2.4.1. ZnS:Mn in Cell Imaging

ZnS:Mn water soluble luminescent nanoparticles have high quantum efficiency and are non-cytotoxic, thereby making them a very good candidate for cell imaging. Figure 2.5 shows images of porcine lens epithelial cells taken by microscope with ZnS:Mn nanoparticles added as a labeling agent. The left image is taken by normal light without using extra excitation or filters. Under UV excitation, red filter are applied and the luminescence clearly display the locations of

ZnS:Mn nanoparticles inside the cell. The cell's morphology can also be seen from the nanoparticle luminescence. The result shows that ZnS:Mn is an efficient labeling agent for cell imaging. Further, water soluble ZnS:Mn nanoparticles can be conjugated with drugs to detect the drug distribution through fluorescence imaging.

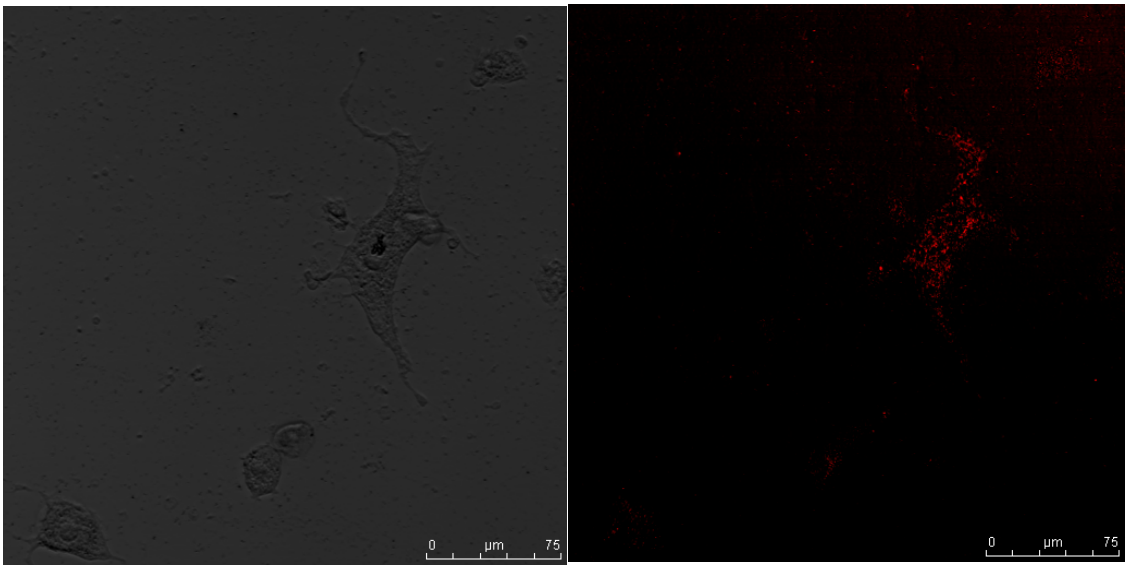

Figure 2.5 The microscope images of porcine lens epithelial cells taken by normal light (left) and UV excitation and red-light-pass filter (right).

2.4.2. ZnS:Mn in Fingerprint Detection

Highly luminescent water soluble nanoparticles have found many biological applications, particularly in tissue and cell labeling and imaging. However, little attention is paid on forensic evidence detection of biomaterials on the surface by using luminescent nanoparticles. As the functional groups of stabilizers coating on nanoparticle surface are able to bond with the target biomaterials, luminescent nanoparticles may also play as labeling agents in trace forensic evidence detection. The challenge is that, in many cases, the forensically relevant surfaces are highly fluorescent, resulting in bright background and thus reducing the imaging contrast. Fortunately, the decay lifetime of most of those background surfaces are very short and in nanosecond regime, which provides opportunities to remove or highly reduce the background fluorescence by collecting images after a certain time delay. The method is so

called time-gated fluorescence detection.[51] The red emission form Mn^{2+} ions in ZnS:Mn has long decay lifetime in milliseconds,[52,53] which is an ideal decay time window for this technique.

Figure 2.5 shows an image of Zn:Mn water soluble nanoparticle labeled fingerprint on polymethylpentene plastic surface, which is taken by the time-gated fluorescence detection technique. A brief sample preparation process is that, after the latent fingerprint is gently pressed on the substrate surface, the solution of water soluble ZnS:Mn nanoparticles is applied and allowed to react with the biomaterials left on the fingerprint for hours. Then, the sample is rinsed gently with DI water and dried by air for future imaging. As nanoparticles are coated by TGA on their surface, the carboxylic group (-COOH) from TGA is able to react with the amine group ($-NH_2$) of the target biomaterials through an amidation reaction.[54] Thus, the ZnS:Mn nanoparticles are bonded with biomaterials on their locations and able to reveal the fingerprint.

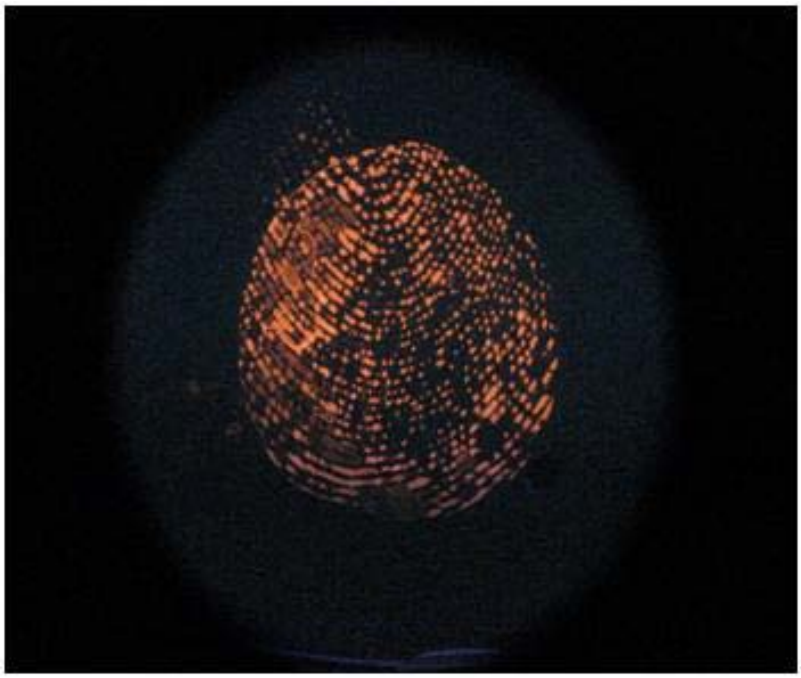

Figure 2.6 The image of a fingerprint on polymethylpentene plastic surface labeled by Zn:Mn water soluble nanoparticles.

It should be stressed that ZnS:Mn water soluble nanopartilces could work for large amount of fingerprint substrates due to its long lifetime and intensive luminescence. Moreover,

by simply changing the functional group on their surface, ZnS:Mn nanoparticles may find more applications in forensic trace evidence detection.

2.5 Applications for Photodynamic Therapy

2.5.1 The Motivation to Combine ZnS:Mn & Hypericin for PDT

While UV light is a good excitation source, the red luminescence due to the characteristic $^4T_1 - {}^6A_1$ transition of Mn^{2+} ions in ZnS:Mn can also be excited by X-ray.[55,56] X-ray is a well-known electromagnetic radiation which is able to penetrate human tissues and has already been widely used in many applications, including cancer treatment. As UV light is largely absorbed and cannot reach to deep tissues in human body, X-ray becomes a good excitation source for luminescent nanoparticles applied for deep cancer treatment or medical imaging. ZnS nanoparticles have been revealed as a cyto-friendly materials for biological applications.[24] Therefore, ZnS:Mn could be a good candidate as a light energy source in PDT for deep cancer treatment.

In order to have a successful energy transfer from a light source to photosensitizer, it is required that the emission from luminescent nanoparticles overlaps with the absorption of the photosensitizer. As the X-ray luminescence of ZnS:Mn is around 600 nm, a proper photosensitizer hypericin has been selected because it has intense absorption peaked at similar wavelength and a high singlet oxygen quantum yield.[57] For an efficient energy transfer, the close distance between luminescent nanoparticles and photosensitizers is also required. The conjugation of luminescent nanoparticles and photosensitizers by chemical bond is a good method to reach a very short distance. However, its synthesis process is usually complicated and inefficient. Here, we encapsulate both ZnS:Mn nanoparticles and hypericin into polylactic-co-glycolic acid (PLGA) nanospheres by using a simple emulsion synthesis method. The ZnS:Mn nanoparticles and hypericin molecules are spatially confined within nano-sized spheres and may have short enough distance for efficient energy transfer. Moreover, PLGA has been intensively studied and approved by the United States Food and Drug Administration as a safe

and biocompatible material for many years. The encapsulation of both luminescent nanoparticles and photosensitizers inside of PLGA nanospheres may provide great convenience for further delivery to tumor cells in patients.

2.5.2 Sample Preparation

Hydrophobic ZnS:Mn nanoparticles were synthesized by using an oil phase method with zinc nitrate hydrate as a precursor. Manganese nitrate hydrate was used for Mn^{2+} doping. Then ZnS:Mn, hypericin and PLGA solutions were mixed together and applied by a standard emulsion process for the preparation of PLGA encapsulated ZnS:Mn & hypericin nanostructures (ZnS:Mn-hypericin-PLGA). For a comparison purpose, ZnS:Mn-PLGA and hypericin-PLGA were also prepared using the same recipe and process.

2.5.3 Results and Discussion

Figure 2.7 shows the spectra of the X-ray luminescence from ZnS:Mn nanoparticles and the absorption of hypericin. The peak of ZnS:Mn X-ray excited emission is at about 610 nm and the peak of hypericin absorption is about 595 nm. Although the two peak positions are not exactly same, the emission spectrum of ZnS:Mn largely overlaps with the hypericin absorption spectrum. Therefore, the overlap requirement for energy transfer is satisfied.

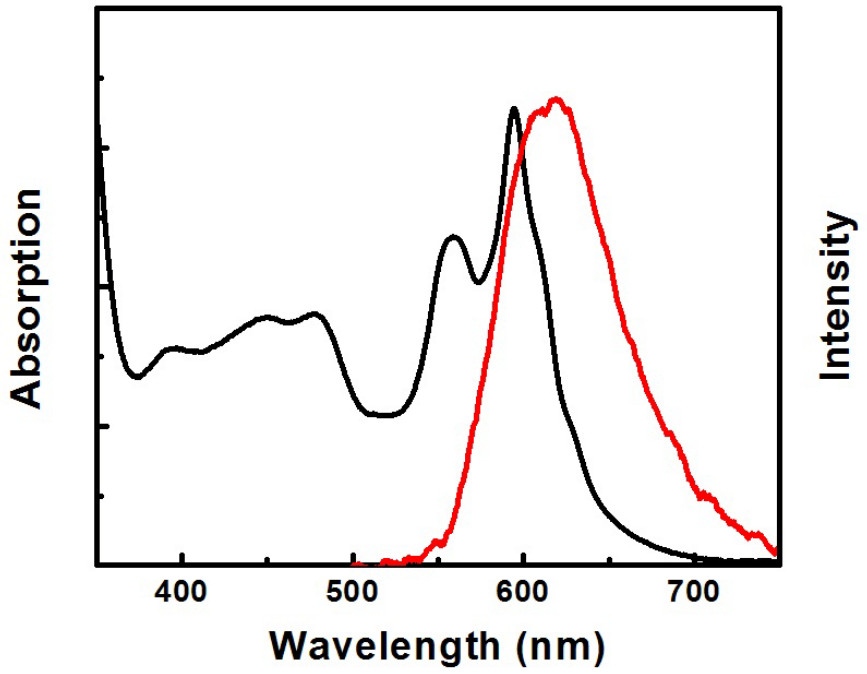

Figure 2.7 The spectra of the X-ray luminescence from ZnS:Mn nanoparticles (red) and the absorption of hypericin (black).

The high resolution transmission electron microscopy (HRTEM) images of PLGA spheres are shown in Figure 2.3. The average size of PLGA spheres is about 200~300 nm. From the image on the left, it can be clearly seen that ZnS:Mn nanoparticles have been highly loaded into the PLGA sphere. For further confirmation, the circled area has been zoomed in and displayed on the right. The lattice spacing is measured as 0.31 nm which is consistent with the spacing value 0.312 nm of the cubic ZnS (111) plane from the standard JCPDS database. Apparently, the edge of the PLGA is distinguishable from the background (shown by the white dash curve). It is very interesting that the ZnS:Mn nanoparticles formed nanorods in the edge area of PLGA sphere, as they are well aligned and perpendicular to the PLGA spherical surface. Further study is needed to reveal the mechanism of their formation. Hypericin molecules could also have been loaded. However, they are not observable by TEM, hence other measurement should be applied for hypericin observation.

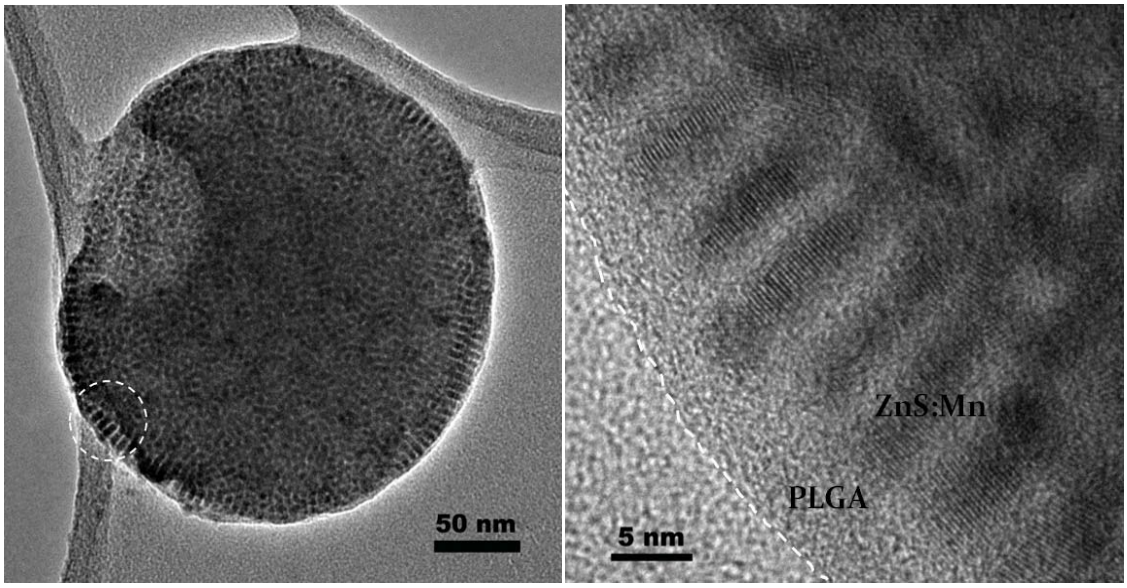

Figure 2.8 HRTEM images of PLGA nanospheres loaded by ZnS:Mn nanoparticles & hypericin. The image on the left shows the entire PLGA sphere. The area circled by the white dash line is zoomed in and shown on the right.

The cytotoxic effects of PLGA encapsulated ZnS:Mn & hypericin combination in human prostate cancer-3 cells are tested by the exposure of X-ray. The X-ray dosage for the cells is about 5 gray. For comparison, same amount of ZnS:Mn-PLGA, hypericin-PLGA and ZnS:Mn&hypericin-PLGA were added into same type of cells respectively and the cells were cultured for 24 hours. Then, the cells were divided into two groups, one group was treated with X-ray (5 gray) and the other was not. The cell viability assay was performed after another 24 hours cell culture. Figure 2.4 displays the percentage cell viabilities for PLGA encapsulated ZnS:Mn, hypericin and ZnS:Mn&hypericin with (light color) and without (deep color) X-ray treatment, respectively. For ZnS:Mn-PLGA treated cells, there is no further cell killing after exposure of X-ray. However, the cell metabolic activity reduced to 87% after the X-ray exposure in the hypericin treated cell samples. A possible reason is that the photosensitizer hypericin absorbed some energy from X-ray radiation and produced singlet oxygen which killed a few cells consequently. After the X-ray exposure, the metabolic activity of ZnS:Mn&hypericin-PLGA treated cells dropped heavier to 71%. This may suggest that energy transfer occurs from

ZnS:Mn nanoparticles to hypericin. As shown previously, ZnS:Mn nanoparticles have X-ray emission which largely overlaps the absorption spectra of hypericn. Therefore, hypericin could absorb the light energy of ZnS:Mn emission which was excited by X-ray.

It should be noticed that the ZnS:Mn&hypericin-PLGA treatment could kill more cells if the X-ray dosage is increased. However, X-ray radiation is harmful to human health, hence lower X-ray energy and shorter exposure time are always preferred. From the data shown, the efficiency of cell killing by ZnS:Mn&hypericin combination is still low (around 30%), this is perhaps due to a possible low hypericin loading in PLGA, further improvement should be focused on increasing the loading level of hypericin in PLGA in the future.

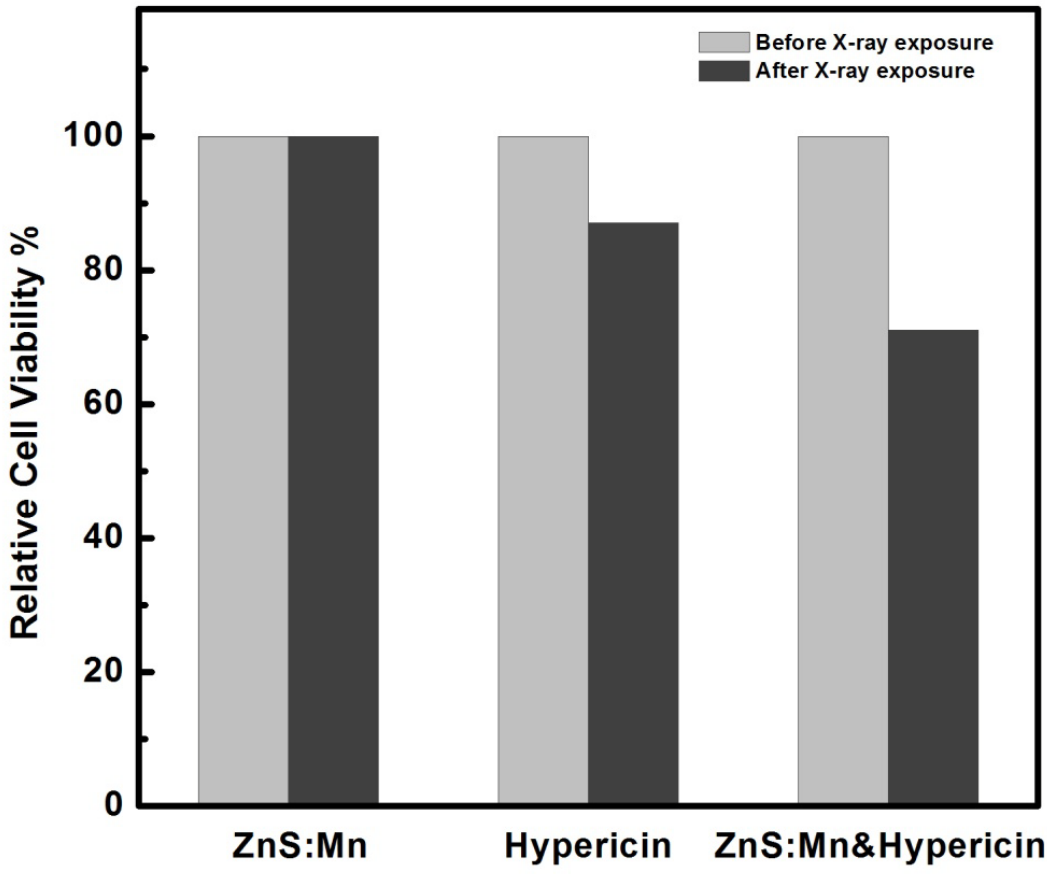

Figure 2.9 The cell viabilities for PLGA encapsulated ZnS:Mn, hypericin and ZnS:Mn-hypericin with (light color) and without (deep color) X-ray treatment respectively.

2.6 Luminescence Enhancement and Quenching in ZnS:Mn by Using Au Nanoparticles

2.6.1. Introduction

Highly intensive luminescence is always an important factor in pursuing highly sensitive fluorescence imaging. There are different methods that have been found effective for enhancing the luminescence intensity or quantum efficiency, such as controlling proper doping species and concentration, adding auxiliary dopants, increasing reaction temperature and pressure, synthesis by microwave or in oil phase, coating with stabilizers, and fabricating a shell layer with higher band gap materials. In the recent decade, noble metal nanoparticles (e.g. Au, Ag) appear much attractive because of their unique physical and chemical characteristics such as plasmon resonance and special effects on optical properties of phosphors nearby. Both luminescence quenching and enhancement have been reported in different applications.[58-60] ZnS:Mn is a very good material for luminescence with much interesting biological applications and it is widely used in electroluminescence and cathodoluminescence displays. There have been many publications on ZnS:Mn nanoparticles.[28,61-63] However, the interaction of metallic surface plasmon with luminescence centers in ZnS:Mn nanoparticles and the influence of surface plasmon on ZnS:Mn luminescence behaviors have not been reported yet. Here, we study the coupling of ZnS:Mn nanoparticles with Au nanoparticles and discuss the interesting luminescence enhancement and quenching of ZnS:Mn nanoparticles by the surface plasmon of Au nanoparticles.

2.6.2. Experment and Characterization

Au/silica/ZnS:Mn core-shell nanocomposites are synthesized in three steps: the preparation of Au nanoparticles, coating Au nanoparticles with silica layer, and the formation of ZnS:Mn nanoparticles on the outshells.

2.6.2.1 Synthesis of Au Nanoparticles

Au nanoparticles were synthesized by a sodium citrate reduction method as reported before.[64,65] To prepare Au nanoparticles, 40 ml of 0.326 mM $HAuCl_4$ solution was added to a

flask with 70 ml deionized (DI) water and heated to boiling temperature. Under vigorous stirring, 10 ml of 1% sodium citrate was then quickly added into the flask. After boiling for half an hour, the color of reaction solution gradually changed from colorless to burgundy, indicating the formation of Au nanoparticles. The solution was then cooled down by air to room temperature and formed Au seeds. To get larger Au nanoparticles, a previous reported seeded growth method[66] was applied. Briefly, 5 ml of Au seeds solution was dropped into a flask containing 60 ml DI water before 10 ml 1% sodium citrate was quickly added. The mixture was heated to 70°C and then 40 ml of 0.326mM $HAuCl_4$ solution was added. The reaction lasted for 1 hour and was cooled down to room temperature. The Au nanoparticles in the solution were washed with water 3 times by centrifugation at 12000 rpm for 30 minutes for each time.

2.6.2.2 Synthesis of Au/Silica Nanoparticles

40 µl of 1 mM MPTMS was added into 40 ml 5×10^{-10} M Au nanoparticle water solution under vigorous stirring. After 10 minutes, the mixture solution was centrifuged at 12000 rpm for 30min. The precipitate of Au nanoparticles was transferred into 20 ml 2-propanol containing 4 ml ammonium hydroxide (30 wt%), immediately followed by adding 40 µl tetramethyl orthosilicate (TEOS) under vigorous stirring. The stirring was allowed to last for 30 minutes. The solution was stored at room temperature overnight and then washed twice by a water-ethanol solution (5:4 in volume). The remaining Au/Silica nanoparticles were re-dispersed in 40 ml ethanol.

2.6.2.3 Formation of ZnS:Mn nanoparticles

ZnS:Mn nanoparticles were synthesized by wet chemical method with zinc acetate and sodium sulfide. Manganese acetylacetonate was used for Mn^{2+} doping. The obtained ZnS:Mn nanoparticles were redispersed in ethanol for later usage. In order to attach ZnS:Mn on the surface of silica coated Au nanoparticles, 20 µl MPTMS was added to 15 ml Au/silica ethanol solution to modify their surfaces. The modification process was conducted at 60 °C for 21 h. Then, 4 ml of the surface modified Au/silica ethanol solution was mixed with 1 ml ZnS:Mn

nanoparticle solution in ethanol and stirred for 3 h. For comparison purpose, ZnS:Mn and silica/ZnS:Mn nanoparticles were also prepared in similar recipes.

2.6.2.4 Characterization

The identity, crystalline structure, size, and shape of the nanoparticles were observed by x-ray diffraction and highresolution transmission electron microscopy (HRTEM). The nanoparticles in solution were brought onto holey carbon covered copper grids for HRTEM observations. The HRTEM images of the particles were obtained with a JEOL JEM-2100 electron microscope with accelerating voltage of 200kV. The excitation, emission, and scattering spectra were measured using a Shimadzu RF-5301PC fluorescence spectrophotometer. The scattering spectra were recorded by synchro measurement. The extinction spectra were recorded using a Shimadzu UV-2450 UV-Vis spectrophotometer.

2.6.3. Results and Discussion

The HRTEM images of Au and Au/silica/ZnS:Mn nanostructures are shown in Figure 2.10. The Au nanoparticles have an average size of 15 nm and the silica shell thickness is around 60 nm. Clearly, ZnS:Mn nanoparticles are attached on the surfaces of silica layers on Au nanoparticles.

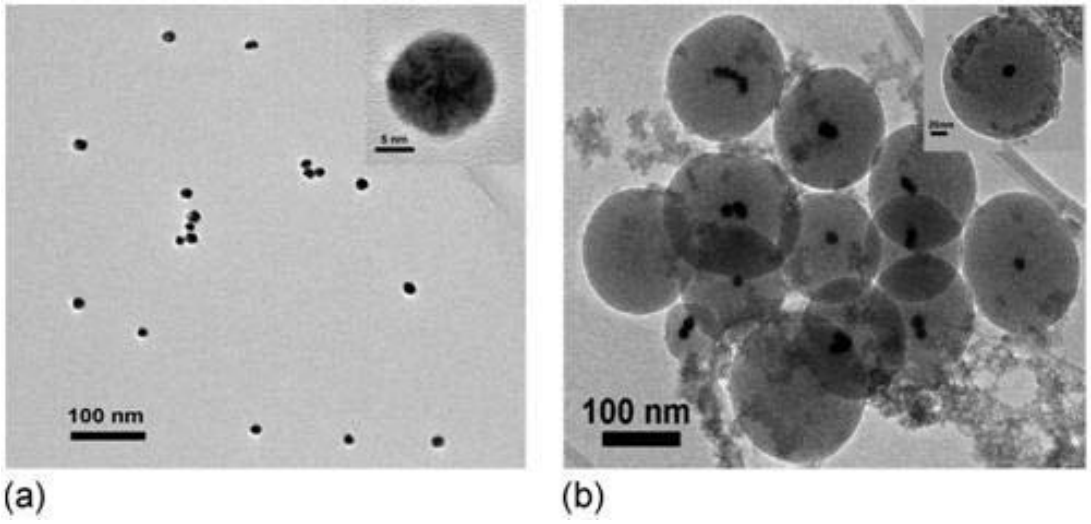

Figure 2.10 HRTEM images of Au nanoparticles (a) and Au/silica/ZnS:Mn nanostructures (b).

Figure 2.11 shows the extinction spectra of Au nanoparticles before and after silica coating. The extinction peak at 520 nm is from the surface plasmon of Au nanoparticles.[67-69] After silica coating and modification with MPTMS, the surface plasmon extinction peak is red-shifted to 535 nm. The red shift is due to the change in the surroundings on Au nanoparticles because the surface plasmon energy is sensitive to the dielectric constant of the surrounding media.[67-69]

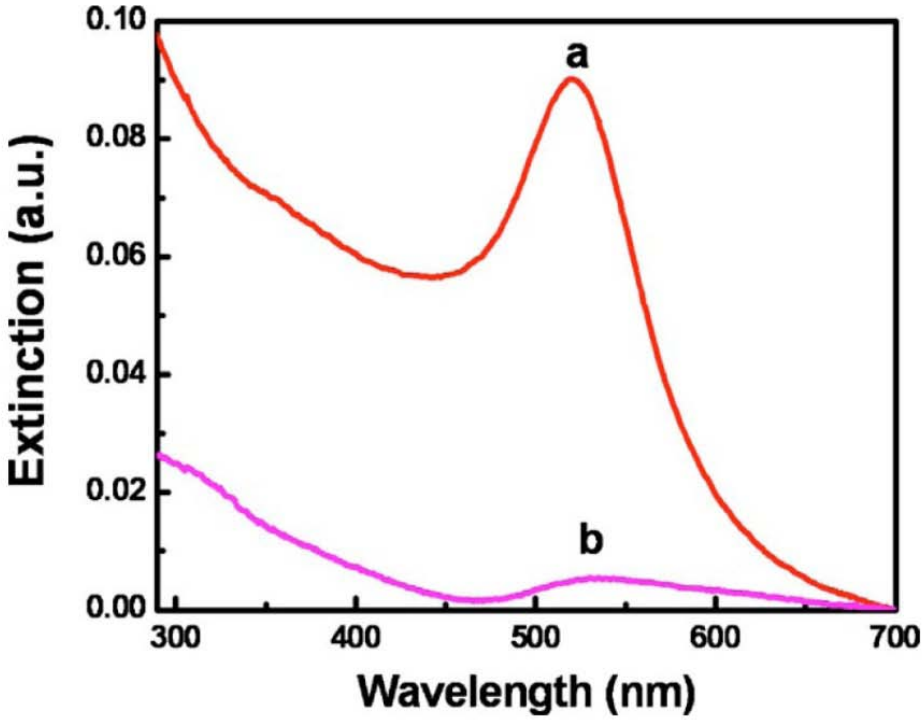

Figure 2.11 The optical extinction spectra of Au nanoparticles before (a) and after (b) silica coating with surface modification.

The emission spectra of ZnS:Mn and Au/silica-MPTMS/ZnS:Mn excited at 310, 320, 330, and 340 nm are shown in Figure 2.12. The emission at 442 nm is from donor-acceptor (D-A) pairs and the emission at 600 nm is from the $^4T_1$– $^6A_1$ transition of Mn^{2+}.[70,71] It is interesting to see that the Mn^{2+} emission at 600 nm is quenched while the blue emission at 442 nm is enhanced in the Au/silica/ZnS:Mn core-shell nanostructures. Furthermore, the enhancement in

the blue emission is increased with increasing the excitation wavelength. The enhancement is 47% at the excitation of 340 nm. However, the quenching at 600 nm is almost the same at different wavelengths of excitation. The results are summarized in Table 1.1 and displayed in Figure 2.13.

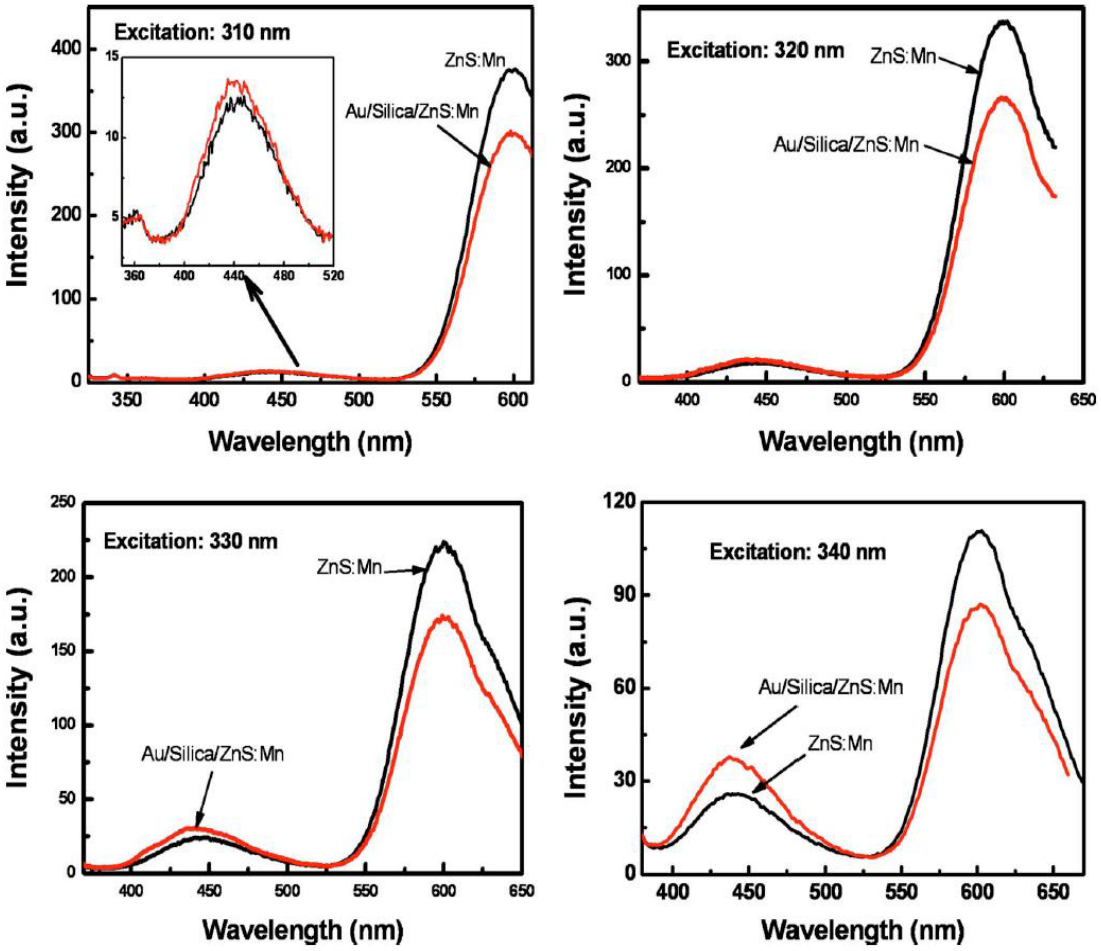

Figure 2.12 The emission spectra of ZnS:Mn and Au/silica/ZnS:Mn excited at 310 nm, 320 nm, 330 nm, and 340 nm, respectively.

Table 2.1 Luminescence Enhancement And Quenching in Au/Silica-MPTMS/ZnS:Mn Core-Shell Nanostructures

Excitation Wavelength	Enhancement at 442 nm	Quenching at 600 nm
310 nm	13 %	21 %
320 nm	16 %	22 %
330 nm	25 %	23 %
340 nm	47 %	22 %

To figure out whether the luminescence enhancement at 442 nm and the quenching at 600 nm are caused by other factors such as the surface passivation from silica, the optical extinction spectra and emission spectra of ZnS:Mn nanoparticles and silica/ZnS:Mn nanocomposites were measured and compared in Figures 2.14 and 2.15, respectively. The procedure for the synthesis of silica/ZnS:Mn nanocomposites is the same as that for Au/silica/ZnS:Mn except Au nanoparticles were not included in the processing. Thus, the relations between the silica and the ZnS:Mn nanoparticles should be similar in silica/ZnS:Mn and Au/silica/ZnS:Mn. As seen in Figure 2.14, the extinction spectrum of silica/ZnS:Mn is almost identical as that of ZnS:Mn nanoparticles. The absorption at the UV range is mainly from band-gap transition of ZnS nanoparticles. Silica is transparent in UV-visible ranges, which is likely the reason why it has no effects on the optical absorption of ZnS:Mn in the nanocomposites.

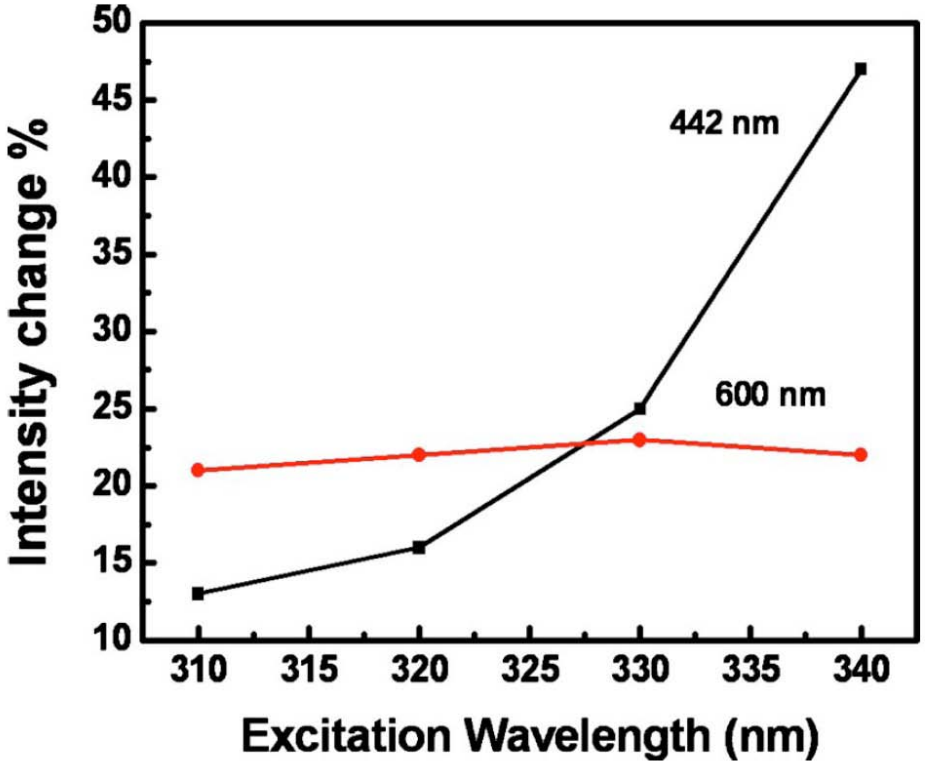

Figure 2.13 The luminescence enhancement at 442 nm and the quenching at 600 nm in Au/silica/ZnS:Mn core-shell nanostructures as a function of excitation wavelength.

In the photoluminescence as shown in Figure 2.15, the emission at 600 nm from Mn^{2+} emission is increased in intensity while the emission at 442 nm from the surface defects or D-A pairs is decreased slightly in silica/ZnS:Mn nanocomposites as compared with that of ZnS:Mn nanoparticles (see Figure 2.15 and the inset). The intensity change is the same for all the excitation wavelengths at 310, 320, 330, and 340 nm, and this change is just reverted as observed in Au/silica/ZnS:Mn nanocomposites. The decrease in the 442 nm emission and the enhancement of the 600 nm emission in silica/ZnS:Mn nanocomposites are likely due to the nanoparticle surface passivation by silica coating that reduces the surface defects and enhance the luminescence of Mn^{2+}.[70,72-74] All these observations indicate that the luminescence enhancement at 442 nm and the quenching at 600 nm in Au/silica/ZnS:Mn nanocomposites are really from the interaction with Au surface plasmon coupling.

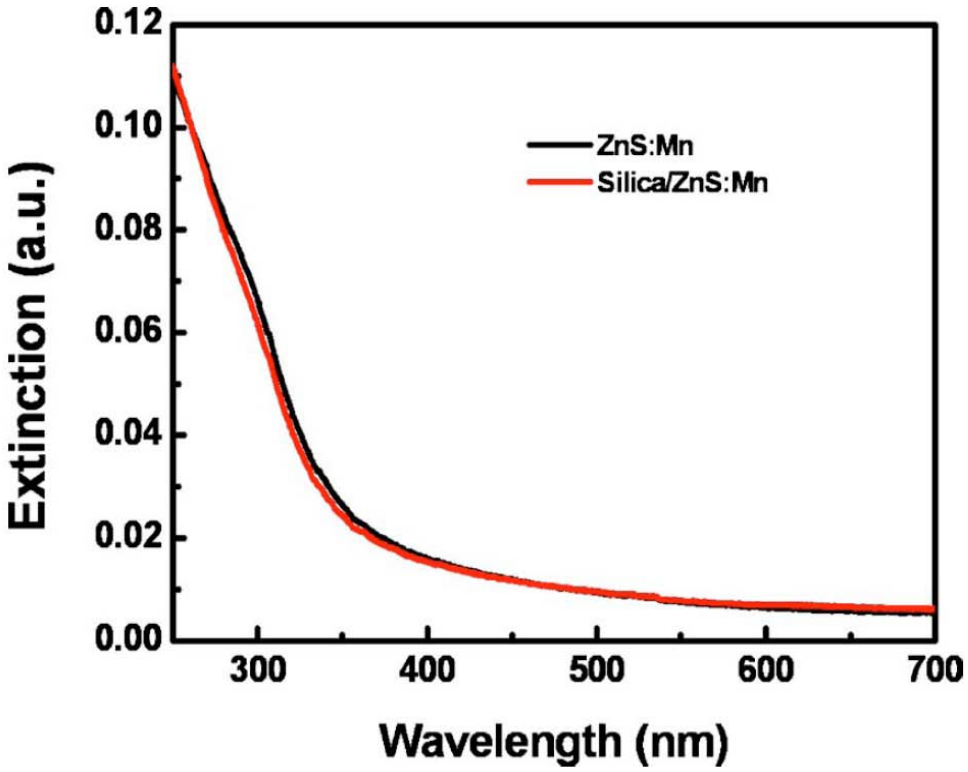

Figure 2.14 Optical extinction spectra of ZnS:Mn nanoparticles and silica/ZnS:Mn nanocomposites.

Luminescence enhancement by metallic surface plasmon coupling has been reported widely.[67-69] However, little attention has been paid to the enhancement of one peak and the quenching of another peak from the same sample. To our knowledge, such phenomenon has been only reported in the light emission of ZnO films by coupling through localized surface plasmons of Ag islands.[75] By sputtering Ag islands onto ZnO films, their band-gap emission at 380 nm was enhanced by three folds, while the defect emission at 530 nm was quenched.[75] Our observation is similar to what was reported in ZnO/Ag island thin films. The photoluminescence enhancement or quenching may be due to the coupling of the light emission with the surface plasmon resonance of Au nanoparticles. According to the radiating plasmon model,[76] when surface plasmon resonance scattering dominates over the absorption process, the surface

plasmon energy can be recovered to free space emission, leading to the enhancement of light emission. Otherwise, light emission will be quenched due to the nonradiative dissipation of surface plasmon absorption.

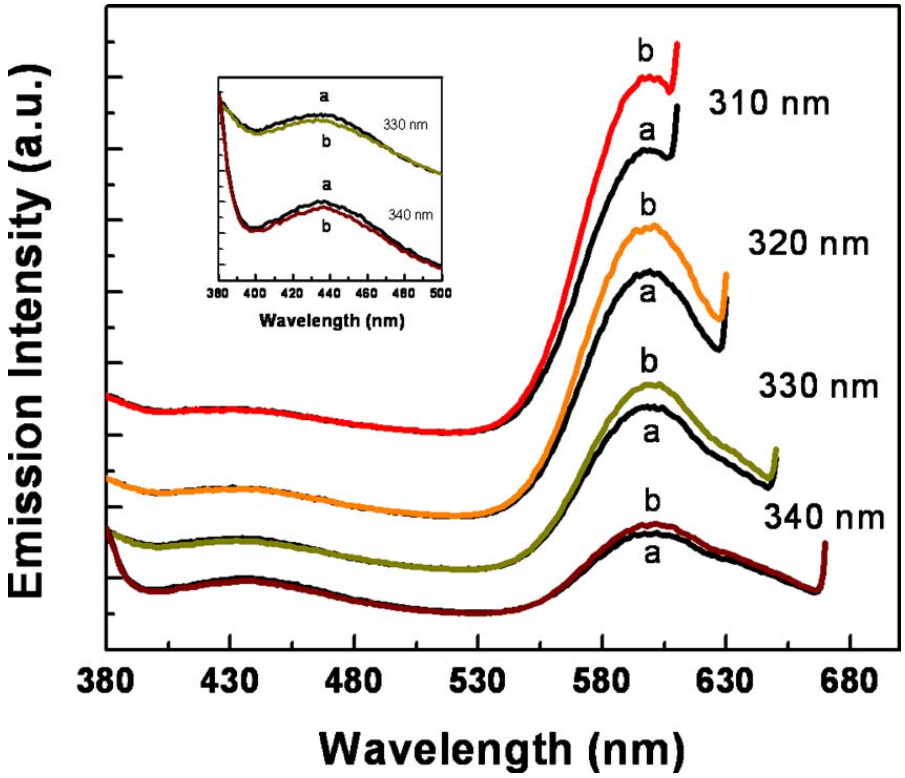

Figure 2.15 Photoluminescence emission spectra of ZnS:Mn nanoparticles (a) and silica/ZnS:Mn nanocomposites (b) excited at 310 nm,320 nm, 330 nm, and 340 nm, respectively.

To determine the origin of the surface enhancement or quenching in our experiments, the extinction spectrum of Au nanoparticles is shown in Figure 2.16 along with the emission spectrum of ZnS:Mn nanoparticles. The extinction spectrum is consistent with both the absorption and scattering of the Au nanoparticles. However, the extinction spectral measurement cannot separate the two components of absorption and scattering. Fortunately, the size dependent extinction, absorption, and scattering spectra of metallic particles have been investigated by Messinger et al.[77] Based on the results reported, the absorption and extinction spectra of a given size Au nanoparticles are very similar, while their scattering spectrum are

very different. For light scattering spectrum, the scattering intensity corresponding to extinction peak range is largely reduced, while the scattering is greatly increased at the short wavelength range.[77]

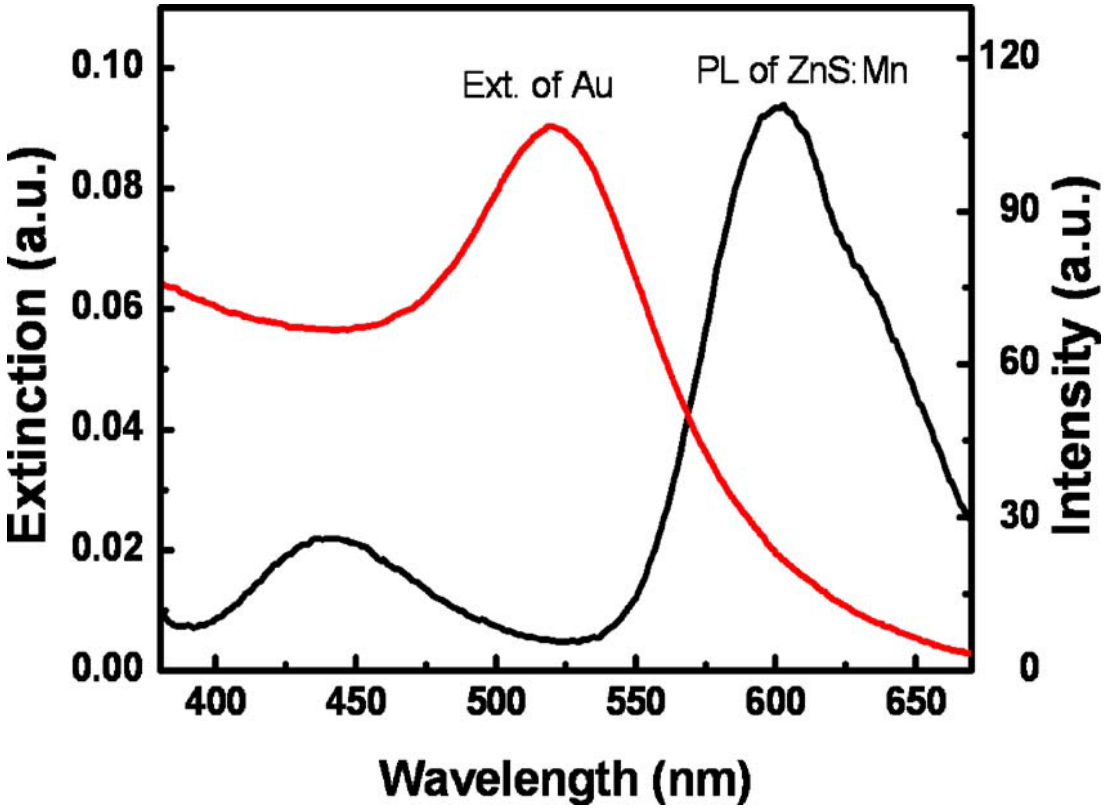

Figure 2.16 Extinction spectrum of Au nanoparticles and emission spectra of ZnS:Mn nanoparticles excited at 340 nm.

To confirm these estimated changes, the light scattering spectra of Au and Au/silica nanoparticles were measured and displayed in Figure 2.17 along with the light scattering spectra of ZnS:Mn, silica/ZnS:Mn and silica nanoparticles. As seen, the light scattering from ZnS:Mn nanoparticles is very weak. Their light scattering spectrum is almost the same as that of the solvent ethanol (not shown). The light scattering from silica nanoparticles (around 100 nm) and silica/ZnS:Mn nanoparticles is stronger than that from ZnS:Mn nanoparticles but still much weaker than that from Au and Au/silica nanoparticles. As for the Au nanoparticles reported here, relative to the extinction spectra, the scattering is very weak at wavelengths longer than 500 nm

and stronger at wavelengths shorter than 500 nm. After coating by silica, the extinction peak at 520 nm is suppressed but the signal at wavelengths shorter than 450 nm is increased (see Figure 2.11). More interestingly, silica coating reduces the light scattering in wavelengths longer than 500 nm but increases the light scattering in 200–500 nm. By comparing with the two emission peak of ZnS:Mn nanoparticles, it is clear that the Mn^{2+} emission peak at 600 nm is partially overlapped with the surface plasmon absorption but hardly overlapped with the scattering of Au nanoparticles. On the contrary, the D-A emission peak at 442 nm is hardly overlapped with the surface plasmon absorption but largely overlapped with the scattering of Au nanoparticles. This is likely the reason why the Mn^{2+} emission at 600 nm was quenched but the D-A emission at 442 nm was enhanced by Au nanoparticles.

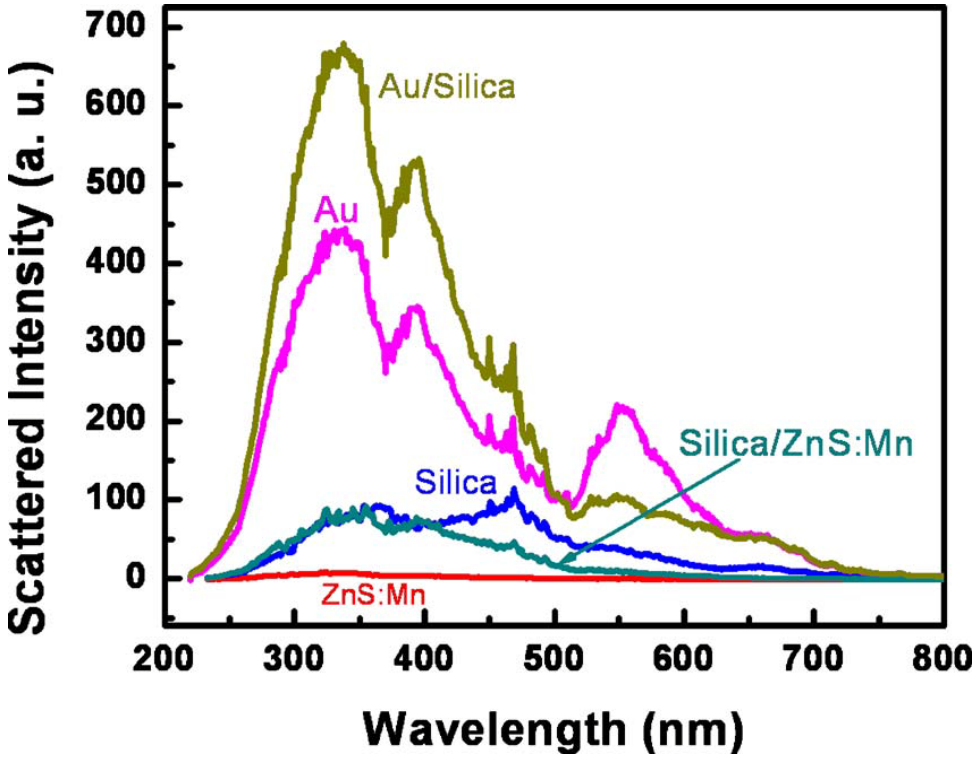

Figure 2.17 Light scattering spectra of Au, Au/silica, ZnS:Mn, silica/ZnS:Mn, and silica nanoparticles.

The suppression of surface plasmon from metallic nanoparticles on the luminescence behaviors reported here may find some practical applications. ZnS:Mn is a phosphor that has

been used for solid state lighting based on its orange emission at 600 nm from Mn^{2+}. The blue D-A emission at 442 nm from ZnS:Mn nanoparticles is an important component for white lights and color displays. However, its low efficacy limits its practical applications. Its enhancement as reported here might make its application possible.

2.7 Summary

In summary, water soluble ZnS:Mn nanoparticles have been synthesized in water by a simple wet chemistry method. The XRD and HRTEM measurement determine that they have cubic zinc blende crystal structure with average size of 4 nm. Three emissions have been observed as ZnS exciton emission (368 nm), defect emission (441 nm), and Mn^{2+} ions $^4T_1 - {}^6A_1$ transition (598 nm) emission. The application on porcine lens epithelial cells shows ZnS:Mn water soluble nanoparticles can act as an non-toxic effective fluorescent probe in cell imaging. Due to its long fluorescence lifetime, successful fingerprint image has been taken with the presence of ZnS:Mn water soluble nanoparticles. This may further open their more applications in forensic trace evidence detection. In addition, excited by X-ray, ZnS:Mn nanoparticles are able to be a new light source for photodynamic therapy. The emulsion process has been applied to encapsulate ZnS:Mn and hypericin together into PLGA spheres. The cell viability study demonstrates that the ZnS:Mn-hypericin combination is more efficient in killing cancer cells. Moreover, Au nanoparticles are found able to affect the emissions from ZnS:Mn nanoparticles due to surface plasmon resonance. The blue emission enhancement may find practical applications in white light display and other fields.

CHAPTER 3

ZnS:Cu,Co WATER SOLUBLE AFTERGLOW NANOPARTICLES – SYNTHESIS, LUMINESCENCE AND POTENTIAL APPLICATIONS

3.1 Introduction

X-ray excited fluorescent nanoparticles have been applied to study PDT for deep cancer treatment.[46,47] Although X-ray is involved, the dosage of X-ray used for nanoparticle excitation is greatly reduced comparing to traditional radiation therapy. Moreover, the X-ray excitation dosage will be further reduced when afterglow nanoparticles are applied as light source for PDT. Once the afterglow nanoparticles get excited, the X-ray can be removed. However, nanoparticles can keep emitting light for a certain time. Thus PDT continues without X-ray. What is more exciting, the afterglow nanoparticles (combined with photosensitizers) may even be excited outside the body and injected directly into cancer locations.

Afterglow phosphors have already found their applications in traffic signs, emergency signs, watches, clocks, paintings, and textile printing as well as in “glow in the dark” toys.[78,79] However, most products of traditional afterglow ZnS:Cu(ZnS:Cu,Co) and newer silicate- or aluminate-based afterglow materials from commercial markets or labs are synthesized through a solid state reaction, which needs a relatively high reaction temperature (above 1300°C) and produces large micrometer-sized particles. Although copper or other metal ions doped ZnS has been studied for many years and rare earth metal ions doped aluminate and silicate afterglow phosphors developed rapidly, little attention has been paid to the potential biological applications of afterglow nanoparticles. Recently, afterglow nanoparticles have been proposed as a light source to activate photodynamic therapy (PDT) for deep cancer treatment.[31,80,81] Moreover, afterglow imaging may be very attractive as it has no background fluorescence or autofluorescence as no excitation source is required. In order to have much smaller sized

particles for biological applications, one method is to ground larger particles into sizes suitable for cell uptake.[82] Besides the particle sizes, the water solubility of nanoparticles is one of the other most important requirements. However, there are challenges to synthesize highly efficient nano-sized water-soluble afterglow particles. First, many nonradiative decay or quenching processes that exist in the water environment can greatly reduce afterglow. Second, the current method to synthesize high-quality afterglow materials usually produce micrometer sized particles. More challengingly, although the electron trap model has been well accepted to explain afterglow,[1,2,7] many details about the traps and mechanism are not clear. From previous reports, wet chemistry method has been applied to synthesize ZnS:Cu and ZnS:Cu,Co nanoparticles.[2,11,13,83-88] However, water soluble afterglow nanoparticles have not been reported before this work. In this chapter, the synthesis, structure and optical properties of water soluble ZnS:Cu,Co afterglow nanoparticles is reported and the potential biological applications will be discussed.

3.2 Experimental Details and Characterization

3.2.1. Material Synthesis

Zinc acetate [$Zn(CH_3COO)_2$, 99.990%)], copper(II) acetylacetonate [$Cu(C_5H_7O_2)_2$, 99.990%], cobalt acetate [$Co(CH_3COO)_2$, 99.995%] and poly(ethylene glycol) bis(carboxymethyl) ether (PEG-COOH) were purchased from Sigma-Aldrich in the USA. Sodium sulfide (Na_2S) is also a product of Sigma but from Canada. All the chemicals were used as obtained. Deionized (DI) water was used as reaction solvent.

Copper and cobalt co-doped zinc sulfide afterglow nanoparticles were synthesized by a simple wet chemistry method. Briefly, 1.836 g $Zn(CH_3COO)_2$ was dissolved in 100 ml DI water and loaded into a 250 ml flask under vigorous stirring. Then, 0.9 ml PEG-COOH and calculated amounts of 1.15 mM $Cu(C_5H_8O_2)_2$ and 0.40 mM $Co(CH_3COO)_2$ aqueous solution were added to the solution and heated to boiling. Next, 6 ml of 1.3 M Na_2S solution was quickly dropped into the solution under vigorous stirring. The reaction was allowed to last for 24 h and finally was

cooled by air to room temperature to form water soluble afterglow nanoparticles. The nanoparticle powder samples can be precipitated from the solutions by centrifuging, and the solid samples can be easily suspended into water by sonication.

3.2.2. Characterization

The identity, crystalline structure, size and shape of the nanoparticles were observed by X-ray diffraction (XRD) and high-resolution transmission electron microscopy (HRTEM). The Energy dispersive X-ray spectroscopy (EDS) was used to carry out the elemental analysis. The X-ray powder diffraction was recorded in a Rigaku Ultima IV X-ray diffractometer with a radiation beam of λ = 1.5406 Å. The ZnS:Cu,Co nanoparticles in aqueous solution were placed onto holey carbon covered copper grids for HRTEM observations. The HRTEM images and EDS spectrum of the particles were obtained with a Hitachi 9500 electron microscope with accelerating voltage of 300 kV. X-ray photoelectron spectroscopy (XPS) analysis was carried out using a Kratos AXIS Ultra DLD high performance spectrometer. The photoluminescence and afterglow spectra were measured using a Shimadzu RF-5301PC fluorescence spectrophotometer.

3.3 Results and Discussion

3.3.1 Structure

Depending on the synthesis conditions such as reaction temperature and precursor concentration, ZnS may have a cubic (β-ZnS) or hexagonal (α-ZnS) structure.[88-90] The XRD pattern of our ZnS:Cu,Co nanoparticles presented in Figure 3.1 reveals a cubic zinc blende structure of ZnS (JCPDS, #05-0566). The main diffraction lines are indexed with the planes of (111), (220), (311), (400), (331) and (422). When ZnS was doped with Cu^{2+} and Co^{2+}, no impurities were observed from the XRD pattern because of the low doping level. As a result of size effect, the XRD peaks were broadened. Based on Debye-Scherer's formula, the average crystal size was estimated at about 3.5 nm. The lattice parameter of obtained ZnS:Cu,Co nanoparticles was also estimated from the XRD pattern, which gives a = 0.5393 nm. This value

is slightly smaller than the standard literature value (JCPDS, #05-0566, a = 0.5406 nm). However, for pure nano-scaled ZnS particles, both larger and smaller lattice parameters than ours have been reported (a = 0.5414 nm[25] and a = 0.5391 nm[91]). Meanwhile, the doping of Cu^{2+} may cause a slight decrease of lattice parameter if Cu^{2+} substitutes Zn^{2+}, as Cu^{2+} has a smaller ionic diameter (0.072 nm) than that of Zn^{2+} (0.074 nm). It would be hard to tell the existence of sulfur or zinc defects by using the change of lattice parameter itself.

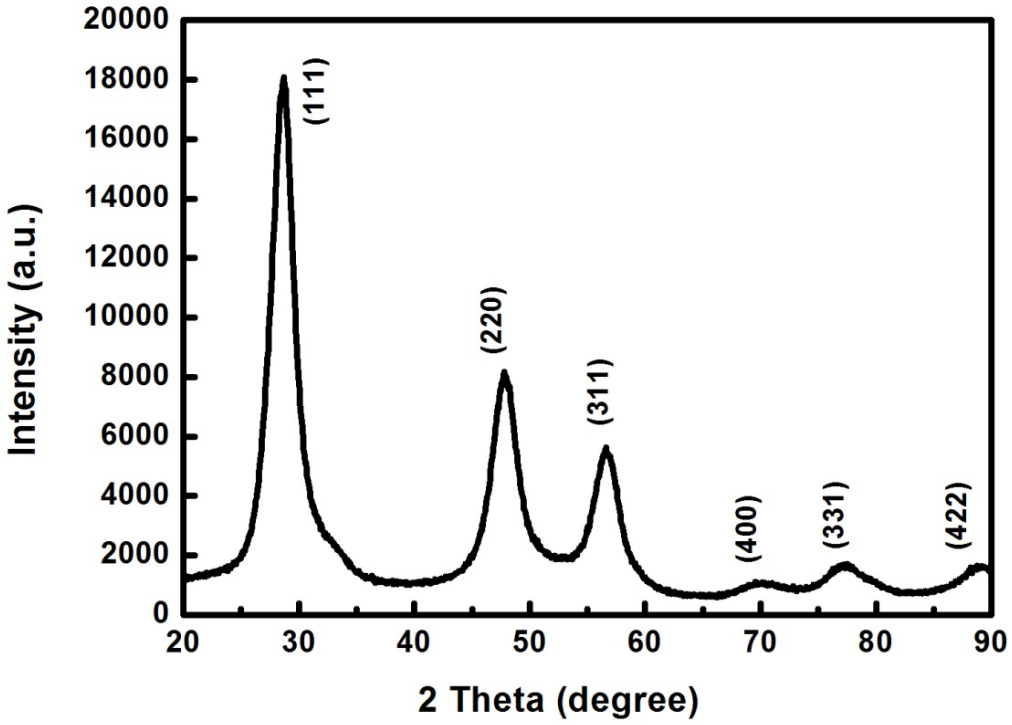

Figure 3.1 The XRD pattern of ZnS:Cu,Conanoparticles (0.07 mol% Cu^{2+}, 0.001 mol% Co^{2+}).

In order to figure out the atomic ratio of Zn and S in ZnS:Cu,Co nanoparticles, the energy dispersive x-ray spectroscopy (EDS) measurements have been done by using a Hitachi H-9500 transmission electron microscope with an accelerating voltage of 300 kV (Figure 3.2). The results show that the atomic percentages of Zn and S are 53% and 47%, respectively, which gives Zn:S = 1:0.88. The results support that the nanoparticles have sulfur vacancy defects

which may increase the surface states (defects) in nanoparticles.

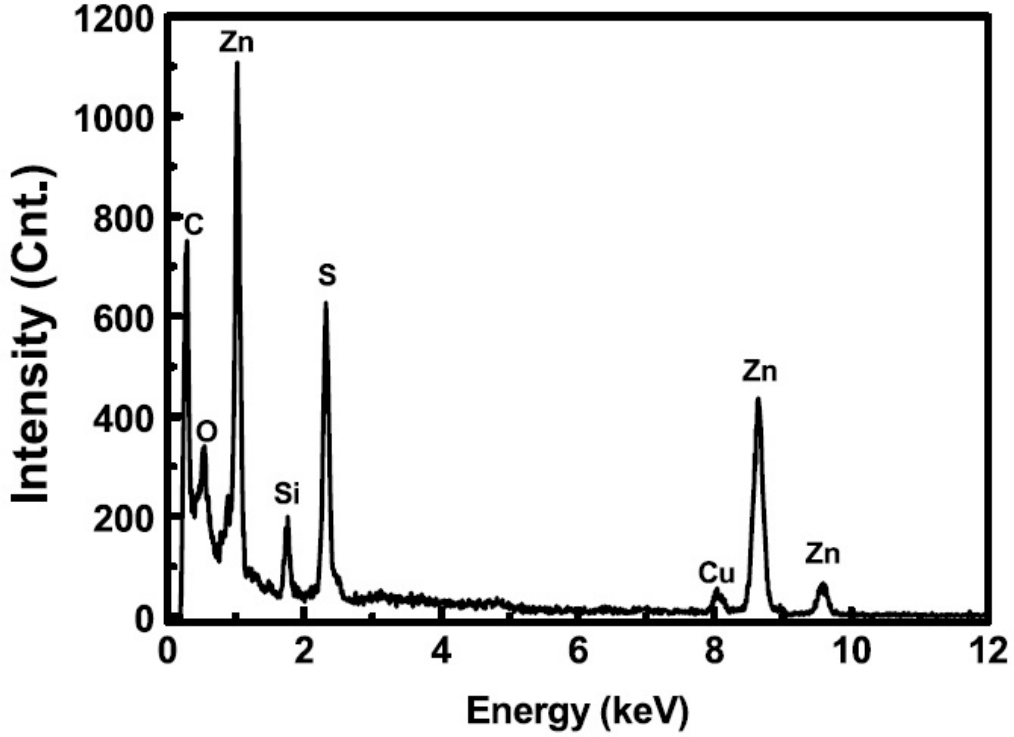

Figure 3.2 EDS spectrum shows the atomic percentage of Zn and S (other elements are not labeled). The atomic ratio of Zn:S = 1:0.88.

Figure 3.3 shows the HRTEM image of our ZnS:Cu,Co solution sample (Cu 0.07 mol%, Co 0.001 mol%). The average size of these nanoparticles is about 4 nm. The obvious lattice fringe display indicates that the nanoparticles are good crystals (inset image). The (111) lattice planes of some particles can mainly be observed, and this lattice spacing is estimated to be about 0.31 nm from the HRTEM image, which is consistent with the cubic ZnS (111) spacing value (0.312 nm) from standard JCPDS database.

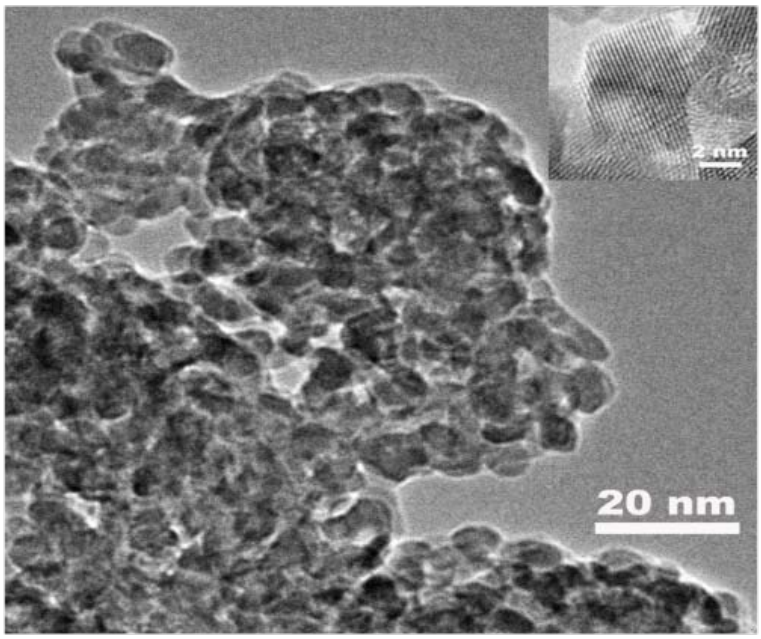

Figure 3.3 The HRTEM image of ZnS:Cu,Co nanoparticles. The Inset is an enlargement of the nanoparticles to show the lattice fringes.

A representative X-ray photoelectron spectroscopy (XPS) image of the ZnS:Cu,Co nanoparticles (Cu 0.07 mol%, Co 0.001 mol%) is shown in Figure 3.4. The analysis identifies significant signals of Zn and S due to a large amount of these elements existed in the crystalline structure. Less amount of O is observed due to the oxidation during sample synthetic and drying procedure. Obviously, the appearance of C is from the stabilizer PEG-COOH. A weak signal from Cu indicates the presence of a small amount in the sample, but Co has no signal because very little amount is present (0.001 mol%).

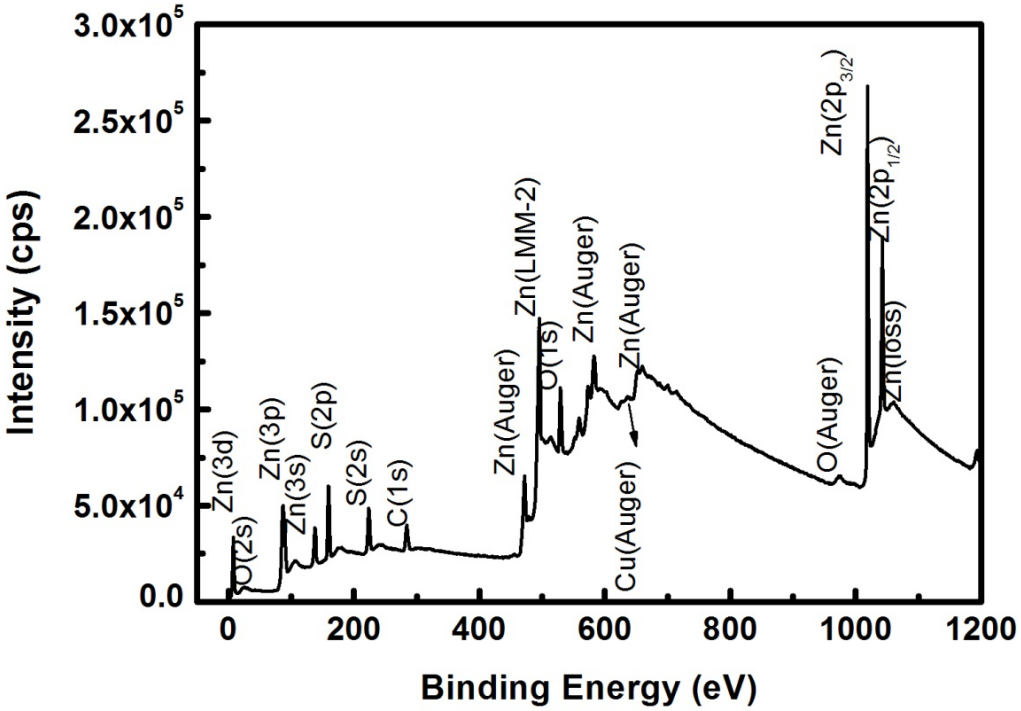

Figure 3.4 The XPS profile of ZnS:Cu,Conanoparticals (0.07 mol% Cu^{2+}, 0.001 mol% Co^{2+}).

3.3.2. Fluorescence and Afterglow Properties

The fluorescence and afterglow of ZnS:Cu,Co nanoparticle aqueous solutions are displayed in Figure 3.5. The fluorescence photos were taken on the samples excited by a UV lamp (360 nm), while the afterglow pictures were taken after the UV excitation was off for 5 s. Both the fluorescence and afterglow increase in intensity with the increase of the reaction time from 4 to 24 h. Their intensities reach the maximum at the reaction time of 24 h. For reactions longer than 24 h, the intensities of the samples are almost the same. This result suggests that a 24 h reaction can form stable and high quality afterglow nanoparticles.

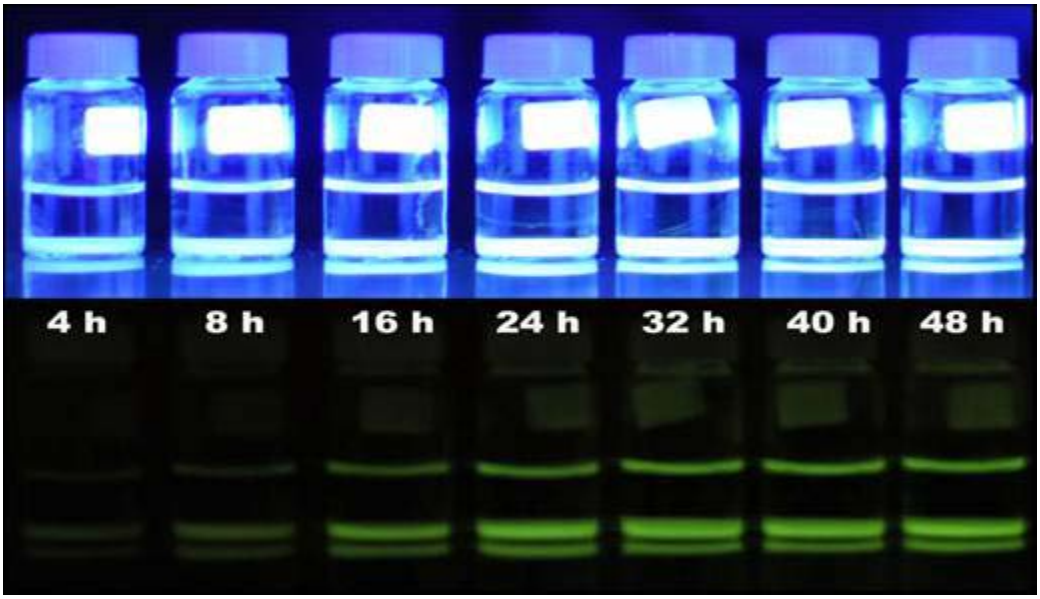

Figure 3.5 The first row represents the luminescence of ZnS:Cu,Co nanoparticles synthesized for different reaction times as indicated under a UV lamp excitation at 360 nm. The second row is the green afterglow emission after UV irradiation at 360 nm was off for 5 s.

The nanoparticles coated with poly(ethylene glycol) bis(carboxymethyl) ether (PEG–COOH) are water-soluble and can be dispersed easily in aqueous solvents. In samples for TEM characterization, the nanoparticle concentration is high (0.5 M), so some nanoparticles are aggregated and precipitated from the solution as seen in Figure 3.6. However, at a reasonably low concentration, the nanoparticle solubility is fairly good. The nanoparticle aqueous solutions are clear, transparent and stable. One example is shown in Figure 3.6 for the photos of nanoparticles in water (0.01 M) and their fluorescence when excited by a UV lamp.

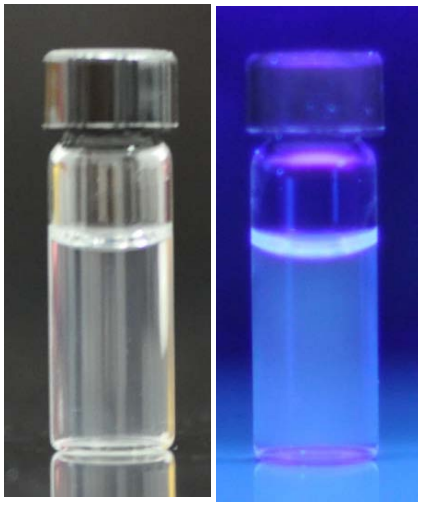

Figure 3.6 The photo of (left) ZnS:Cu,Co nanoparticles in water (0.01 M) and (right) its photoluminescence under UV lamp (360 nm).

Figure 3.7 shows the excitation and emission spectra of ZnS:Cu^{2+},Co^{2+} (0.07 mol%, Co^{2+} 0.001 mol%) nanoparticles in aqueous solutions. Two emission bands peaking at 470 and 510 nm are observed from samples. Under excitation at 310 and 320 nm, the peak at 510 nm is stronger, but the peak at 470 nm is dominant when excited at 348 and 360 nm. The excitation spectra have a sharp peak at 348 nm and a shoulder from 250 to 330 nm. The excitation spectra are found to be almost identical in shape and position by monitoring the emission peaks at 470 and 510 nm.

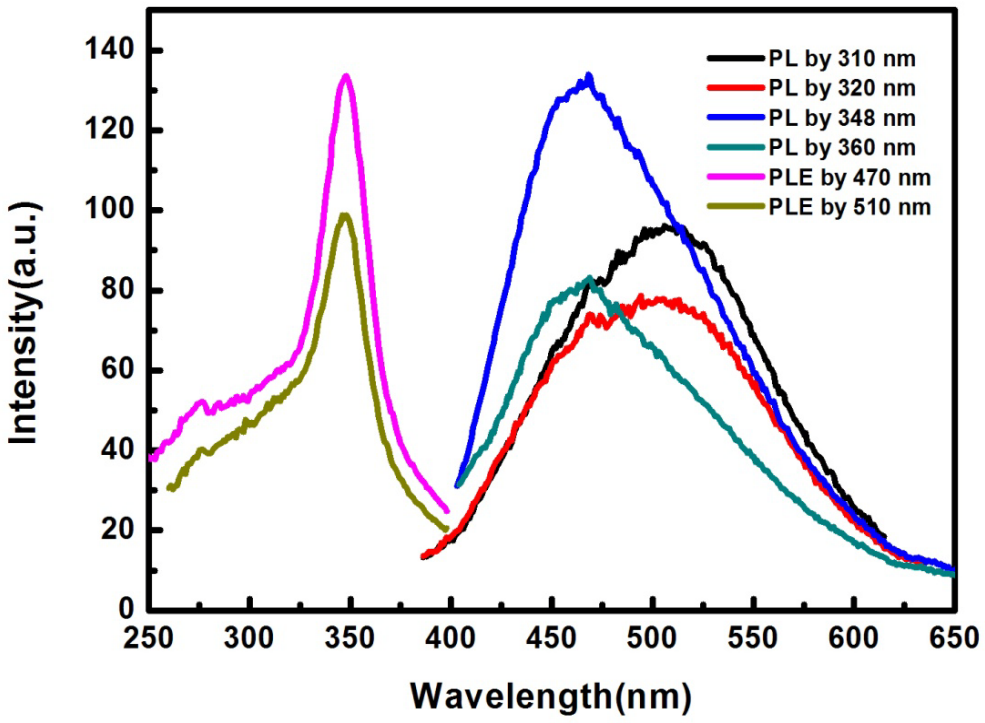

Figure 3.7 The excitation (PLE, left) and emission (PL, right) spectra of ZnS:Cu,Co nanoparticles (0.07 mol% Cu^{2+} and 0.001 mol% Co^{2+}).

The afterglow emission spectra of ZnS:Cu,Co nanoparticle aqueous solution after excitation at 360 for 1 and 5 min are shown in Figure 3.8. Unlike the fluorescence, the afterglow has only one emission peak at 525 nm,suggesting that the luminescence centers for the blue fluorescence at 470 nm have no contribution to the afterglow. The afterglow is from the luminescence centers that are related to the green fluorescence. It was reported that the co-doping of Co^{2+} in ZnS:Cu,Co only reduces or enhances the luminescence intensity of ZnS:Cu, but it does not cause any new emission peaks.[2] It was also reported that in ZnS nanoparticles, Co^{2+} may also just function as a sensitizing agent, which only changes the intensity but not the emission wavelength of the defect emission in ZnS.[92] This means the luminescence centers at ZnS:Cu are also responsible for the luminescence in ZnS:Cu, Co. The co-doping of Co^{2+} may

change the concentrations of these centers but cannot add any new centers or remove any existing centers.

There are still some debates about the origin of the emissions in ZnS:Cu^{2+} phosphors. Zinc vacancies have been suggested to cause an emission of 480 nm in ZnS:Cu^{2+} nanoparticles.[85] The same vacancies were also used to explain a blue emission at 450 nm.[11] Xu et al.[83] explained an emission at 460 nm in ZnS:Cu for the electron transition from the ZnS conduction band to the t_2 state level of Cu^{2+}. One emission at 470 nm from ZnS:Cu^{2+} was explained by electron recombination from a shallow donor level at the doped Cu^{2+} ions.[84] Moreover, the host ZnS nanoparticles can also display a range of blue emission bands peaking from 420 nm to 470 nm due to sulfur or zinc defects.[11,13-20] In the nanoparticles presented here, it is noticed that the blue emission is largely reduced by silica coating, and it is well known that silica coating can largely reduce surface defects. This indicates that the blue emission at 470 nm is from surface states or defects. It has been widely agreed that the green emission is from the electron transition between the sulfur defect level just below the conduction band and the Cu^{2+} center.[11,17,83-86] Therefore, we may conclude that the transition from the sulfur defect state to the Cu^{2+} center is responsible for the green afterglow emission in ZnS:Cu,Co water soluble nanoparticles.

To support the above conclusion, pure ZnS and ZnS:Cu^{2+} nanoparticles were prepared and their luminescence properties were measured and compared. The emission spectra of pure ZnS (blue) and ZnS:Cu^{2+} (green) nanoparticles excited at 320 nm (dotted) and 340 nm (solid) are shown in Figure 3.8. Pure ZnS nanoparticles have a strong blue emission peaking at 454 nm which is assigned to the surface defects or surface states.[84,93,94] The spectra are similar to emission spectra of ZnS:Cu^{2+} nanoparticles[11,84,95] and support that the green emission is from Cu^{2+}. In bulk ZnS: Cu^{2+} phosphors[96,97] the green emission of Cu^{2+} is dominant, while in ZnS: Cu^{2+} nanoparticles, the blue emission is dominant because the surface states in nanoscale materials are much higher than in the bulk. However, it is interesting to see that only the Cu^{2+}

related green emission contributes to the afterglow, while the surface state blue emission has no contribution to the afterglow emission.

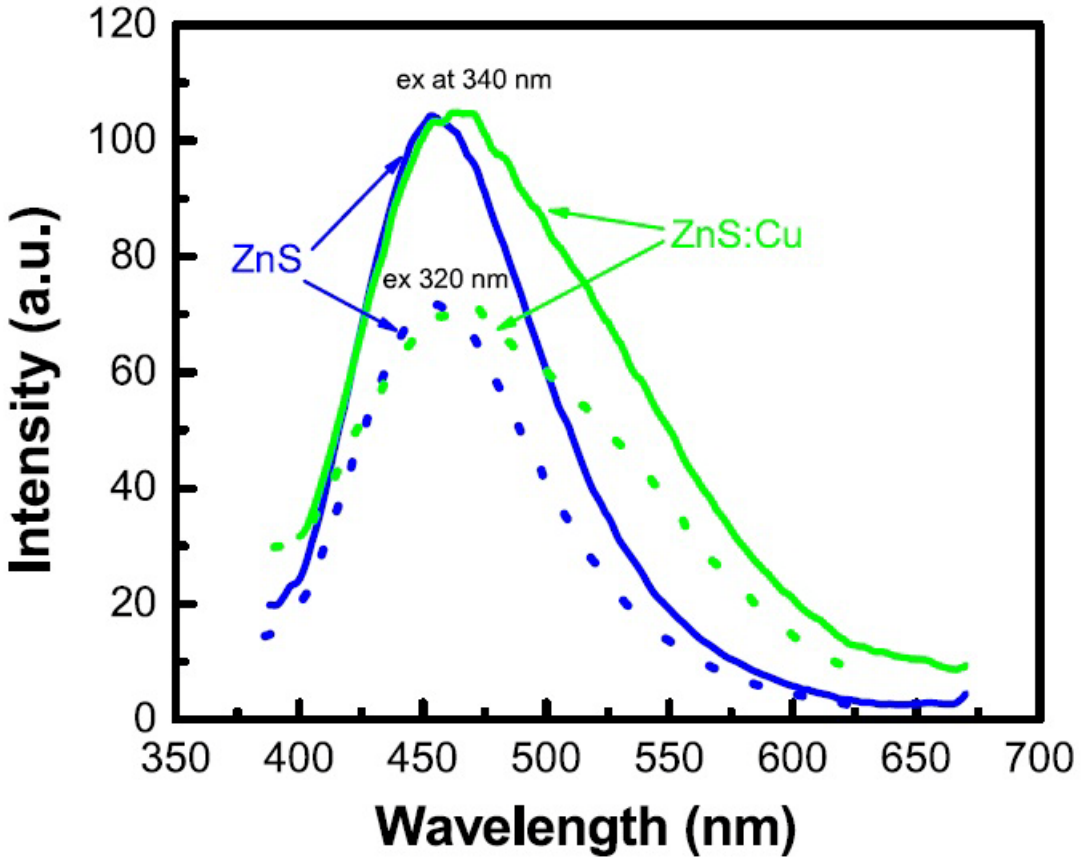

Figure 3.8 Photoluminescence emission spectra of pure ZnS (blue) and ZnS:Cu^{2+} (green, 0.07 mol% Cu^{2+}) nanoparticles excited at 320 nm (dotted) and 340 nm (solid).

Figure 3.9 shows the variation of the afterglow spectra of ZnS:Cu, Co nanoparticles at the Cu^{2+} concentrations of 0.02, 0.07 and 0.14%, while the concentration of Co^{2+} (0.001%) is the same for all three samples. The afterglow intensity increases from 0.02 mol% to 0.07 mol%, but decreases at the concentration of 0.14 mol%. This is a typical dependence of a luminescence on the dopant concentrations. At low concentration, the intensity increases with the dopant concentration because the luminescence centers increase and then reach critical concentration for the maximum peak. At concentrations higher than the critical value, the luminescence

quenching begins due to energy migration among the luminescence centers. Therefore, the emission intensity begins to decrease.[98-100]

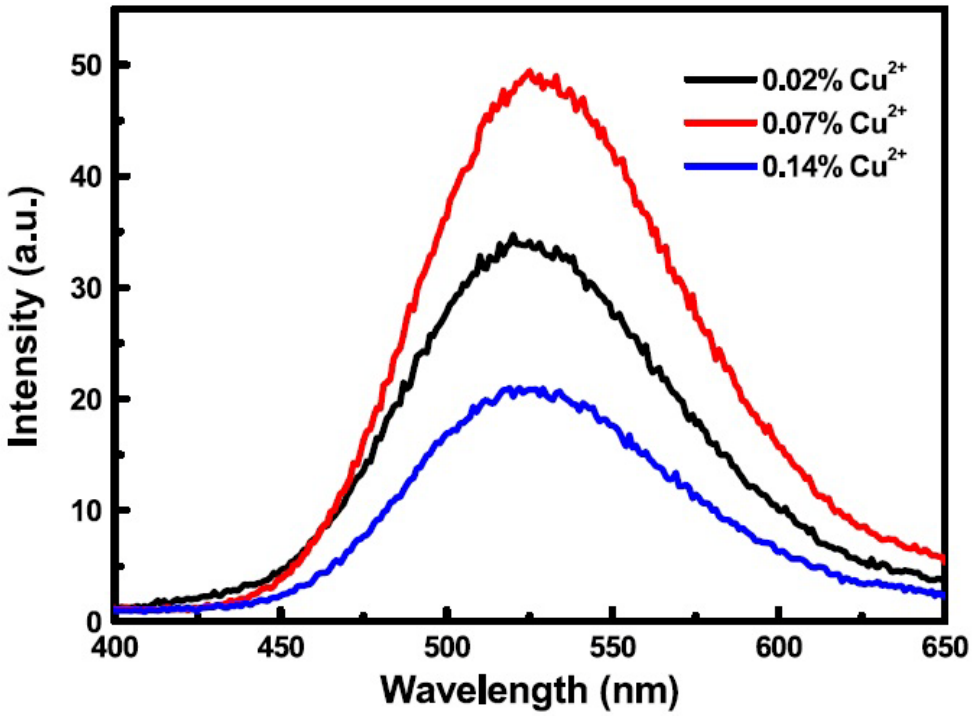

Figure 3.9 The afterglow spectra of ZnS:Cu,Co nanoparticles at different Cu^{2+} levels as indicated. The concentration of Co^{2+} is the same in all the samples (0.001 mol%). The afterglow spectra were taken after UV irradiation at 360 nm for 60 s.

The introduction of cobalt at a certain level has been shown to quench the luminescence of ZnS:Cu,Co solid state phosphors but enhance their afterglow intensity.[1,2] In our experiments, we found that ZnS:Cu nanoparticles themselves without co-doping with cobalt display no afterglow at all. The intensity change of the afterglow from ZnS:Cu,Co nanoparticles with the concentration of Co^{2+} is shown in Figure 3.10 while the concentration of Cu^{2+} (0.07 mol%) is the same for all the five samples. The dependence of the afterglow intensity on Co^{2+} concentration is similar to the concentration dependence of most doped phosphors, which can be explained by "concentration quenching".[98-100] However, it is well known that Co^{2+} is not a luminescence center in ZnS:Cu^{2+}, Co^{2+}. It is only a sensitizer that activates the Cu^{2+} related

luminescence and may change the concentration of some defects.[2,92] Thus, its effect on the afterglow intensity is complicated. At a certain low concentration range, Co^{2+} may function as a sensitizer to enhance the afterglow emission. At high concentrations, it might function as a quencher to suppress the afterglow luminescence. Much work is required in order to reveal its contribution and mechanism to the afterglow of ZnS:Cu^{2+},Co^{2+} nanoparticles.

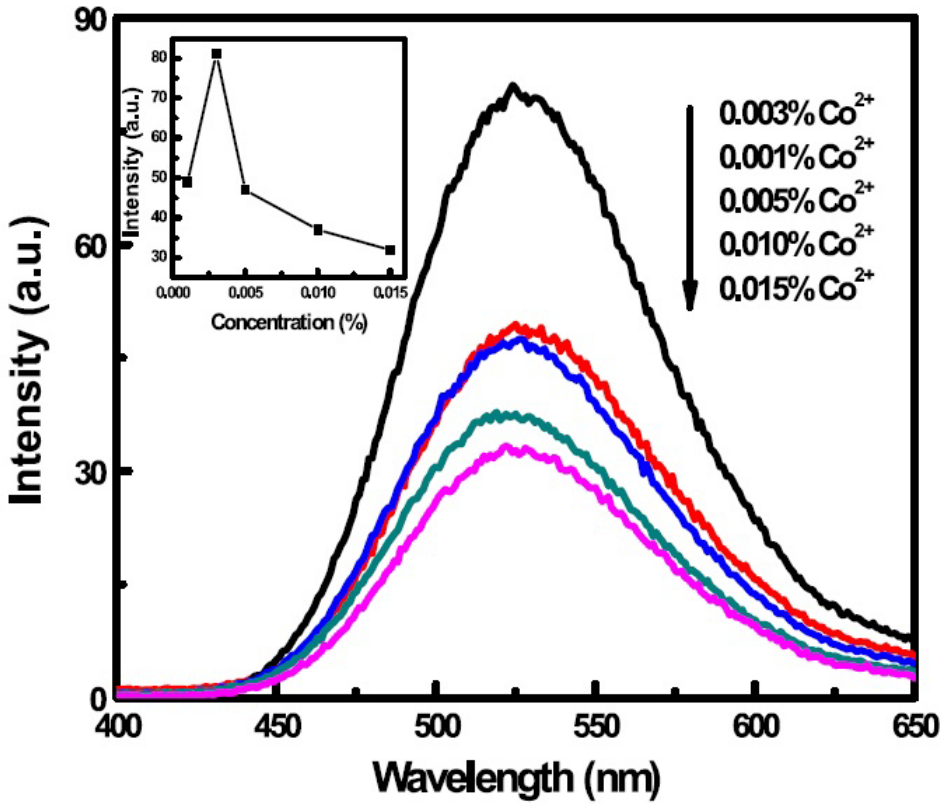

Figure 3.10 The afterglow spectra of ZnS:Cu,Co nanoparticles at different Co^{2+} levels as indicated. The concentration of Cu^{2+} is the same in all samples (0.07 mol%). The afterglow spectra were taken after UV irradiation at 360 nm for 60 s.

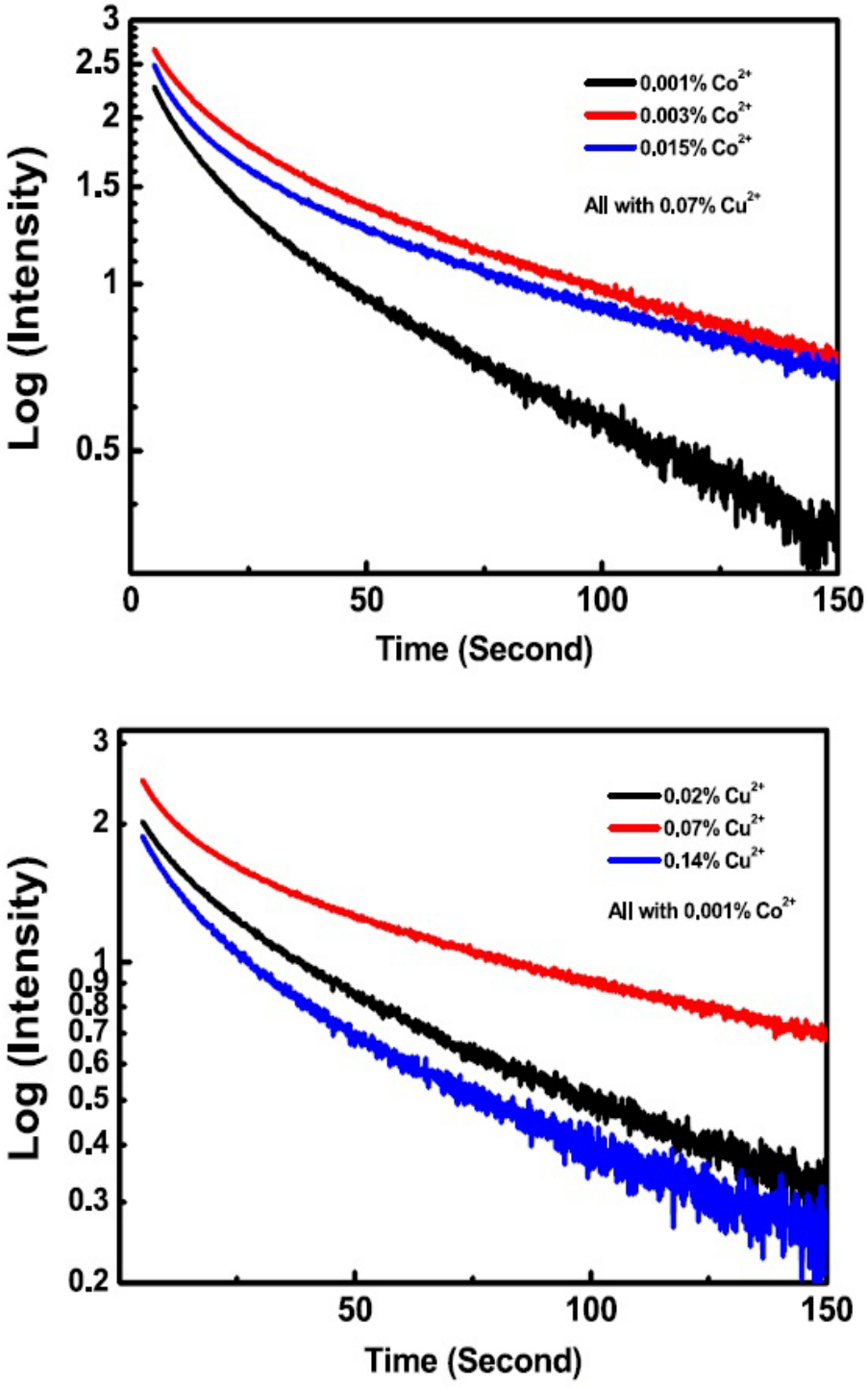

Figure 3.11 The afterglow decay curves of ZnS:Cu,Co nanoparticles after UV irradiation at 360 nm for 60 s.

The afterglow decay curves of ZnS:Cu^{2+},Co^{2+} nanoparticles are shown in Figure 3.11. In the measurements, a sample was first activated by a UV lamp (360 nm) for 60 s, and then, the sample was loaded into the sample chamber of a fluorometer for the decay measurement. The loading of the sample took 5 s. Here, we define the decay lifetime as the time when the afterglow reaches its half intensity and the longevity as the time when the afterglow is totally gone. Based on the decay curves and the sample loading time, the afterglow decay lifetimes of our samples are estimated to be within a time scale of several seconds. Their longevities are also estimated and shown in Table 3.1. It should be noted that the decay lifetime and longevity is longer if the UV activation time is longer.

Table 3.1 The Longevities of ZnS:Cu^{2+},Co^{2+} Nanoparticles After UV Excitation for 60 s.

Sample	Concentration	Longevity
ZnS:Cu^{2+} (0.07%),Co^{2+}	0.001% Co^{2+}	140 s
	0.003% Co^{2+}	150 s
	0.015% Co^{2+}	75 s
ZnS:Cu^{2+}, Co^{2+} (0.001%)	0.02% Cu^{2+}	65 s
	0.07% Cu^{2+}	140 s
	0.14% Cu^{2+}	50 s

3.4 Application of ZnS:Cu,Co in PDT

For medicinal applications of luminescent nanoparticles, one example is for photodynamic therapy in which a photosensitizer is activated by light to produce singlet oxygen for cancer cell destruction.[101,102] PDT has been widely used for skin cancer treatment but rarely for deep cancer treatment because light cannot penetrate deeply into tissue. Recently, a new concept of PDT called nanoparticle self-lighting photodynamic therapy was proposed by Chen.[80,81] In this now modality, afterglow nanoparticles are used as a light source for PDT activation, which will make PDT useful for deep cancer treatment.[80,81] Here, the ZnS:Cu,Co afterglow nanoparticles

are conjugated with photosensitizer tetrabromorhodamine-123 (TBrRh123) and applied to cancer cell viability study by using PDT method.

3.4.1 Photosensitizer Selection and Sample Preparation

As it is described previously, the absorption of selected photosensitizer needs to match the emission form nanoparticles to reach efficient energy transfer. In this case, the afterglow emission from ZnS:Cu,Co is chosen and the photosensitizer TBrRh123 has been selected because its maximum absorption overlaps the afterglow emission spectrum. Figure 3.12 shows the afterglow and fluorescence of ZnS;Cu,Co and TBrRh123 absorption spectra together.

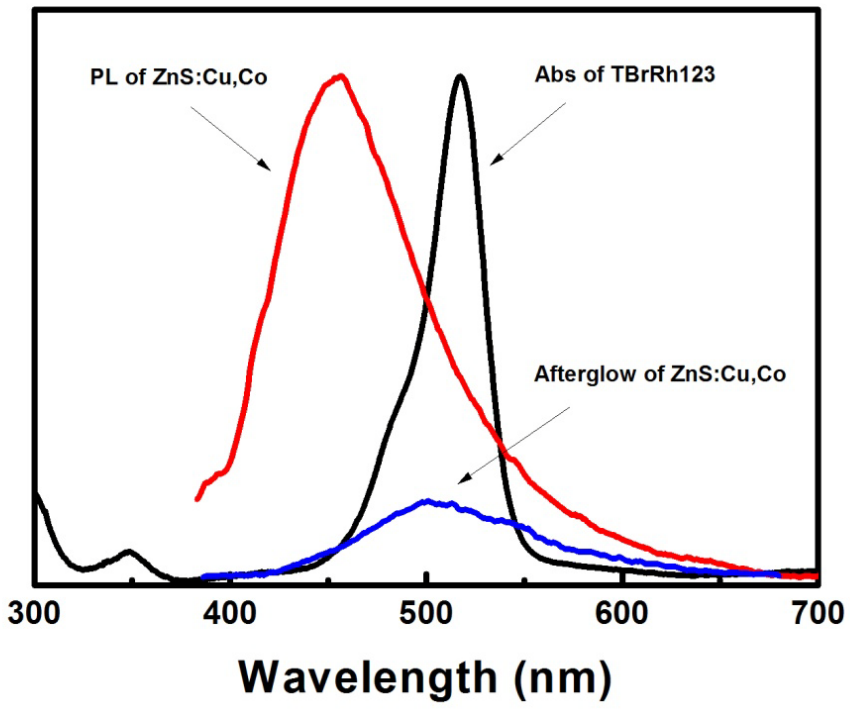

Figure 3.12 The afterglow and fluorescence of ZnS;Cu,Co (excited by 360nm) and TBrRh123 absorption spectra together.

The conjugation of ZnS:Cu,Co nanoparticles and TBrRh123 is synthesized by a standard amidation method. For comparison, the sample of ZnS:Cu,Co solution and the sample of TBR123 solution are also prepared by using the same procedure.

3.4.2 Results and Discussion

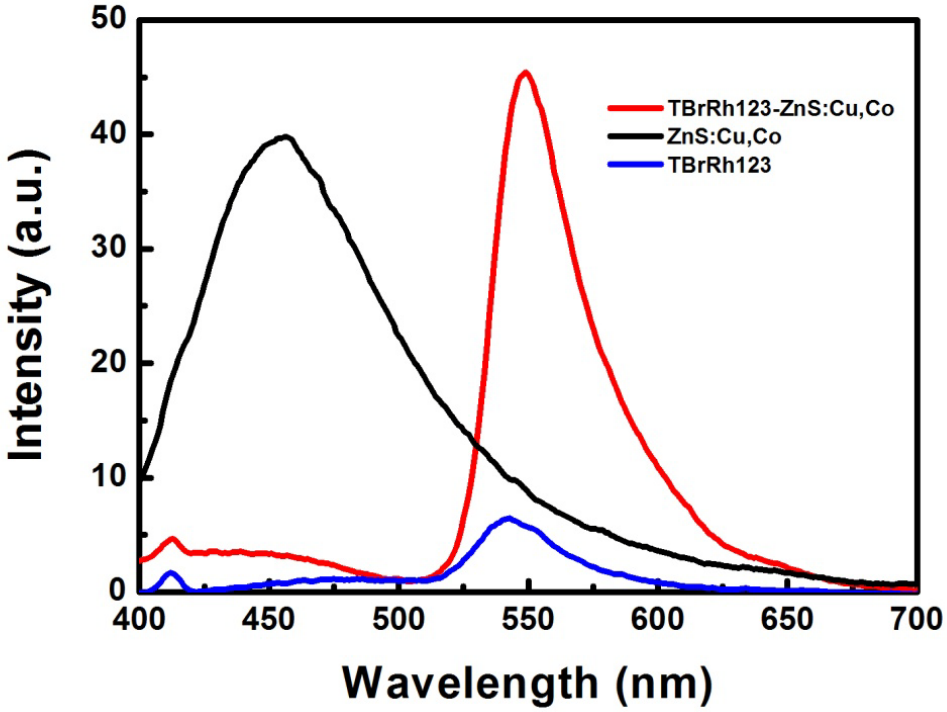

Figure 3.13 The emission spectra of ZnS:Cu,Co (black), TBrRh123 (blue) and ZnS:Cu,Co-TBrRh123 conjugation.

In Figure 3.13, excited by 360 nm, the emission spectra of ZnS:Cu,Co (black) and TBrRh123 (blue) are peaked at 456 nm and 544 nm respectively. After their conjugation, the ZnS:Cu,Co emission almost disappears and the intensity of TBrRh123 emission increases to almost 7 times higher , associated with a little red shift. The possible reason could be that, TBrRh123 absorbs the afterglow and fluorescence energy from ZnS:Cu,Co nanoparticles because of the absorption-emission overlap and thus emits much stronger light. At this point, the enhancement of ZnS:Cu,Co and TBrRh123 conjugation emission indicates a successful energy transfer from the nanoparticles to photosensitizer.

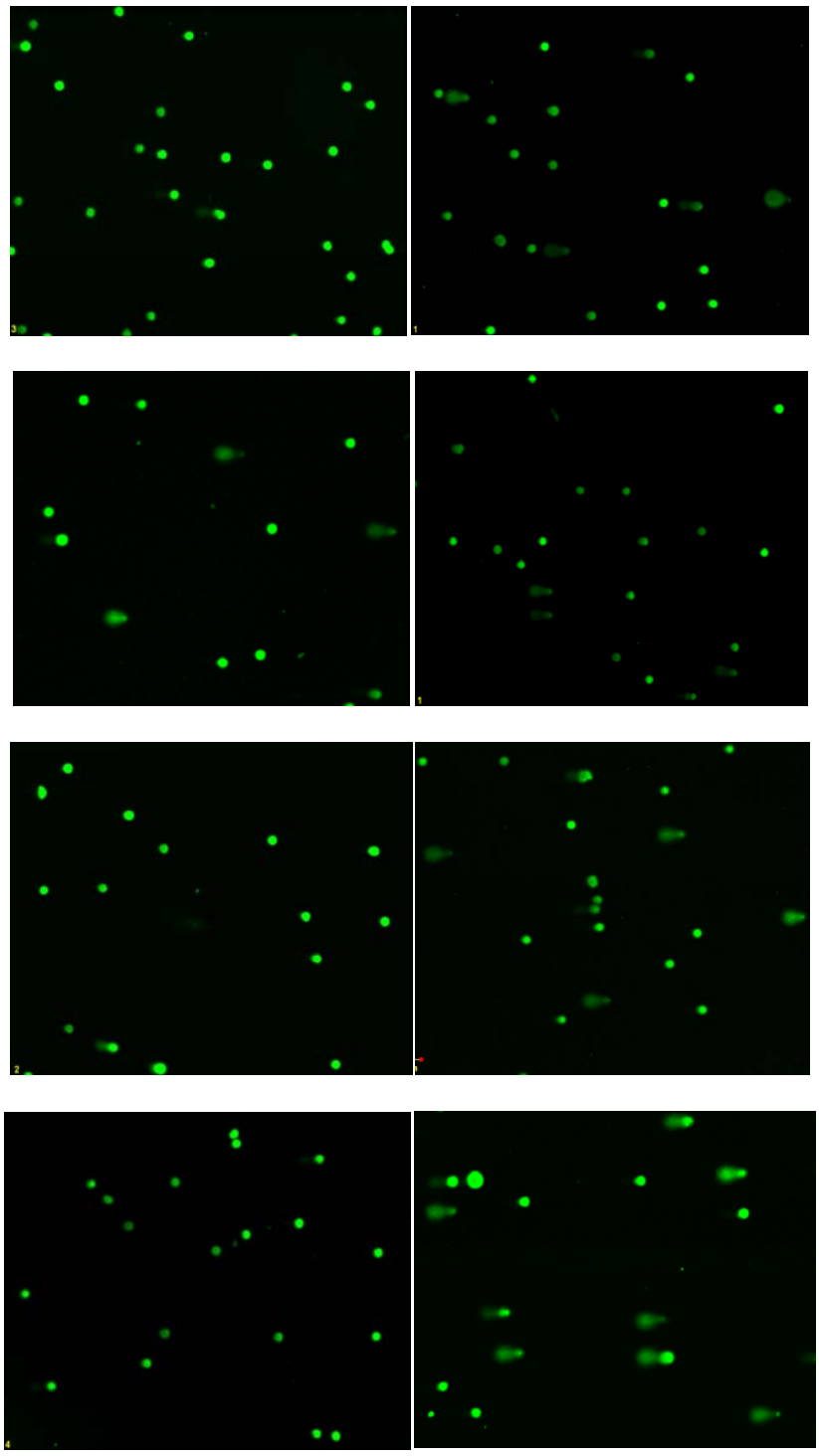

Figure 3.14 Comet Assay images of human prostate cancer-3 cells before (left) and after (right) UV light treatment (360nm, 3 min) for control (the first row), ZnS:Cu,Co (the second row), TBrRh123 (the third row), and ZnS:Cu,Co-TBrRh123 conjugation (the fourth row), respectively.

The same amount of ZnS:Cu,Co, TBrRh123, and ZnS:Cu,Co-TBrRh123 conjugation are applied to human prostate cancer-3 cells for a 24 h culture. The Comet Assay of cells before and after UV light treatment (360nm, 3 min) for different samples is shown in Figure 3.14. It is seen that there is very little cell killing after the UV light treatment in both the control and ZnS:Cu,Co samples. However, about 30% cells are dead after the UV light treatment in TBrRH123 added sample. The percentage of cell killed increases to 56% in ZnS:Cu,Co-TBrRh123 conjugation added sample. As the singlet oxygen generated by photosensitizer has been proposed as the reason of killing cancer cells, this result indicates that the afterglow ZnS:Cu,Co nanoparticles have transferred emission energy to activate TBrRh123, which then created singlet oxygen resulting in the death of much more cells.

3.5 X-ray Excited ZnS;Cu,Co Afterglow

X-ray is an efficient energy source widely used in biological imaging and treatment. The soft tissues in the body (such as blood, skin, fat, and muscle) allow most of the X-ray to pass through. However, X-ray is capable to damage or kill tissues cells depending on its dosage and radiation time. Thus, less X-ray radiation is always a target being pursued in medical treatment. As it has been mentioned previously, using afterglow nanoparticles as a light source in PDT for deep cancer treatment can largely reduce the usage of X-ray radiation.[45] For a future practical deep cancer PDT application by using ZnS:Cu,Co afterglow nanoparticles, it would be very necessary to test their afterglow properties firstly with X-ray excitation.

In order to examine X-ray excited ZnS:Cu,Co afterglow, the ZnS:Cu,Co nanoparticle aqueous solution was loaded inside of a small glass vial and put on a stage under a X-ray tube (X-RAD 320 irradiator, Precision X-Ray, Inc.). The afterglow pictures were taken by a digital camera with exposure time fixed at 30 s. Figure 3.15 shows The ZnS:Cu,Co afterglow photo pictures excited by X-ray at different working voltages and radiation time. Clearly, the X-ray excited afterglow has been seen after X-ray is turned off. By using same operation voltage (120KV), the ZnS:Cu,Co afterglow intensity gradually increases with X-ray radiation time

increasing from 0.5 min to 4 min (image 1 to 4). On the other hand, with same radiation time of 2 min, the afterglow intensity increases apparently by increasing X-ray operation voltage from 120KV to 160KV.

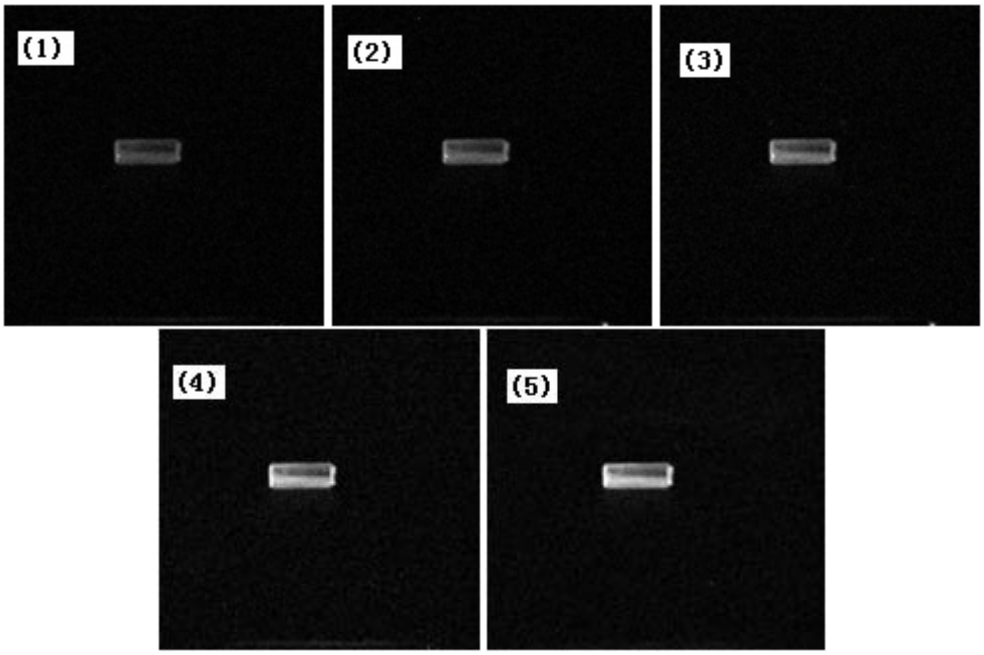

Figure 3.15 The ZnS:Cu,Co afterglow photo pictures (in black and white) excited by X-ray at different working voltages and time, (1) 120KV, 0.5 min; (2) 120KV, 1 min; (3) 120KV, 2 min; (4) 120KV, 4 min; (5) 160KV, 2 min.

This preliminary observation firstly demonstrates the X-ray excited afterglow from water soluble ZnS:CuCo nanoparticles. As X-ray can penetrate most body tissues, this study offers ZnS:CuCo afterglow nanoparticles great opportunities in future deep cancer PDT and other potential applications.

3.6 Other Potential Applications

As mentioned, afterglow phosphors have been widely investigated and used in traffic signs, emergency signs, watches, clocks, paintings and textile printing[99] as well as in “glow in the dark” toys.[79] However, little attention has been paid to the potential biological applications of afterglow nanoparticles. Actually, afterglow nanoparticles have many potential applications in biology and medical science. For example, long lasting afterglow nanoparticles can be used for

in vitro and in vivo imaging while no excitation light is needed because some afterglow phosphors can last longer than 10 h after activation.[103] In biological systems, many cells and biological processes are light sensitive, and light has tremendous applications in biology and medicine.[104,105] In addition, light therapy or phototherapy has been applied to treat Acne vulgaris, Psoriasis and eczema, vitiligo, jaundice, and wound healing.[105-107] Many skin diseases are light sensitive, and both phototherapy and photodynamic therapy have been applied for their treatment. The immune system and many enzymes are also light sensitive. [104,105] Some bacteria and organisms use light to harvest energy and nutrients.[104,105] Potentially, afterglow nanoparticles can find applications to activate or/and accelerate these biological processes. For these potential applications, the afterglow nanoparticles must be water soluble and must be able to be delivered and targeted to cancer cells. The synthesis of doped nanoparticles in aqueous solutions presents an additional challenge due to luminescence quenching by the solvent. In aqueous solutions, the dominant mode of luminescence quenching of the excited ions occurs via the coupling of the excited states of the lanthanide ions to the O–H oscillators of water molecules coordinated to the cation.[108] The result of the coupling is the energy transfer from excited states of emitters to O–H oscillators of bound water molecules. Ligands with N–H oscillators that have vibronic frequencies similar to the O–H oscillators are also effective quenchers of nanoparticle luminescence in solution. Therefore, appropriate coating to prevent the coupling of nanoparticle luminescence centers with O–H or N–H oscillators would be an efficient way to enhance the luminescence of water-soluble doped nanoparticles. The present work represents the first investigation of water soluble afterglow nanoparticles and their potential applications in biology and medical science.

3.7 Summary

In summary, green afterglow is observed from ZnS:Cu,Co water soluble nanoparticles. Cu^{2+} is responsible for the afterglow from nanoparticles but the co-doping of Co^{2+} is critical in obtaining the afterglow. The ZnS:Cu,Co nanoparticles have a cubic zinc blende structure with

average size of about 4 nm. The afterglow intensity and longevity are dependent on the concentrations of both Cu^{2+} and Co^{2+}. Our ZnS:Cu,Co nanoparticles are almost non-cytotoxic to human prostate cancer-3 cells, while the ZnS:Cu,Co-TBrRh123 conjugation kills more cells than TBrRh123 itself by applying UV light. For the first time, X-ray excited afterglow from water soluble ZnS:Cu,Co nanoparticles is observed. The successful observation of afterglow from water soluble nanoparticles opens their new applications in biological imaging, labeling and therapy.

CHAPTER 4

ENHANCEMENT OF AFTERGLOW IN ZNS:Cu,Co WATER-SOLUBLE NANOPARTICLES BY AGING

4.1 Introduction

Afterglow efficiency and longevity are the key parameters for practical applications in disease treatment and medical imaging. The afterglow of higher brightness and longer persistent time can greatly improve the imaging and disease treatment results. In order to reach a high quality afterglow material, lots of efforts have been done by developing new materials or applying different dopants into the lattice structure of phosphors.[6,7,40,109,110] Meanwhile, new synthesis methods appeared to seek high optical performance of long persistent luminescence materials.[9,22,37,111] Recently, our research group found the afterglow property increment in $CaZnGe_2O_6:Tb^{3+}$ phosphor by using ZnO nanopowder instead of ZnO bulk materials, and a optimized ratio of ZnO nanopowder to bulk material was suggested as 0.71:1 to enhance the afterglow intensity and other optical properties.[112] However, these efforts are mainly dealing with large phosphor particles (in micrometers) from solid state reaction. There is still not a general method to enhance the afterglow properties. Although researchers promoted various models for afterglow emissions, the real mechanism of afterglow is so complicated and remains unclear. As for nano-sized afterglow materials, it is still almost a blank area except this work and the other work in which large particles were physically grinded into small sizes.[82] Afterglow nanoparticles may be a better candidate comparing with fluorescent nanoparticles in medical imaging as the background fluorescence or autofluorescence can be avoided by removing the excitation source. However, in general, afterglow intensity is much lower than fluorescent phosphors although there might be some compensation from afterglow's long persistent time. Therefore, it would be very promising if the afterglow intensity can be enhanced to a high level.

This work becomes more challenging because there is also a requirement of particle water solubility for biological applications. ZnS is a good afterglow material for biological applications due to its low toxicity and wide gap for doping. In the previous work, we have prepared water-soluble ZnS:Cu,Co afterglow nanoparticles. In this chapter, we report our new observations on their afterglow enhancement by aging.

4.2 Sample Preparation and Characterization

4.2.1 Chemicals

Zinc acetate [$Zn(CH_3COO)_2$, 99.990%)], copper(II) acetylacetonate [$Cu(C_5H_7O_2)_2$, 99.990%], cobalt acetate [$Co(CH_3COO)_2$, 99.995%], sodium hydroxide [NaOH, 98%], and 3-mercaptopropionic acid (MPA) [$HSCH_2CH_2COOH$, 99%] were purchased from Sigma-Aldrich in the USA. Sodium sulfide (Na_2S) is also a product of Sigma but from Canada. All chemicals were used without further purification. Deionized (DI) water was used as the reaction solvent.

4.2.2 Sample Preparation

In a typical synthesis, 0.918 g of $Zn(CH_3COO)_2$ was dissolved in 200 mL of DI water and then mixed with 12 mL of 1.15 mM $Cu(C_5H_8O_2)_2$ and 0.15 mL of 0.40 mM $Co(CH_3COO)_2$ aqueous solutions in a 250 mL flask under mild stirring. The molar ratios of copper and cobalt ions to zinc ions are 0.28% and 0.001%, respectively. Then, 2 mL of MPA was added to the solution, and the PH value was adjusted to 10.4 by using 2 M NaOH. The solution was degassed by N_2 gas for 30 min before 5 mL of 0.46 M Na_2S solution was quickly injected under vigorous stirring. The reaction was allowed for 15 min and then heated to boiling temperature and lasted for 24 h to form the water-soluble afterglow nanoparticles. Finally, the solution was cooled by air to room temperature and then separated into two halves: one half was used for immediate measurements, and the other half was sealed and stored for 2 weeks at room temperature before any measurements. By adding the proper amount of ethanol, the nanoparticle powder samples can be obtained using centrifuging followed by drying in a vacuum oven. The solid powder can be easily redispersed into DI water.

4.2.3 Characterization

The identity, crystalline structure, size, and shape of the nanoparticles were observed by X-ray diffraction and high-resolution transmission electron microscopy. The X-ray powder diffraction was recorded in a Rigaku Ultima IV X-ray diffractometer with a radiation beam of λ = 1.5406 Å. The ZnS:Cu,Co nanoparticles in aqueous solution were placed onto holey carbon-covered copper grids for HRTEM observations. The HRTEM images of the particles were obtained with a Hitachi 9500 electron microscope with accelerating voltage of 300 kV. The X-ray photoelectron spectroscopy analysis was carried out by using a Kratos AXIS Ultra DLD high performance spectrometer. The photoluminescence and afterglow spectra were measured by using a Shimadzu RF-5301PC fluorescence spectrophotometer. The absorption spectra were recorded by using a Shimadzu UV-2450 UV-vis spectrophotometer. A 15 W UV lamp with an irradiation peak at 360 nm from UtiliTech (product F15T8) was used as the excitation source for afterglow measurement.

4.3 Results and Discussion

4.3.1 Fluorescence and Afterglow Enhancement

The photo pictures of aqueous ZnS:Cu,Co afterglow nanoparticles before and after aging are displayed in Figure 4.1. The left column shows the samples under normal light. The fluorescence pictures under a UV lamp (360 nm) are shown on the middle column. The afterglow pictures (right column) were taken after the same UV lamp excitation was off for 2 s. As shown in pictures, the clear ZnS:Cu,Co aqueous sample turned to semi-transparent after aging for 2 weeks at room temperature. Under UV light, the aged sample exhibited a much intensive blue emission. The afterglow has been observed from both samples, although it is pretty low for the sample without aging. Obviously, the afterglow increased significantly after aging.

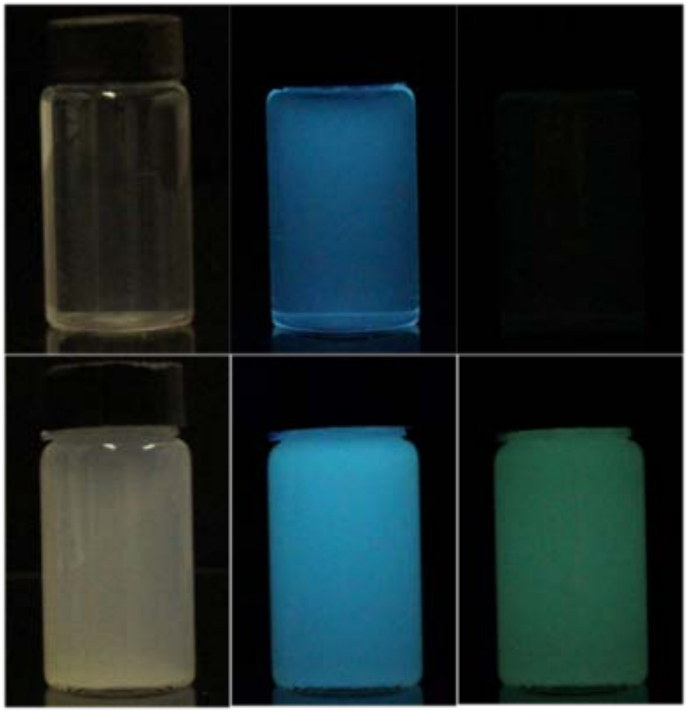

Figure 4.1 The photo pictures of non-aged (top row) and aged (bottom row) aqueous ZnS:Cu,Co nanoparticle samples under normal light (left), UV lamp (middle), and their afterglows (right) that were taken after the UV lamp was off for 2 seconds.

Figure 4.2 shows the fluorescence spectra of both ZnS:Cu,Co aqueous samples described above by using excitation of 360 nm. The blue emission from the samples is at around 466 nm, which is related to ZnS surface defect (S vacancy).[113] The fluorescence intensity apparently increased after the aging for 2 weeks at room temperature and the emission of the aged sample is red shifted to 469 nm from 466 nm in the fresh sample. The doping of Cu^{2+} and Co^{2+} in ZnS:Cu,Co nanopartiles has been discussed in our previous work.[113] Basically, Cu^{2+} doping shifts the blue emission (454 nm) of ZnS to 472 nm and is responsible to a green emission shoulder located at about 510 nm. As for the co-doping of Co^{2+}, it may change the emission intensity but not the emission wavelength on ZnS:Cu,Co nanoparticles.

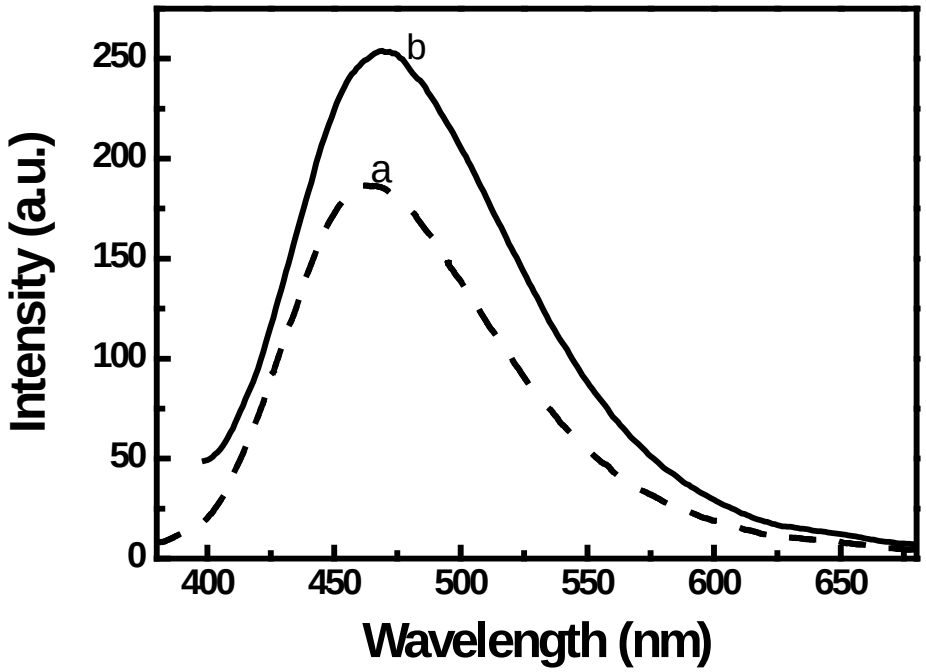

Figure 4.2 Fluorescence spectra of nonaged (a) and aged (b) ZnS:Cu, Co nanoparticles in water by using excitation of 360 nm.

Figure 4.3 shows the afterglow emission spectra of the non-aged and aged ZnS:Cu,Co samples. The spectra were recorded after a 2 minute exposure using the UV lamp peaked at 360 nm. Similar to our previous report,[113] unlike their blue fluorescence, the afterglow emission is green with a peak at around 500 nm. As pointed out in our previous work, the green afterglow from ZnS:Cu,Co water-soluble nanoparticles is attributed to the electron transition from S vacancies to Cu^{2+} centers.[113] After aging for two weeks at room temperature, the afterglow intensity is increased more than 7 times while the fluorescence is only increased 1.4 times in intensity.

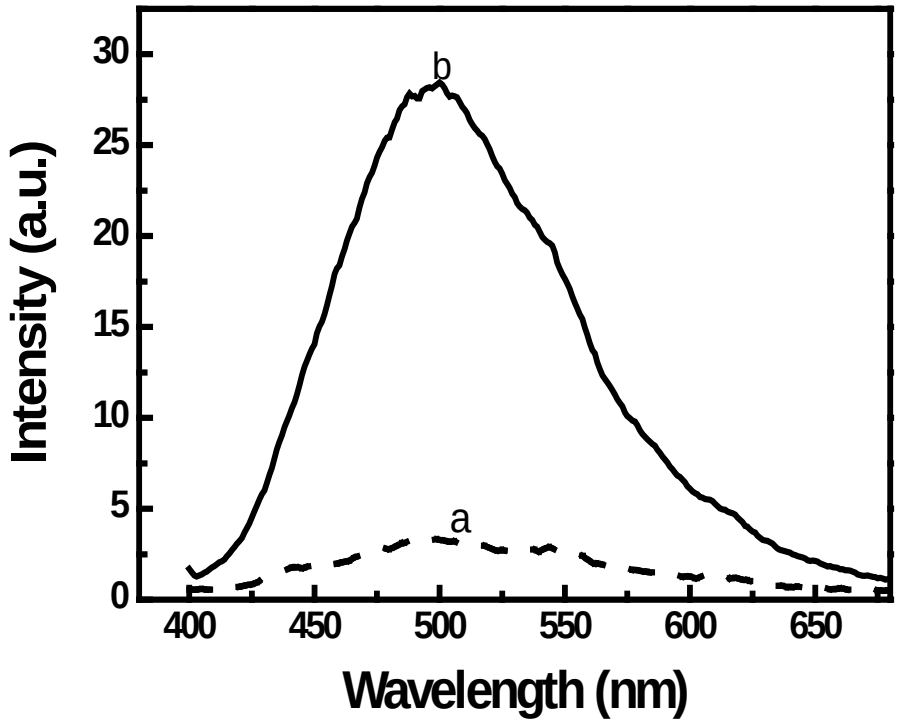

Figure 4.3 Afterglow emission spectra of nonaged (a) and aged (b) aqueous ZnS:Cu,Co nanoparticle samples. The spectra were recorded after 2 min exposure under the UV lamp (360 nm).

The afterglow decay spectra for the non-aged and aged aqueous ZnS:Cu,Co samples excited by the UV lamp are displayed in Figure 4.4. The decay curves show a close linear property in the logarithmic scale plot, which means that the afterglow intensity is not decaying in time by a simple power function relationship. Here we define decay lifetime as the time when the afterglow intensity reduces to its half level and longevity as the time cost when afterglow is gone (not detectable to the fluorescence spectrophotometer, which means the intensities below 1 on the spectra). The decay lifetimes of the samples are estimated from the plot and they are both at a same range of several seconds. The longevities of them can be seen as around 40 s and 180 s, respectively. The luminescence and afterglow intensities of the two samples are

summarized in Table-4.1. Our observations indicate that the aging increases both the fluorescence and afterglow.

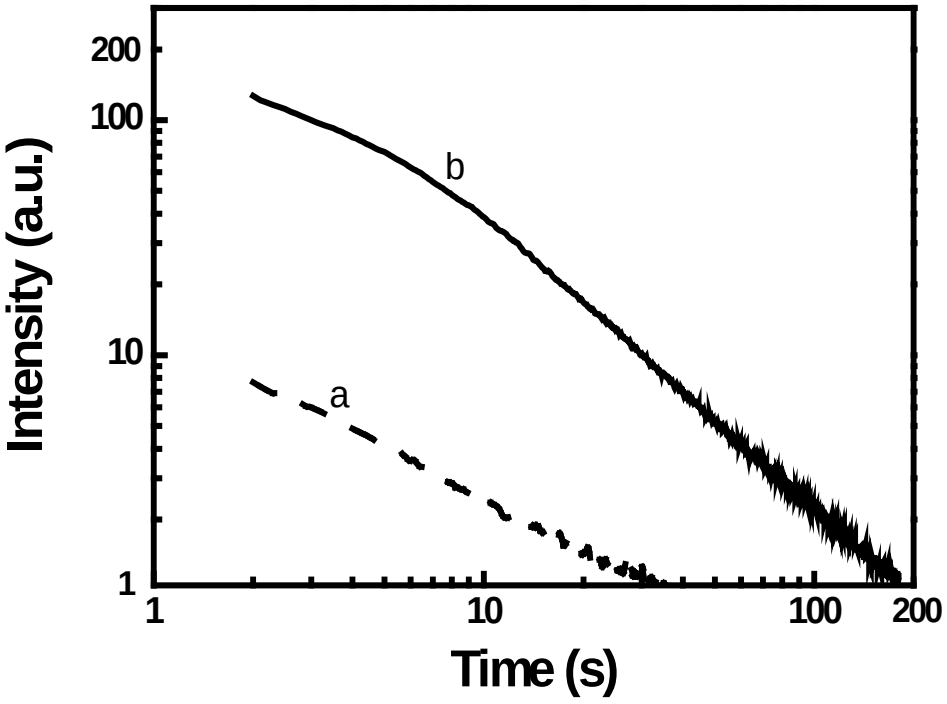

Figure 4.4 Afterglow decay spectra (monitored at 500 nm) of non-aged (a) and aged (b) aqueous ZnS:Cu,Co nanoparticles. The spectra were recorded after 2 min exposure to the UV lamp (360 nm).

Table 4.1 Photoluminescence (466 nm) and Afterglow (500 nm) Intensities From the Non-aged and Aged Samples

Samples	Non-aged	Aged
Emission Intensity (a.u.)	187	255
Afterglow Intensity (a.u.)	3.4	28.5
Afterglow Longevity (s)	40	180

4.3.2 Mechanisms for Afterglow Enhancement

We are interested in why ageing can largely enhance the afterglow of the nanoparticles. For this purpose, we investigated the nanoparticle crystal structure, size and surface characteristics before and after ageing. The X-ray diffraction patterns in Figure 4.5 demonstrate that ZnS:Cu,Co nanoparticles prepared in water have a cubic zinc blende structure (JCPDS, no. 05-0566) regardless of the non-aged or aged samples. There is no apparent difference found in the XRD patterns for the both samples. No Cu^{2}+ or Co^{2+} impurities are observed from the measurements, which indicates that Cu^{2+} and Co^{2+} were doped into the crystal lattice. By comparing with the standard cubic ZnS structure, the main diffraction peaks are indexed with the lattice planes of (111), (220), (311), (400), and (331), respectively, although all of them slightly shift to larger diffraction angles. This can be seen obviously with setting up the standard peak positions of pure ZnS (dash lines). The broad XRD peaks are indicative of the small size effect of nanoparticles. From the width of the peak broadening, the average crystal size is calculated by using Debye-Scherrer formula and gives similar size results of 3±1 nm for the both samples without or with aging. Further, the lattice constant is obtained from the XRD patterns respectively by using software Jade 5.0, which gives a = 0.5383 nm (non-aged) and a = 0.5380 nm (aged). The two values are similar but both are slightly smaller than the lattice constant of pure ZnS (JCPDS, no. 05-0566, a = 0.5406 nm). The resulted smaller lattice constants are also consistent with the observation of peak right shifting described above. It is possibly due to the partial substitution of some Zn^{2+} ions by Cu^{2+} and Co^{2+} ions as the radius of Cu^{2+} (0.72 Å) and Co^{2+} (0.58 Å) are smaller than Zn^{2+} (0.74 Å). This further proves that Cu^{2+} and Co^{2+} ions were doped into the ZnS nanoparticle lattices.

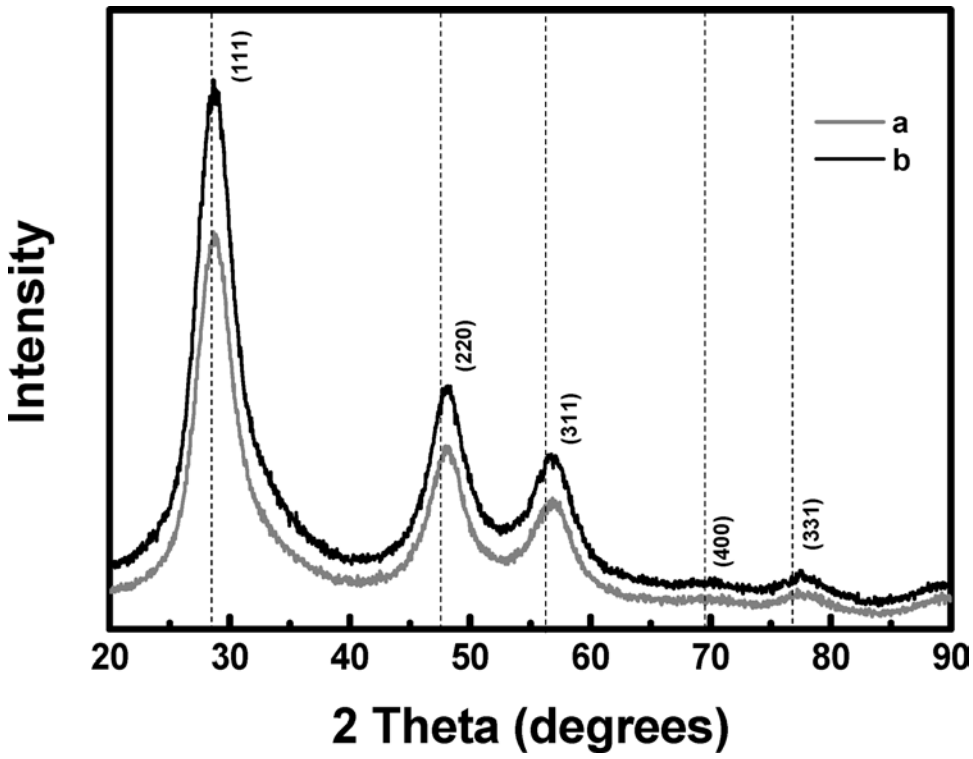

Figure 4.5 X-ray diffraction patterns of non-aged (a) and aged (b) ZnS:Cu,Co water soluble nanoparticles. The dash lines indicate the standard peak positions of pure ZnS (JCPDS, no. 05-0566).

From high resolution transmission electron microscope (HRTEM) measurement, the images do not show apparent mean size changes for the non-aged and aged ZnS:Cu,Co afterglow nanoparticles. Figure 4.6 displays the HRTEM images of the two samples. The average sizes of the non-aged and aged particles are similar, both about 4 nm. This is also in agreement with the size estimated from XRD measurements. It is interesting to see the average sizes of the ZnS:Cu,Co nanoparticles remain almost the same even they were aged at room temperature for 2 weeks. This is quite different from the work done by Zang et al., in which the ZnS particles were stabilized by polyphosphate and their size was found to get increased after aging at 10 °C for a few days.[114] However, some of the nanoparticles are aggregated after aging for 2 weeks as shown in the image (right). Aggregation may cause the red-shift of the emission due to particle-particle interaction which has been reported in literature.[115]

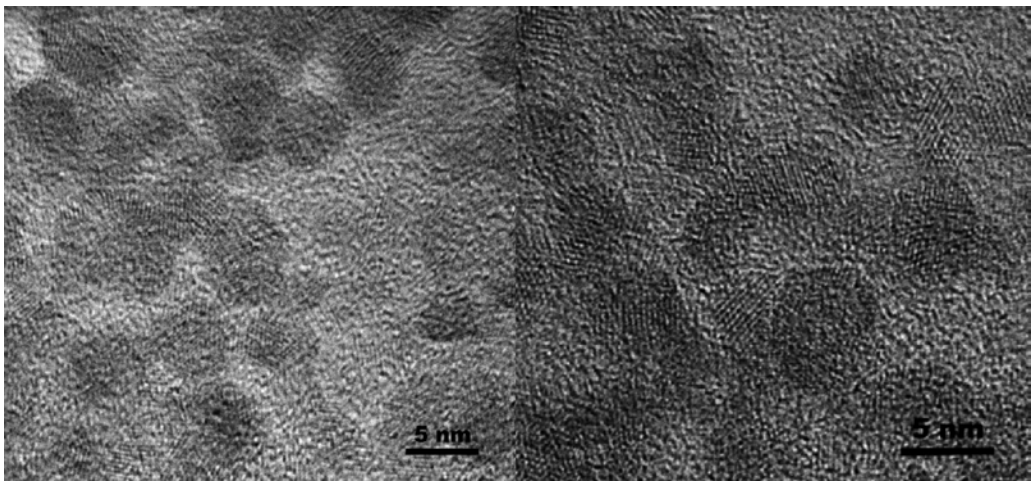

Figure 4.6 HRTEM images of non-aged (left) and aged (right) ZnS:Cu,Co nanoparticles in water.

Optical absorption spectra have been widely used to estimate the size of ZnS nanoparticles as the band gap of semiconductor nanoparticles is largely related to their size known as quantum confinement.[11,50,116,117] To further study the size change of ZnS:Cu,Co nanoparticles in aqueous solution before and after long time aging, the absorption spectra of two samples were measured and shown in Figure 4.7. A pronounced shoulder appears at 315 nm (3.93 eV), which is from the confined excitons in ZnS nanoparticles. The exciton absorption is shifted to shorter wavelengths or higher energies comparing to the band gap of bulk ZnS (~3.6 eV) as a result of quantum size confinement. From works done by other researchers, the absorption (~315 nm) of undoped or doped ZnS usually means an average particle size of 3~5 nm which is consistent with the results from XRD and HRTEM measurements. [11,50,116,117]

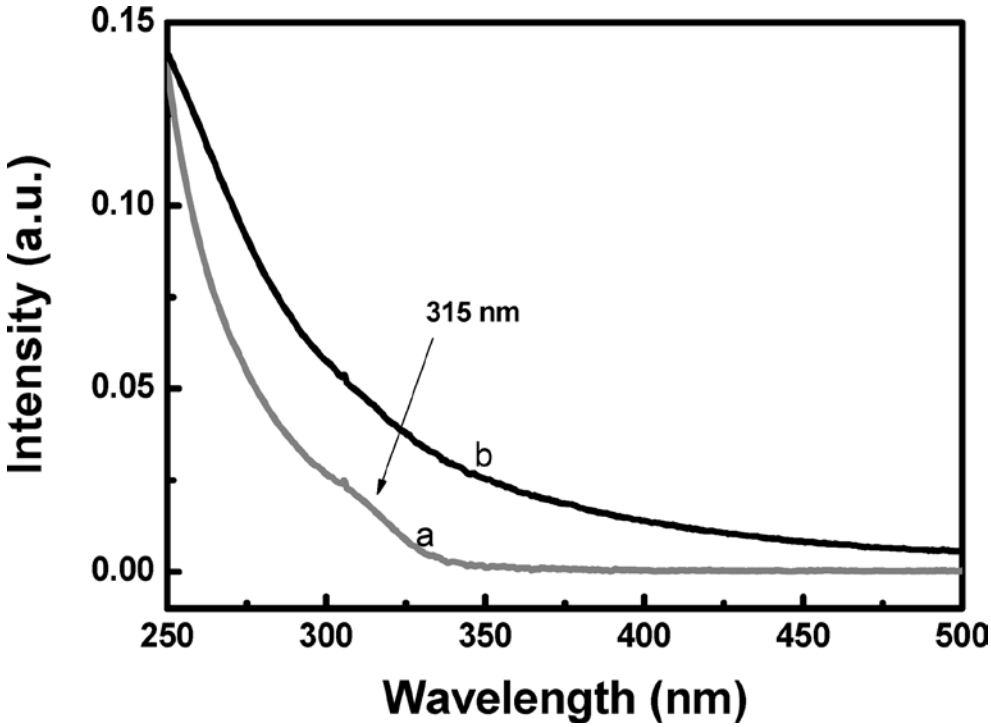

Figure 4.7 Absorption spectra of non-aged (a) and aged (b) ZnS:Cu,Co water soluble nanoparticles.

Regarding to the aged samples, it displays a stronger but smoothly decreasing curve with no apparent ZnS absorption peak. As shown in Figure 4.1, after aging at room temperature for 2 weeks, the clear sample became semi-transparent due to the particle aggregation that has been mentioned in above. The optical semi-transparent solution may absorb and scatter or even partially block the light passing through, therefore the absorption (extinction) of the aged sample is more intensive. As it will be discussed in the following section, there is slow oxidation occurring on ZnS and this might affect ZnS band gap structure and weaken its absorption, so the weak peak is submerged in the intensive absorptions and cannot be seen.

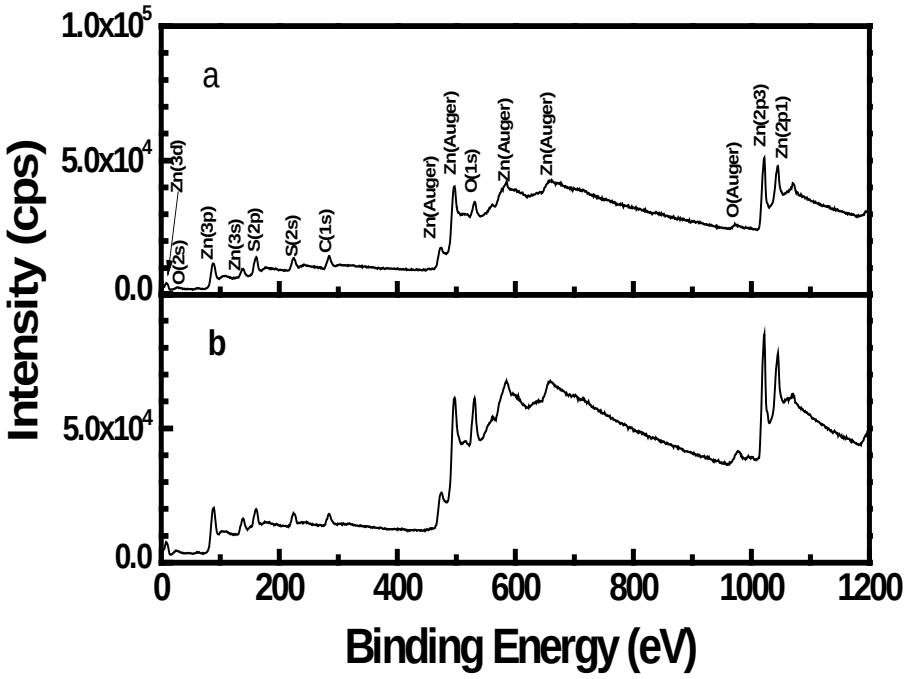

Figure 4.8 XPS spectra of non-aged (a) and aged (b) ZnS:Cu,Co nanoparticles. The binding energy peaks are labeled with corresponding elements, as shown only in the top plot (a) representatively.

It is well known that the surface effect becomes significantly important as particles shrink to very small sizes. In order to give further insight into the surface properties of ZnS:Cu,Co nanoparticles, the X-ray photoelectron spectroscopy (XPS) of the samples without and with aging was investigated and shown together in Figure 4.8. The XPS spectra of the two samples perform as almost identical and the element labels are just shown in one of them. Significant signals of Zn, S, and O were found from each sample. C also can be seen from the spectra but it should be from stabilizer 3-mercaptopropionic acid (MPA). Further quantification analysis gives the atomic ratio of Zn:S:O for the two samples separately, which is shown together in Table 4.2. Either sample has a ratio of Zn:S lower than the starting precursor ratio in synthesis. The increasing S is also due to thiol groups from the stabilizer MPA that are attached on

particle surfaces. The existence of large ratio of O in both samples indicates that there was oxidation process occurring in the long time reaction and air cooling (~30 h totally). After aging, the O increased to a higher amount while the amount of S decreased to a lower level. The ratio of O to S is much higher in the aged sample (2.45) than in the fresh sample (0.87). As the oxidation is able to remove S^{2-} ions ($S^{2-} \rightarrow SO_4^{2-}$),[114,118], this could produce tow results. Firstly, the thiol groups from the stabilizer could be destroyed and leave the particle surface which further lead to particle aggregation as described before. This also explains the decreasing amount of S on the ZnS:Cu,Co particle surfaces shown from the XPS measurement. Secondly, more S vacancies could be left on the surface of ZnS:Cu,Co nanoparticles associated with the slow oxidation process to particles themselves. As the surfaces with absent atoms have high surface energy and have tendency to accept other species,[119], oxygen may be preferred to site on or enter the particle crystal structure as a SO_4^{2-} form, combining with Zn^{2+} ions, and/or staying at interstitials. The particle surfaces then become much rich with oxygen. This is why an increasing amount of O has been found in the XPS measurements. However, there is no ZnO found from the XRD patterns, which means that no ZnO crystal structure formed even the O may enter the ZnS structure or possibly substitute S. In a word, the oxidation can generated more S vacancies which then contribute to the much intensive blue emission from ZnS:Cu,Co nanoparticles. Moreover, the increased S vacancies and appearance of O in ZnS:Cu,Co crystal structure may produce more electron traps, which in turn enhance the afterglow intensity and longevity from ZnS:Cu,Co nanoparticles.

Table 4.2 XPS Quantification Report of the Atomic Ratio of Zn:S:O of Non-aged and Aged ZnS:Cu,Co Nanoparticles.

	Zn	S	O	O/S
Non-aged	1	1.33	1.16	0.87
Aged	1	0.76	1.86	2.45

4.4 Summary

In summary, it is observed that aging can enhance the luminescence and particularly the afterglow of water-soluble ZnS:Cu,Co nanoparticles. The structure and size of the particles remains the same but some particles are slightly aggregated. XPS measurements indicate that more oxygen are entered into the nanoparticles and more defects appeared after aging. The partial oxidation is perhaps responsible for the afterglow enhancement as this could provide more electron storage which is a source for afterglow emission.

CHAPTER 5

BLUE AFTERGLOW FROM ZnS:Ag,Co WATER SOLUBLE NANOPARTICLES

5.1 Introduction

Doped ZnS materials are able to emit visible colors from blue to red by varying the dopants. Comparing with photoluminescence, afterglow has similar luminescent centers. Based on our previous work, we have suggested that the green afterglow from ZnS:Cu,Co nanoparticles is due to the electron transition from sulfur vacancies to Cu^{2+} luminescent centers. Thus, it is possible to obtain other afterglows from ZnS based materials by simply changing the doped luminescent centers. As the doped luminescent centers vary and create new energy levels in ZnS host, afterglow nanoparticles of different wavelengths could be synthesized. This may greatly increase the opportunities of ZnS based afterglow materials in further applications. For example, the photosensitizers in PDT are mostly having their maximum absorptions in a UV-blue range, hence blue afterglow nanoparticles can work with them more efficiently. Therefore, the synthesis of blue afterglow nanoparticles is promising, especially for the PDT in deep cancer treatment. What is more, the success of synthesis of other afterglow materials by using same preparation method may provide further evidence to the afterglow mechanism in ZnS:Cu,Co nanoparticles that was promoted before. In this chapter, we synthesized ZnS:Ag,Co blue afterglow water soluble nanoparticles by using the same preparation method for ZnS:Cu,Co afterglow nanoparticles. It is also the first time, to my best knowledge, that the blue afterglow were obtained from doped ZnS water soluble nanoparticles.

5.2 Synthesis and Characterization

5.2.1 Chemicals

Zinc acetate [$Zn(CH_3COO)_2$, 99.990%)], silver nitrate [$AgNO_3$, 99%], cobalt acetate [$Co(CH_3COO)_2$, 99.995%], sodium hydroxide [NaOH, 98%], and 3-mercaptopropionic acid

(MPA) [$HSCH_2CH_2COOH$, 99%] were purchased from Sigma-Aldrich in the USA. Sodium sulfide (Na_2S) is also a product of Sigma but from Canada. All chemicals were used without further purification. Deionized (DI) water was used as the reaction solvent.

5.2.2 Sample Preparation and Characterization

The silver and cobalt doped water soluble ZnS afterglow nanoparticles were prepared by following the same method described in the previous chapter. For Ag^+ dopping, silver nitrate was applied in the experiment instead of copper(II) acetylacetonate. After the reaction was finished, the solution was sealed with air left in the container and stored for 3 weeks at room temperature. The solution turned from clear to semi-transparent after aging. To obtain powder samples, ethanol was added to precipitate the particles and the white cloudy solution was centrifuged at 8000 rpm. The supernatant of the solution was removed and the precipitation was washed with DI water twice and dried in a vacuum oven. The solid powder can be easily redispersed into DI water.

The identity, crystalline structure, size, shape, composition and optical properties of the nanoparticles were characterized by using the same instruments and methods described in the previous chapter.

5.3 Results and Discussion

5.3.1 Optical Properties

The photo pictures of aqueous ZnS:Ag,Co nanoparticle samples under normal light, UV lamp, and their afterglow are displayed in Figure 5.1. The nanoparticle solution is semi-transparent as the scales from the other side of the flask are clearly seen through the solution. Under UV light, the solution emits bright blue color. The blue afterglow from ZnS:Ag,Co nanoparticles is taken after the UV light is off for 2 s.

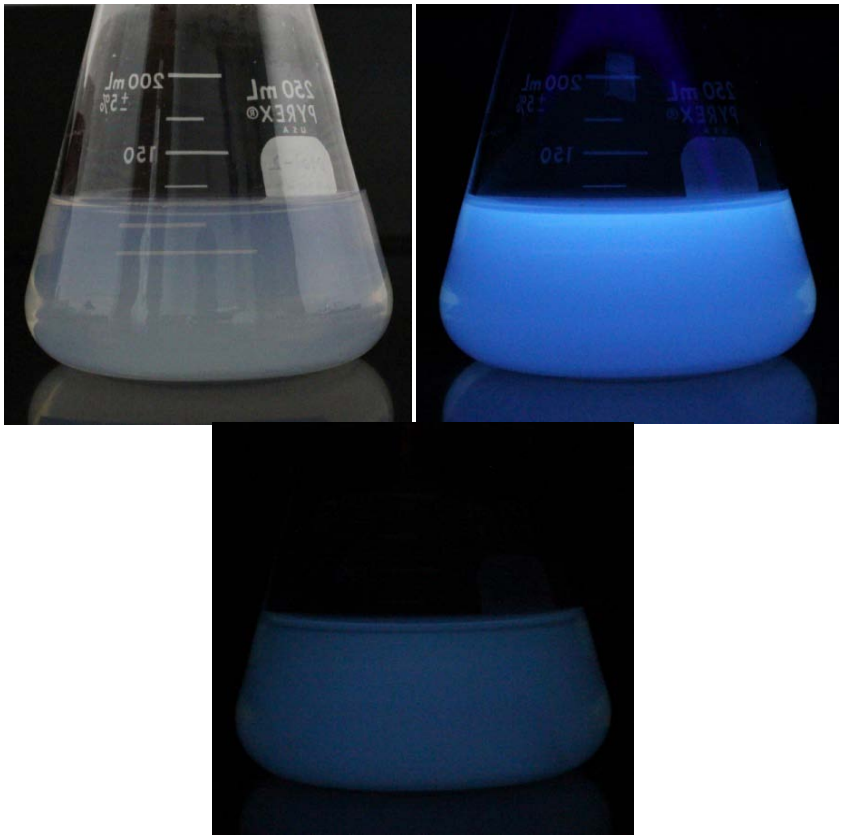

Figure 5.1 The photo pictures of aqueous ZnS:Ag,Co nanoparticle sample under normal light (top,left), UV lamp (top,right), and their afterglow (bottom) that were taken after the UV lamp was off for 2 seconds.

Figure 5.2 reveals the photoluminescence and afterglow spectra of water soluble ZnS:Ag,Co nanoparticles. The photoluminescence spectrum is obtained by using excitation wavelength of 360 nm and afterglow is using the UV lamp which emits UV light peaked at 360 nm. The blue emission from ZnS:Ag,Co is at around 441 nm, which is due to the transition from surface defects to Ag^{+} luminescent centers and consistent with ZnS:Ag emission reported before.[120,121] As it is already discussed in previous chapters, the Co^{2+} doping may affect the emission intensity but not wavelength. Although the dopant Co^{2+} often acts as a luminescence quencher,[2] it is important for the green afterglow from ZnS:Cu,Co nanoparticles and the blue afterglow of ZnS:Ag,Co nanoparticles herein. Actually, the afterglow can be barely observed without Co^{2+} co-doping for both cases. While the real role of Co^{2+} ions in afterglow is still

unclear, they might help to form deeper electron traps which result in slower trapped electron release. The blue afterglow band centered at 475 nm is broad and covers the whole their dominant radiative electron transitions are in different energy ranges.

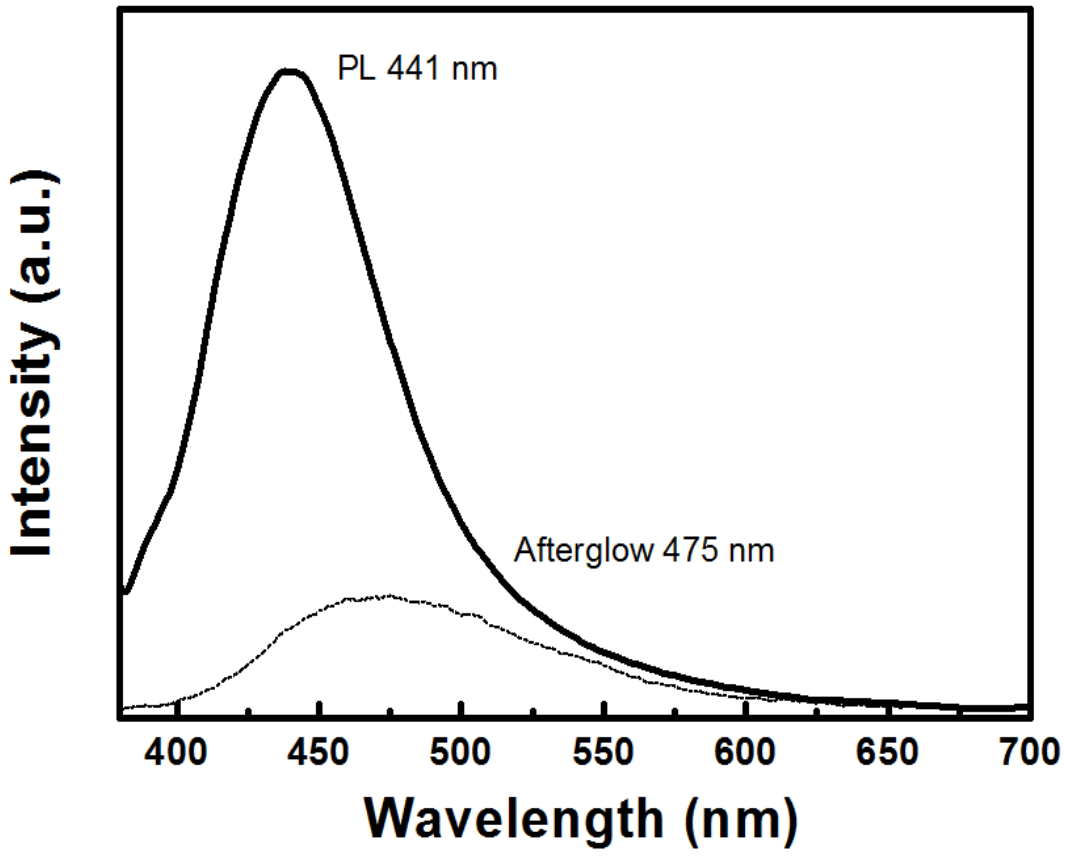

Figure 5.2 The photoluminescence (solid curve, excitation=360 nm) and afterglow (dash curve) spectra of water soluble ZnS:Ag,Co nanoparticles. The afterglow spectra were recorded after 2 min exposure under the UV lamp (360 nm).

The absorption spectrum of ZnS:Ag,Co water soluble nanoparticles is displayed in Figure 5.4. A pronounced shoulder appears at 315 nm (3.93 eV), which is known as the exciton absorption in ZnS nanoparticles. It is shifted to shorter wavelengths or higher energies comparing to the band gap of bulk ZnS (~3.6 eV) as a result of quantum size confinement. The exciton absorption of undoped or doped ZnS is related to the particle average size. Based on

previous works, the exciton absorption at around 315 nm of undoped or doped ZnS nanoparticles usually means an average particle size of 3~5 nm.[11,50,116,117]

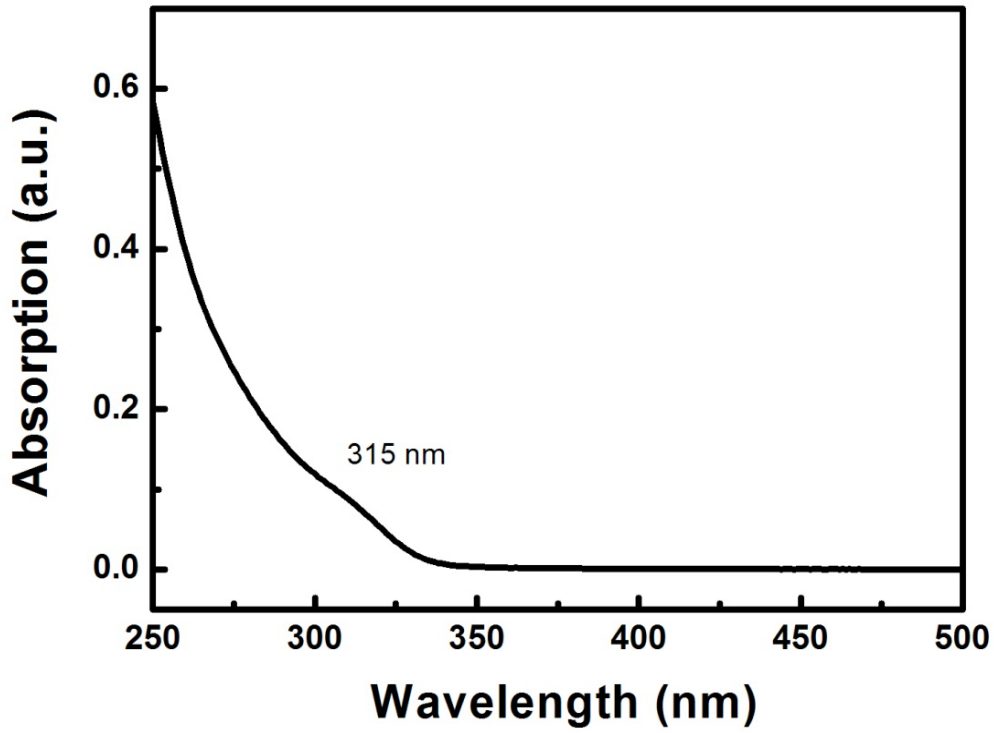

Figure 5.3 Absorption spectra of ZnS:Ag,Co water soluble nanoparticles.

Figure 5.4 shows the afterglow decay spectrum of ZnS:Ag,Co nanoparticles excited by a UV lamp. By using a logarithmic scale plot, the afterglow intensity displayed an almost linear (but not exactly) relationship to the decay time. Differing from those afterglow decay of solid powder materials,[3] the afterglow from nanoparticles in water solution may be much complicated and is not following a simple power function relationship. For water soluble nanoparticles, many factors affect their optical properties, such as sizes, surface defects, stabilizers, solvents, and possible interactions of liquid molecules and nanoparticles. Under the same definitions of afterglow decay lifetime and longevity described in the last chapter, the decay lifetime of ZnS:Ag,Co nanoaparticles estimated from the plot is about 2.5 seconds. The longevity can be

seen as about 90 seconds. It should be noticed that varying the Ag^{+} and Co^{2+} doping levels may optimize both afterglow intensity and longevity. Thus, future work is necessary for obtaining higher afterglow properties.

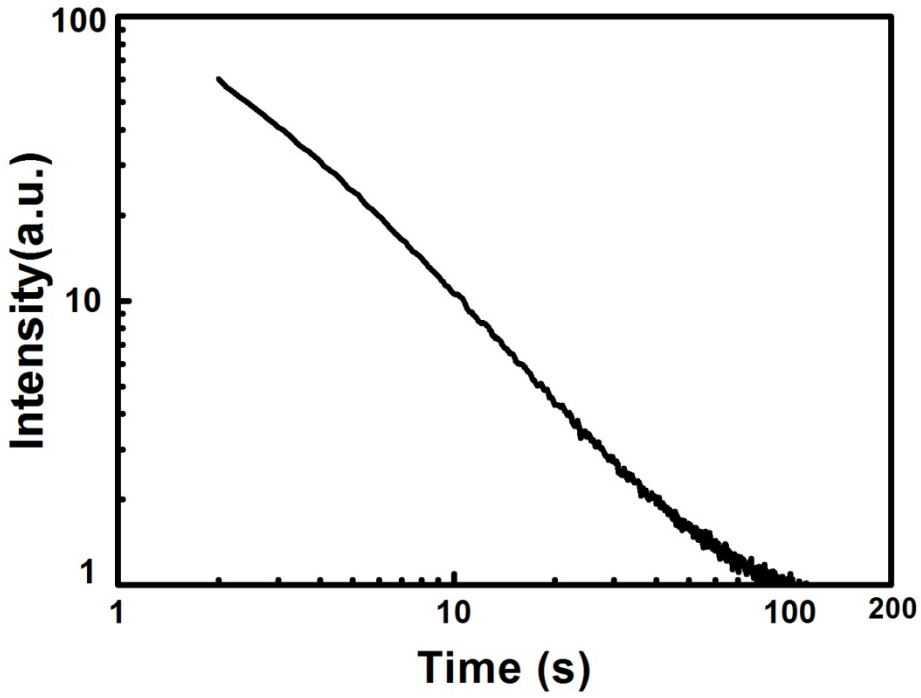

Figure 5.4 Afterglow decay spectra (monitored at 475 nm) of aqueous ZnS:Ag,Co nanoparticles. The spectra were recorded after 2 minute exposure to the UV lamp (360 nm).

5.3.2 Structure

The X-ray diffraction pattern shown in Figure 5.5 demonstrates that the ZnS:Ag,Co nanoparticles have a cubic zinc blende structure (JCPDS, no. 05-0566). The main peaks can be indexed with the lattice planes of (111), (220), (311), and (331), respectively. The broadening of the diffraction peaks is indicative of the small size effect of nanoparticles. From the width of the peak broadening, the mean crystal size D is determined as 4±1 nm by using Scherrer equation $D=0.9\lambda/(\beta\cos\theta)$, where λ is the X-ray wavelength (here λ = 1.54060 Å), β is the full width at half maximum (FWHM) and θ is the diffraction angle.

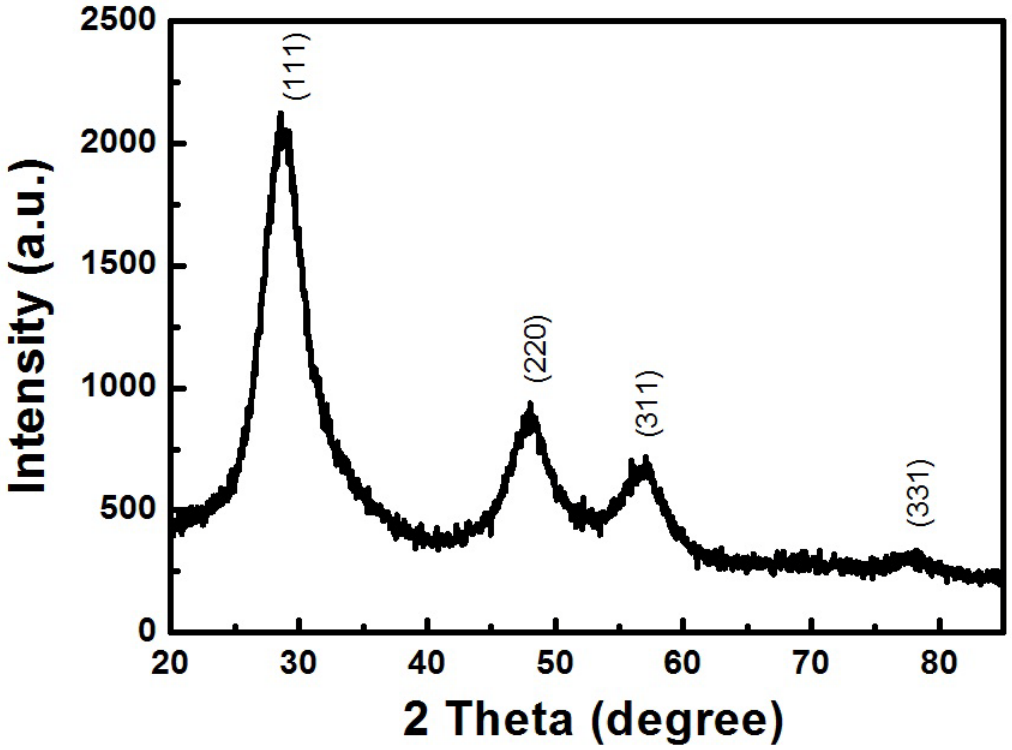

Figure 5.5 X-ray diffraction patterns of ZnS:Ag,Co water soluble nanoparticles.

The high resolution transmission electron microscope (HRTEM) image of ZnS:Ag,Co water soluble nanoparticles is displayed in Figure 5.6. The mean diameter of these nanoparticles is estimated to be 4 nm, which is consistent with the calculated value from XRD measurement. The obvious lattice fringe display indicates that the nanoparticles are crystals. The (111) lattice planes of some particles can mainly be observed and this lattice spacing is measured to be about 0.31 nm from the HRTEM image, which agrees with the spacing value (0.312 nm) of cubic ZnS (111) plane from the standard JCPDS database.

Figure 5.6 HRTEM images of ZnS:Ag,Co water soluble nanoparticles.

5.3.3 Oxidation on the Particle Surface

Figure 5.7 shows the X-ray photoelectron spectroscopy (XPS) measurement of ZnS:Ag,Co nanoparticles. Significant signals of Zn, S, C, and O have been found from the sample. The C measured from the spectra should be from stabilizer 3-mercaptopropionic acid (MPA) and is not concerned for ZnS:Ag,Co crystal structure. There is no silver or cobalt displayed in the XPS spectra as their doping levels are low. For comparison purpose, the XPS quantification measurement is also done for fresh sample of ZnS:Ag,Co before aging. The quantification reports of the atomic ratio of Zn:S:O for both fresh and aged samples are shown in Table 5.1. Similar to the results obtained for ZnS:Cu,Co nanoparticles, we observe that the S level reduced and O level increased significantly. It is due to the oxidation process on the surface of ZnS:Ag,Co nanoparticles. Similarly to the discussion in Chapter 4, the oxidation removes the S^{2-} ions ($S^{2-} \rightarrow SO_4^{2-}$) and produces two results. One is that the oxidation destroyed some thiol groups from the stabilizer and results in a decreased S level (Table 5.1) and particle

aggregation (Figure 5.1). On the other hand, as the surfaces with less atoms have high surface energy and have tendency to accept other species,[119], oxygen may be preferred to site on or enter the particle crystal structure and thus a large increasing of oxygen is observed. We can reach a same conclusion for ZnS:Ag,Co, as that for ZnS:Cu,Co water soluble nanoparticles. In a word, the surface oxidation produces more S vacancies and then possibly forms more electrons traps, a large amount of trapped electrons may finally result in the apparent blue afterglow observed.

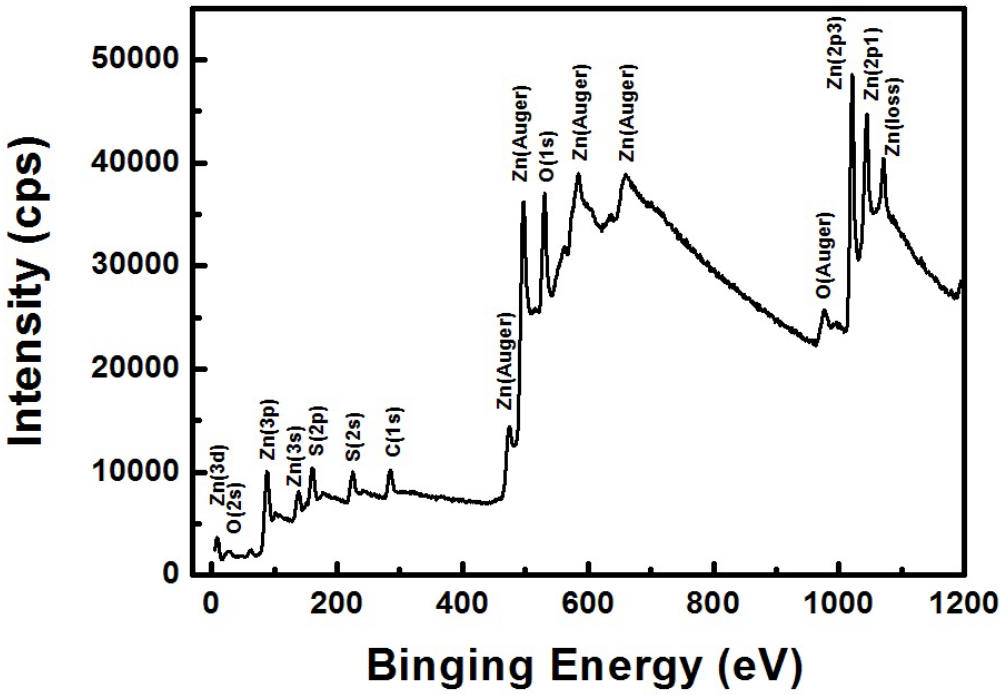

Figure 5.7 XPS spectra of ZnS:Ag,Co nanoparticles. The binding energy peaks are labeled with corresponding elements.

Table 5.1 XPS Quantification Report of the Atomic Ratio of Zn:S:O of ZnS:Ag,Co Nanoparticles Before and After Aging.

	Zn	S	O	O/S
Before aging	1	1.28	1.50	1.17
After aging	1	0.76	2.22	2.92

5.4 Summary

In summary, we have successfully synthesized water soluble ZnS:Ag,Co blue afterglow nanoparticles by using the same strategy developed in the last chapter for ZnS:Cu.Co nanoparticles. The crystal structure and size of the nanoparticles remain the same as expected. The blue afterglow centered at 475 nm has a longevity of about 90 s. The XPS measurements also indicate that the same oxidation process occurred on ZnS:Ag,Co nanoparticles. The oxidation removes S on nanoparticle surfaces and produces more S vacancies that could act as electron traps for afterglow. Thus, apparent afterglow can be obtained by aging (oxidation) method. The blue afterglow ZnS:Ag,Co nanoparticles may have more potential PDT applications because the absorptions of many photosensitizers are in UV-blue range. Cobalt co-doping is necessary for doped ZnS afterglow nanoparticles. By changing the dopant in ZnS based materials, new ZnS based water soluble afterglow nanoparticles can be synthesized by using similar method developed in this work.

APPENDIX A

LIST OF PUBLICATIONS

LIST OF PUBLICATIONS

(1) **Lun Ma** and Wei Chen, The Enhancement of Afterglow in ZnS:Cu,Co Water-Soluble Nanoparticles by Aging, *Journal of Physical Chemistry C, Vol.115, 8940 (2011)*

(2) Xing Zhang, Zhongxin Liu, **Lun Ma**, Marius Hossu, and Wei Chen, Interaction of porphyrins with CdTe quantum dots, *Nanotechnology, Vol.22 , 195501 (2011)*

(3) **Lun Ma** and Wei Chen, ZnS:Cu,Co water-soluble afterglow nanoparticles: synthesis, luminescence and potential applications, *Nanotechnology, Vol. 21, 385604 (2010)*

(4) **Lun Ma** and Wei Chen, Luminescence enhancement and quenching in ZnS:Mn by Au nanoparticles, *Journal of Applied Physics, Vol.107, 123513 (2010)*

(5) Mingzhen Yao, Xing Zhang, **Lun Ma**, Wei Chen, Alan G. Joly, Jinsong Huang, and Qingwu Wang, Luminescence enhancement of CdTe nanostructures in LaF_3:Ce/CdTe nanocomposites, *Journal of Applied Physics, Vol.108, 103104 (2010)*

(6) Yuebin Li, Zhong Sun, **Lun Ma**, Xing Zhang, Mingzhen Yao, Alan G Joly, Zuli Liu and Wei Chen, Synthesis and Luminescence of CePO4:Tb/LaPO4 Core/Sheath Nanowires, *Nanotechnology, Vol.21, 125604 (2010)*

(7) Marius Hossu, **Lun Ma**, Wei Chen, Nonlinear enhancement of spontaneous biophoton emission of sweet potato by silver nanoparticles, *Journal of Photochemistry and Photobiology B: Biology Vol.99, 44 (2010)*

(8) Zhong Sun, Yuebin Li, Xing Zhang, Mingzhen Yao, **Lun Ma** and Wei Chen Luminescence and Energy Transfer in Water Soluble CeF3 and CeF3:Tb3+ Nanoparticles, *Journal of Nanoscience and Nanotechnology, Vol.9, 1 (2009)*

(9) Yuebin Li, **Lun Ma**, Xing Zhang, Alan G. Joly, Zuli Liu and Wei Chen, Synthesis and Optical Properties of Sulfide Nanoparticles Prepared in Dimethylsulfoxide, *Journal of Nanoscience and Nanotechnology, Vol.8, 1 (2008)*

(10) Kwan H. Cheng, Jacob Aijmo, **Lun Ma**, Mingzhen Yao, Xing Zhang, John Como, Louisa J. Hope-Weeks, Juyang Huang and Wei Chen, Luminescence Decay Dynamics and Trace Biomaterials Detection Potential of Surface-Functionalized Nanoparticles, *Journal of Physical Chemistry C, Vol. 112, 17931 (2008)*

REFERENCES

(1) Clabau, F.; Rocquefelte, X.; Le Mercier, T.; Deniard, P.; Jobic, S.; Whangbo, M. H. *Chemistry of Materials* 2006, *18*, 3212.

(2) Levshin, B. L.; Mitrofanova, N. V.; Timofeev, Y. P.; Fridman, S. A.; Shchaenko, V. V. *Proceedings (Trudy) of the P.N. Lebedev Physics Institute* 1972, *59*, 54.

(3) Van den Eeckhout, K.; Smet, P. F.; Poelman, D. *Materials* 2010, *3*, 2536.

(4) Katsumata, T.; Toyomane, S.; Tonegawa, A.; Kanai, Y.; Kaneyama, U.; Shakuno, K.; Sakai, R.; Komuro, S.; Morikawa, T. *J. Cryst. Growth* 2002, *237-239*, 361.

(5) Nag, A.; Kutty, T. R. N. *Materials Research Bulletin* 2004, *39*, 331.

(6) Wang, J.; Su, Q.; Wang, S. *Materials Research Bulletin* 2005, *40*, 590.

(7) Matsuzawa, T.; Aoki, Y.; Takeuchi, N.; Murayama, Y. *Journal of the Electrochemical Society* 1996, *143*, 2670.

(8) Zitoun, D.; Bernaud, L.; Manteghetti, A.; Filhol, J.-S. *Journal of Chemical Education* 2009, *86*, 72.

(9) Pan, W.; Ning, G.; Zhang, X.; Wang, J.; Lin, Y.; Ye, J. *Journal of Luminescence* 2008, *128*, 1975.

(10) Trindade, T.; O'Brien, P.; Pickett, N. L. *Chemistry of Materials* 2001, *13*, 3843.

(11) Peng, W. Q.; Cong, G. W.; Qu, S. C.; Wang, Z. G. *Optical Materials* 2006, *29*, 313.

(12) Li, L. S.; Pradhan, N.; Wang, Y.; Peng, X. *Nano Letters* 2004, *4*, 2261.

(13) Ben, P. V.; Tue, P. T. *VNU Journal of Science, Mathematics - Physics* 2008, *24*, 7.

(14) Borse, P. H.; Deshmukh, N.; Shinde, R. F.; Date, S. K.; Kulkarni, S. K. *Journal of Materials Science* 1999, *34*, 6087.

(15) Chatterjee, A.; Priyam, A.; Bhattacharya, S. C.; Saha, A. *Colloids and Surfaces A: Physicochemical and Engineering Aspects* 2007, *297*, 258.

(16) Han, S.-D.; Singh, K. C.; Lee, H.-S.; Cho, T.-Y.; Hulme, J. P.; Han, C.-H.; Chun, I.-S.; Gwak, J. *Materials Chemistry and Physics* 2008, *112*, 1083.

(17) Lee, S.; Song, D.; Kim, D.; Lee, J.; Kim, S.; Park, I. Y.; Choi, Y. D. *Materials Letters* 2004, *58*, 342.

(18) Murase, N.; Jagannathan, R.; Kanematsu, Y.; Watanabe, M.; Kurita, A.; Hirata, K.; Yazawa, T.; Kushida, T. *The Journal of Physical Chemistry B* 1999, *103*, 754.

(19) Thuy, P. T.; Thuy, U. T. D.; Chi, T. T. K.; Phuong, L. Q.; Liem, N. Q.; Li, L.; Reiss, P. *Journal of Physics: Conference Series* 2009, 012014.

(20) Wageh, S.; Ling, Z. S.; Xu-Rong, X. *J. Cryst. Growth* 2003, *255*, 332.

(21) Panda, S. K.; Datta, A.; Chaudhuri, S. *Chemical Physics Letters* 2007, *440*, 235.

(22) Cheng, B. C.; Wang, Z. G. *Advanced Functional Materials* 2005, *15*, 8.

(23) KARAR, N.; Chander, H. *Journal of nanoscience and nanotechnology* 2005, *5*, 5.

(24) Koyakutty, M.; et al. *Nanotechnology* 2009, *20*, 065102.

(25) Mohagheghpour, E.; Rabiee, M.; Moztarzadeh, F.; Tahriri, M. *Journal of Ceramic Processing Research* 2010, *11*, 6.

(26) Okamoto, S.; Tanaka, K. *physica status solidi (c)* 2006, *3*, 1059.

(27) Kolny-Olesiak, J.; Kloper, V.; Osovsky, R.; Sashchiuk, A.; Lifshitz, E. *Surface Science* 2007, *601*, 2667.

(28) Chen, W.; Zhang, J. Z.; Joly, A. G. *Journal of Nanoscience and Nanotechnology* 2004, *4*, 919.

(29) Chen, W.; Malm, J.-O.; Zwiller, V.; Huang, Y.; Liu, S.; Wallenberg, R.; Bovin, J.-O.; Samuelson, L. *Physical Review B* 2000, *61*, 11021.

(30) Chen, W. *Doped Nanomaterials and Nanodevices* 2010, *Chapter 1*, 30.

(31) Chen, W. *Nalwa, H. S., Webster,T. J., Eds.; American Scientific Publishers: Los Angeles, CA,* 2007, 24.

(32) Pradhan, N.; Battaglia, D. M.; Liu, Y.; Peng, X. *Nano Letters* 2006, *7*, 312.

(33) Kynev, K.; Schanda, J. D. *Journal of Luminescence* 1982, *27*, 199.

(34) Froelich, H. C. *U.S. Patent* 1946, *2392814*, 2.

(35) Abbruscato, V. *Journal of the electrochemical society* 1971, *118*, 4.

(36) Tang, Z.; Zhang, F.; Zhang, Z.; Huang, C.; Lin, Y. *Journal of the European Ceramic Society* 2000, *20*, 2129.

(37) Chen, I.-C.; Chen, T.-M. *Materials Research Society* 2001, *16*, 8.

(38) Aitasalo, T.; Hölsä, J.; Jungner, H.; Lastusaari, M.; Niittykoski, J. *Journal of Alloys and Compounds* 2002, *341*, 76.

(39) Aitasalo, T.; Holsa, J.; Jungner, H.; Lastusaari, M.; Niittykoski, J. *The Journal of Physical Chemistry B* 2006, *110*, 4589.

(40) Lin, Y.; Tang, Z.; Zhang, Z.; Wang, X.; Zhang, J. *Journal of Materials Science Letters* 2001, *20*, 2.

(41) Pathak, S.; Choi, S.-K.; Arnheim, N.; Thompson, M. E. *Journal of the American Chemical Society* 2001, *123*, 4103.

(42) Alivisatos, P. *Nat Biotech* 2004, *22*, 47.

(43) Bruchez, M.; Moronne, M.; Gin, P.; Weiss, S.; Alivisatos, A. P. *Science* 1998, *281*, 2013.

(44) Yong, K.-T.; Ding, H.; Roy, I.; Law, W.-C.; Bergey, E. J.; Maitra, A.; Prasad, P. N. *ACS Nano* 2009, *3*, 502.

(45) Chen, W. *Journal of Biomedical Nanotechnology* 2008, *4*, 8.

(46) Liu, Y.; Chen, W.; Wang, S.; Joly, A. G. *Applied Physics Letters* 2008, *92*, 043901.

(47) Yang, W.; Read, P. W.; Mi, J.; Baisden, J. M.; Reardon, K. A.; Larner, J. M.; Helmke, B. P.; Sheng, K. *International Journal of Radiation Oncology*Biology*Physics* 2008, *72*, 633.

(48) Rosenthal, S. J.; Tomlinson, I.; Adkins, E. M.; Schroeter, S.; Adams, S.; Swafford, L.; McBride, J.; Wang, Y.; DeFelice, L. J.; Blakely, R. D. *Journal of the American Chemical Society* 2002, *124*, 4586.

(49) Bhargava, R. N.; Gallagher, D.; Hong, X.; Nurmikko, A. *Physical Review Letters* 1994, *72*, 416.

(50) Zhuang, J.; Zhang, X.; Wang, G.; Li, D.; Yang, W.; Li, T. *Journal of Materials Chemistry* 2003, *13*.

(51) Roorda, R. D.; Ribes, A. C.; Damaskinos, S.; Dixon, A. E.; Menzel, E. R. *Journal of Forensic Sciences* 2000, *45*, 5.

(52) Smith, B. A.; Zhang, J. Z.; Joly, A.; Liu, J. *Physical Review B* 2000, *62*, 2021.

(53) Bol, A. A.; Meijerink, A. *Physical Review B* 1998, *58*, R15997.

(54) Cheng, K. H.; Aijmo, J.; Ma, L.; Yao, M.; Zhang, X.; Como, J.; Hope-Weeks, L. J.; Huang, J.; Chen, W. *The Journal of Physical Chemistry C* 2008, *112*, 17931.

(55) Putiev, I. T.; Chenets, V. N.; Tukhlibaev, A. *Russian Physics Journal* 1974, *17*, 290.

(56) Murphy, M.; Zhou, X.-T.; Heigl, F.; Regier, T.; Sham, T.-K. *X-RAY ABSORPTION FINE STRUCTURE - XAFS13: 13th International Conference. AIP Conference Proceedings.* 2007, *882*, 3.

(57) Kamuhabwa, A.; Agostinis, P.; Ahmed, B.; Landuyt, W.; Cleynenbreugel, B. V.; Poppel, H. V.; Witte, P. d. *Photochemical & Photobiological Sciences* 2004, *3*, 9.

(58) Zhu, J. *Physics Letters A* 2005, *341*, 212.

(59) Fu, Y.; Zhang, J.; Lakowicz, J. R. *Chemical Communications* 2009, 313.

(60) Chowdhury, M. H.; Ray, K.; Geddes, C. D.; Lakowicz, J. R. *Chemical Physics Letters* 2008, *452*, 162.

(61) Chen, W.; Aguekian, V. F.; Vassiliev, N.; Serov, A. Y.; Filosofov, N. G. *The Journal of Chemical Physics* 2005, *123*, 124707.

(62) Suyver, J. F.; Wuister, S. F.; Kelly, J. J.; Meijerink, A. *Nano Letters* 2001, *1*, 429.

(63) Chen, W.; Joly, A. G.; Zhang, J. Z. *Physical Review B* 2001, *64*, 041202.

(64) Enüstün, B. V.; Turkevich, J. *Journal of the American Chemical Society* 1963, *85*, 3317.

(65) Liu, N.; Prall, B. S.; Klimov, V. I. *Journal of the American Chemical Society* 2006, *128*, 15362.

(66) Jana, N. R.; Gearheart, L.; Murphy, C. J. *Langmuir* 2001, *17*, 6782.

(67) Liz-Marzán, L. M. *Langmuir* 2005, *22*, 32.

(68) Hutter, E.; Fendler, J. H. *Advanced Materials* 2004, *16*, 1685.

(69) Zhang, J.; Noguez, C. *Plasmonics* 2008, *3*, 127.

(70) Chen, W.; Sammynaiken, R.; Huang, Y.; Malm, J.-O.; Wallenberg, R.; Bovin, J.-O.; Zwiller, V.; Kotov, N. A. *Journal of Applied Physics* 2001, *89*, 1120.

(71) Chen, W.; Su, F.; Li, G.; Joly, A. G.; Malm, J.-O.; Bovin, J.-O. *Journal of Applied Physics* 2002, *92*, 1950.

(72) Chen, W.; Sammynaiken, R.; Huang, Y. *Journal of Applied Physics* 2000, *88*, 5188.

(73) Gan, L. M.; Liu, B.; Chew, C. H.; Xu, S. J.; Chua, S. J.; Loy, G. L.; Xu, G. Q. *Langmuir* 1997, *13*, 6427.

(74) Bol, A. A.; Meijerink, A. *The Journal of Physical Chemistry B* 2001, *105*, 10197.

(75) Cheng, P.; Li, D.; Yuan, Z.; Chen, P.; Yang, D. *Applied Physics Letters* 2008, *92*, 041119.
(76) Lakowicz, J. R. *Analytical Biochemistry* 2001, *298*, 1.

(77) Messinger, B. J.; von Raben, K. U.; Chang, R. K.; Barber, P. W. *Physical Review B* 1981, *24*, 649.

(78) Yen, W. M.; Shionoya, S.; Yamamoto, H. *PHOSPHOR HANDBOOK (Second Edition), CRC Press* 2007.

(79) Juzenas, P.; Chen, W.; Sun, Y.-P.; Coelho, M.; Generalov, R.; Generalova, N.; Christensen, I. *Adv. Drug Deliv. Rev.* 2008, *60*, 1600.
(80) Chen, W.; Zhang, J. *J. Nanosci. Nanotechnol.* 2006, *6*, 1159.

(81) Chen, W. *J. Biomed. Nanotechnol.* 2008, *4*, 369.

(82) le Masne de Chermont, Q.; Chanéac, C.; Seguin, J.; Pellé, F.; Maîtrejean, S.; Jolivet, J.-P.; Gourier, D.; Bessodes, M.; Scherman, D. *Proceedings of the National Academy of Sciences* 2007, *104*, 9266.

(83) Xu, S. J.; Chua, S. J.; Liu, B.; Gan, L. M.; Chew, C. H.; Xu, G. Q. *Applied Physics Letters* 1998, *73*, 478.

(84) Bol, A. A.; Ferwerda, J.; Bergwerff, J. A.; Meijerink, A. *Journal of Luminescence* 2002, *99*, 325.

(85) Jayanthi, K.; Chawla, S.; Chander, H.; Haranath, D. *Crystal Research and Technology* 2007, *42*, 976.

(86) Yang, P.; Lü, M.; Zhou, G.; Yuan, D.; Xu, D. *Inorganic Chemistry Communications* 2001, *4*, 734.

(87) Wang, W.; Huang, F.; Xia, Y.; Wang, A. *Journal of Luminescence* 2008, *128*, 610.

(88) Song, H.; Leem, Y.-M.; Kim, B.-G.; Yu, Y.-T. *Journal of Physics and Chemistry of Solids* 2008, *69*, 153.

(89) Fitzpatrick, B. J. *J. Cryst. Growth* 1990, *86*, 106.

(90) Ihanus, J.; Ritala, M.; Leskelä, M.; Prohaska, T.; Resch, R.; Friedbacher, G.; Grasserbauer, M. *Applied Surface Science* 1997, *120*, 43.

(91) Yang, H.; Huang, C.; Su, X.; Tang, A. *Journal of Alloys and Compounds* 2005, *402*, 274.

(92) Yang, P.; Lü, M.; Xü, D.; Yuan, D.; Song, C.; Zhou, G. *Journal of Physics and Chemistry of Solids* 2001, *62*, 1181.

(93) Baea, W.; Mehra, R. K. *Journal of Inorganic Biochemistry* 1998, *70*, 11.

(94) Chen, W.; Wang, Z.; Lin, Z.; Lin, L. *Journal of Applied Physics* 1997, *82*, 3111.

(95) Wang, M.; Sun, L.; Fu, X.; Liao, C.; Yan, C. *Solid State Communications* 2000, *115*, 493.

(96) Kandarakisa, I.; ∗, D. C.; Nikolopoulosa, D.; Anastasioua, A.; Dimitropoulosb, N.; Kalivasc, N.; Ventourasa, E.; Kalatzisa, I.; Nomicosd, C.; Panayiotakis, G. *Radiation Measurements* 2005, *39*, 13.

(97) Kao, C.-c.; Liu, Y.-c. *Materials Chemistry and Physics* 2009, *115*, 463.

(98) Nakazawa, E. In *Phosphor Handbook*; Shionoya, S., Yen, W. M., Eds.; CRC Press: New York, 1999, p 85.

(99) *Phosphor Handbook*; Shionoya, S.; Yen, W. M., Eds.; CRC Press: New York, 1999.

(100) Lakowicz, J. R. *Principles of Fluorescence Spectroscopy* 3 edition ed.; Springer, 2006.

(101) Dougherty, T. J.; Gomer, C. J.; Henderson, B. W.; Jori, G.; Kessel, D.; Korbelik, M.; Moan, J.; Peng, Q. *Journal of the National Cancer Institute* 1998, *90*.

(102) Brown, J. E.; Brown, S. B.; Vernon, D. I. *JSDC* 1999, *115*, 249.

(103) Jia, W.; Yuan, H.; Holmstrom, S.; Liu, H.; Yen, W. M. *Journal of Luminescence*, *83/84*, 465.

(104) Douglas, R. H.; Moan, J.; Dall'Acqua, F. *Light in Biology and Medicine*; Plenum Press: New York and London, 1987; Vol. 1.

(105) Douglas, R. H.; Moan, J.; Ronto, G. *Light in Biology and Medicine*; Plenum Press: New York and London, 1991; Vol. 2.

(106) Papageorgiou, P.; Katsambas, A.; Chu, A. *Br. J. Dermatol.* 2000, *142*, 973.

(107) Posten, W.; Wrone, D. A.; Dover, J. S.; Arndt, K. A.; Silapunt, S.; Alam, M. *Dermatol Surg* 2005, *31*, 334.

(108) Lis, S. *J. Alloys. Compounds.* 2002, *341*, 45.

(109) Bartwal, K. S.; Ryu, H. *Resources Processing* 2008, *55*, 120.

(110) Li, W.; Liu, Y.; Ai, P. *Materials Chemistry and Physics* 2010, *119*, 52.

(111) Peng, T.; Huajun, L.; Yang, H.; Yan, C. *Materials Chemistry and Physics* 2004, *85*, 68.

(112) Woo, B. K.; Luo, Z.; Li, Y.; Singh, S. P.; Joly, A. G.; Hossu, M.; Liu, Z.; Chen, W. *Optical Materials* 2011.

(113) Lun, M.; Wei, C. *Nanotechnology* 2010, *21*, 385604.

(114) Zang, L.; Liu, C.-Y.; Ren, X.-M. *Journal of Photochemistry and Photobiology A: Chemistry* 1994, *79*, 189.

(115) Reitinger, N.; Hohenau, A.; Köstler, S.; Krenn, J. R.; Leitner, A. *physica status solidi (a)* 2010, n/a.

(116) Yang, Y.; Huang, J.; Liua, S.; Shen, J. *Journal of Materials Chemistry* 1997, *7*, 3.

(117) Murugadoss, G.; Rajamannan, B.; Ramasamy, V. *Journal of Luminescence* 2010, *130*, 2032.

(118) Kolhe, S.; Kuljarni, S. K.; Nigavekar, A. S.; Sharma, S. K. *Solar Energy Materials* 1984, *10*, 47.

(119) Mehta, S. K.; Kumar, S.; Chaudhary, S.; Bhasin, K. K. *Nanoscale Research Letters* 2009, *4*, 12.

(120) Jian, W.; Zhuang, J.; Zhang, D.; Dai, J.; Yang, W.; Bai, Y. *Materials Chemistry and Physics* 2006, *99*, 494.

(121) Qu, H.; Cao, L.; Su, G.; Liu, W.; Sun, Y.; Dong, B. *Journal of Applied Physics* 2009, *106*, 093506.

BIOGRAPHICAL INFORMATION

The author received his early academic education in China, graduated with a degree of Bachelor of Science in Physics from Shannxi Normal University. Before pursuing the doctoral program in the University of Texas at Arlington in 2007, he spent two years and obtained the degree of Master of Science in Physics from the same University. The author is currently working in the research area of luminescent nanomaterials and their biological applications.